

Comprehensive Analysis of Charged Lepton Flavour Violation in the Symmetry Protected Type-I Seesaw

Andreas Crivellin^{a,b} Fiona Kirk^{a,b} Claudio Andrea Manzari^{a,b}

^a*Physik-Institut, Universität Zürich, Winterthurerstrasse 190, CH-8057 Zürich, Switzerland*

^b*Paul Scherrer Institut, CH-5232 Villigen PSI, Switzerland*

E-mail: andreas.crivellin@cern.ch, fiona.kirk@psi.ch,
claudioandrea.manzari@physik.uzh.ch

ABSTRACT: The type-I seesaw model is probably the most straightforward and best studied extension of the Standard Model that can account for the tiny active neutrino masses determined from neutrino oscillation data. In this article, we calculate the complete set of one-loop corrections to charged lepton flavour violating processes within this model. We give the results both using exact diagonalisation of the neutrino mass matrix, and at leading order in the seesaw expansion (i.e. $\mathcal{O}(v^2/M_R^2)$). Furthermore, we perform the matching onto the $SU(2)_L$ invariant Standard Model Effective Field Theory at the dimension 6 level. These results can be used as initial conditions for the renormalisation group evolution from the right-handed neutrino scale down to the scale of the physical processes, which resums large logarithms. In our numerical analysis, we study the inverse seesaw limit, i.e. the symmetry protected type-I seesaw, where the Wilson coefficient of the Weinberg operator is zero such that sizeable neutrino Yukawas are permissible and relevant effects in charged lepton flavour violating observables are possible. We correlate the different charged lepton flavour violating processes, e.g. $\ell \rightarrow \ell' \gamma$, $\ell \rightarrow 3\ell'$, $\mu \rightarrow e$ conversion and $Z \rightarrow \ell\ell'$, taking into account the constraints from electroweak precision observables and tests of lepton flavour universality.

Contents

1	Introduction	1
2	Setup	2
3	Matching onto the SMEFT	5
3.1	Conventions	7
3.2	Tree Level Matching	9
3.3	One-Loop Matching	10
3.3.1	Modified Gauge-Boson Couplings ($\mathcal{O}_{\varphi\ell}^{(1)}$ and $\mathcal{O}_{\varphi\ell}^{(3)}$)	10
3.3.2	Four-Lepton Operators ($\mathcal{O}_{\ell\ell}$ and $\mathcal{O}_{\ell e}$)	12
3.3.3	Two-Lepton-Two-Quark Operators ($\mathcal{O}_{\ell q}^{(1)}$, $\mathcal{O}_{\ell q}^{(3)}$, $\mathcal{O}_{\ell u}$ and $\mathcal{O}_{\ell d}$)	13
3.3.4	Magnetic Operators (\mathcal{O}_{eW} and \mathcal{O}_{eB})	13
4	Observables	13
4.1	Lepton Flavour Universality Tests	14
4.2	$Z \rightarrow \nu\nu$	17
4.3	$Z \rightarrow \ell\ell'$	17
4.4	$\ell \rightarrow \ell'\gamma$	19
4.5	$\ell \rightarrow 3\ell'$ and $\ell \rightarrow \ell'\ell''\ell'''$	19
4.6	$\mu \rightarrow e$ Conversion in Nuclei	21
5	Phenomenology	24
6	Conclusions	26
A	Neutrino Mixing Matrix	30
B	Contributions to charged lepton flavour violating processes within the EFT	32
B.1	$\ell \rightarrow \ell'\gamma$	32
B.2	Four Lepton Amplitudes	33
B.3	Two-Lepton-Two-Quark Interactions	34
C	Exact diagonalisation and/or R_ξ Dependence	36
C.1	Anomalous Magnetic Moments and Radiative Leptonic Decays	36
C.2	$Z \rightarrow \ell\ell'$	37
C.3	$\ell \rightarrow \ell'\ell''\ell'''$	40
C.3.1	Photon Penguin Contributions	40
C.3.2	Z Penguin Contributions	40
C.3.3	Box Contributions	41
C.4	$\mu \rightarrow e$ Conversion in Nuclei	44

C.4.1	Photon Penguin Contributions	45
C.4.2	Z Penguin Contributions	45
C.4.3	Box Contributions	45
D	Integrals	46

1 Introduction

Since neutrinos are massless within the Standard Model (SM), any explanation of the non-vanishing neutrino masses determined from neutrino oscillation data must involve new particles. The most studied scenario in this context is the extension of the SM by right-handed neutrinos, which reproduces a situation similar to that in the quark and charged lepton sector, where each left-handed field has a right-handed counterpart. This allows for Yukawa interactions, which, after electroweak symmetry breaking, give rise to Dirac mass terms for neutrinos. This minimal extension of the SM, referred to as the ν SM [1], appeals due to its simplicity, however, it is often considered unnatural since extremely small Yukawa couplings would be necessary to reproduce the observed neutrino masses, which are at most at the eV scale. Furthermore, the small ν SM Yukawa couplings do not lead to any observable new physics effects in precision observables. Indeed, within the ν SM e.g. charged lepton flavour violating processes suffer from a GIM-like suppression by the active neutrino masses, leading to branching ratios below 10^{-45} , which are unobservable.

A more natural explanation of the smallness of the neutrino masses can be provided by seesaw mechanisms, such as the type I seesaw [2–6], which assigns large Majorana masses, M_R , to the right-handed neutrinos. In this case, the light neutrinos masses turn out to be proportional to $M_D M_R^{-1} M_D^T$, where M_D denotes the Dirac mass term. Depending on the scale of M_R , the type-I seesaw model can be probed at colliders [7–17], it can be used as a framework for leptogenesis [18–21] or the right-handed neutrinos can be viewed as dark matter candidates [20, 22–25]. The discovery potential of the generic type-I seesaw is, however, limited, since the smallness of the active neutrino masses, as inferred from neutrino oscillation data, excludes sizeable Yukawa couplings to TeV-scale right-handed neutrinos.

Sizeable Yukawa couplings are admissible if an (approximate) lepton number symmetry [8, 26–36] is imposed, which suppresses the Wilson coefficient of the Weinberg operator [37], and therefore the observed neutrino masses. This strategy is adopted in the inverse seesaw model [27, 28, 30, 38, 39], therefore we refer to the limit with vanishing active neutrino masses as the inverse-seesaw limit. In this symmetry-protected type-I seesaw, admissibly sizeable Yukawa couplings can significantly modify the neutrino couplings to SM gauge bosons. At tree-level, this leads to effects in processes such as $\pi \rightarrow \ell\nu$, $\tau \rightarrow \mu\nu\nu$, $Z \rightarrow \nu\nu$ and beta decays [6, 11, 40–68], and at the loop level to effects in $\ell \rightarrow \ell'\gamma$, $\ell \rightarrow 3\ell'$, and $Z \rightarrow \ell^+\ell^-$ [6, 11, 40–75], which have also been studied in the SM Effective Field Theory (SMEFT) [34, 37, 70, 72, 76–85].

In this article we perform a comprehensive analysis of charged lepton flavour violation in the symmetry protected type-I seesaw: We calculate these effects both using exact diagonalisation of the neutrino mass matrix and by expanding the amplitudes in v^2/M_R^2 , which corresponds to the seesaw limit. Furthermore, we match the type-I seesaw model onto the $SU(2)_L$ gauge invariant SMEFT, which allows for the use of renormalisation group improved perturbation theory that resums the large logarithms between the right-handed neutrino scale and the scale of the physical processes. We state our conventions for the type-I seesaw model in Sec. 2. In Sec. 3, we give the 1-loop SMEFT matching conditions that are relevant for flavour observables, in Sec. 4 we list the fixed-order results for the flavour observables of interest, before performing our phenomenological analysis in Sec. 5 and concluding Sec. 6. In the appendix we provide results using exact diagonalisation of the neutrino mass matrix and/or in a general R_ξ gauge.

2 Setup

In the most general type-I seesaw setup, the SM is supplemented by n generations of right-handed neutrinos N_R , i.e. by fermions that are singlets under the SM gauge group. These new fields can have Majorana mass terms, as well as Yukawa-like interactions with the lepton doublet $L = (\nu_L, \ell_L)$ and the Higgs doublet Φ . In the interaction basis, the Lagrangian is given by

$$\mathcal{L}_N = \bar{N}_R i\partial^\mu N_R - \left(\bar{L} Y^\nu \tilde{\Phi} N_R + \frac{1}{2} \bar{N}_R^c M_R N_R + \text{h.c.} \right), \quad (2.1)$$

where c stands for charge conjugation and we have suppressed flavour indices for better readability, i.e. M_R is an $n \times n$ matrix, that, without loss of generality, can be chosen to be diagonal and real, Y^ν is a $3 \times n$ matrix. After electroweak symmetry breaking, the Higgs doublet acquires a vacuum expectation value of $v/\sqrt{2} \approx 175$ GeV and takes the form

$$\Phi \equiv \begin{pmatrix} \varphi^+ \\ \frac{v+h+i\varphi^0}{\sqrt{2}} \end{pmatrix}, \quad \tilde{\Phi} \equiv i\sigma_2 \Phi^* = \begin{pmatrix} \frac{v+h-i\varphi^0}{\sqrt{2}} \\ -\varphi^- \end{pmatrix}, \quad (2.2)$$

where σ_2 is the second Pauli matrix. Electroweak symmetry breaking generates the $3 \times n$ Dirac mass matrix

$$M_D = \frac{v}{\sqrt{2}} Y^\nu. \quad (2.3)$$

We can now write the mass terms resulting from Eq. (2.1) as

$$\mathcal{L}_N = -\frac{1}{2} \left(\bar{\nu}_L \bar{N}_R^c \right) M_\nu \begin{pmatrix} \nu_L^c \\ N_R \end{pmatrix} + \text{h.c.} , \quad (2.4)$$

with the mass matrix

$$M_\nu = \begin{pmatrix} \mathbb{O}_3 & M_D \\ M_D^T & M_R \end{pmatrix}. \quad (2.5)$$

Next we move to the mass eigenbasis in which M_ν is diagonal,

$$\mathcal{L}_N = -\frac{1}{2}\bar{n}_R^c M_\nu^{\text{diag}} n_R + \text{h.c.} , \quad (2.6)$$

with

$$M_\nu^{\text{diag}} = V^\dagger M_\nu V^* \equiv \begin{pmatrix} m^l & 0 \\ 0 & m^h \end{pmatrix} . \quad (2.7)$$

Here V is a unitary $(3+n) \times (3+n)$ matrix, m^l is a 3×3 matrix containing the light neutrino masses, while m^h is an $n \times n$ matrix with masses of $\mathcal{O}(M_R)$. Since the light neutrinos are mostly composed of the ones within the lepton doublet L_i , they are commonly referred to as *active* neutrinos, whereas the heavy neutrinos, which are mostly aligned with the gauge singlets N_R , are known as *sterile* neutrinos. The neutrino mass eigenstates ($3+n$ vectors) are defined as

$$n_R = V^T \begin{pmatrix} \nu_L^c \\ N_R \end{pmatrix} \equiv \begin{pmatrix} n_R^l \\ n_R^h \end{pmatrix}, \quad \bar{n}_R^c = \begin{pmatrix} \bar{\nu}_L \\ \bar{N}_R^c \end{pmatrix}^T V \equiv \begin{pmatrix} \bar{n}_R^{l,c} \\ \bar{n}_R^{h,c} \end{pmatrix}^T . \quad (2.8)$$

In the following, we will consider the seesaw limit $v \ll M_R$ and expand our results in v/M_R . The full results, obtained by exact diagonalisation of the neutrino mass matrix, are given in Appendix C.

In a first step, we block-diagonalise M_ν , such that $\tilde{M}_\nu = \text{diag}(\tilde{m}^l, \tilde{m}^h)$, where \tilde{m}^l is a 3×3 matrix and \tilde{m}^h is an $n \times n$ matrix in flavour space. At leading order in v/M_R , we find

$$V = \begin{pmatrix} \mathbb{1}_3 - \frac{1}{2}M_D M_R^{-2} M_D^\dagger & M_D M_R^{-1} \\ -M_R^{-1} M_D^\dagger & \mathbb{1}_n + \mathcal{O}\left(\frac{v^2}{M_R^2}\right) \end{pmatrix} + \mathcal{O}\left(\frac{v^3}{M_R^3}\right) , \quad (2.9)$$

$$\tilde{m}^l = -M_D M_R^{-1} M_D^T , \quad (2.10)$$

$$\tilde{m}^h = M_R + \mathcal{O}\left(\frac{v^2}{M_R^2}\right) . \quad (2.11)$$

Note that the off-diagonal blocks induce *active-sterile* mixing, while the correction to the upper-left block induces (apparent) PMNS unitarity violation. Since our focus will be on charged lepton flavour violation, to which the active neutrino masses do not contribute in any observable way, we assume

$$\tilde{m}^l \approx -M_D M_R^{-1} M_D^T \equiv 0 , \quad (2.12)$$

which we will refer to as the *inverse seesaw limit* [8, 27–30, 33, 70] of the type-I seesaw. In this scenario, which is also known as the symmetry protected seesaw, the Wilson coefficient of the Weinberg operator is zero, implying that the neutrino mass matrix is automatically diagonal after block diagonalisation, and given by

$$M_\nu^{\text{diag}} \approx \text{diag}(0, 0, 0, M_{R,1}, M_{R,2}, M_{R,3}) + \mathcal{O}\left(\frac{v^2}{M_R^2}\right) , \quad (2.13)$$

while $\mathcal{O}(1)$ Yukawa couplings remain possible.

In presence of a single sterile neutrino, Eq. (2.12) only has a trivial solution (i.e. $Y^\nu = 0$), while for two sterile neutrinos, the solutions to Eq. (2.12) are given by [70]

$$Y^\nu = \begin{pmatrix} \lambda_e \pm i\lambda_e \sqrt{\frac{M_{R,2}}{M_{R,1}}} \\ \lambda_\mu \pm i\lambda_\mu \sqrt{\frac{M_{R,2}}{M_{R,1}}} \\ \lambda_\tau \pm i\lambda_\tau \sqrt{\frac{M_{R,2}}{M_{R,1}}} \end{pmatrix}. \quad (2.14)$$

If three sterile neutrinos are added to the SM,

$$Y^\nu = \begin{pmatrix} \lambda_e z \lambda_e \sqrt{\frac{M_{R,2}}{M_{R,1}}} \pm i\sqrt{1+z^2} \lambda_e \sqrt{\frac{M_{R,3}}{M_{R,1}}} \\ \lambda_\mu z \lambda_\mu \sqrt{\frac{M_{R,2}}{M_{R,1}}} \pm i\sqrt{1+z^2} \lambda_\mu \sqrt{\frac{M_{R,3}}{M_{R,1}}} \\ \lambda_\tau z \lambda_\tau \sqrt{\frac{M_{R,2}}{M_{R,1}}} \pm i\sqrt{1+z^2} \lambda_\tau \sqrt{\frac{M_{R,3}}{M_{R,1}}} \end{pmatrix}. \quad (2.15)$$

Here z is an arbitrary complex number, and λ_e , λ_μ and λ_τ can be chosen to be real and positive. In the seesaw-expanded results, we will encounter the combination

$$S_{ij} = (M_D M_R^{-2} M_D^\dagger)_{ij} \quad (2.16)$$

or equivalently,

$$T_{ij} = (Y^\nu M_R^{-2} Y^{\nu\dagger})_{ij} = \frac{2}{v^2} S_{ij}. \quad (2.17)$$

For two sterile neutrinos with degenerate masses $M_{R,1} = M_{R,2} = M_R$, T_{ij} is given by

$$T_{ij} = 2 \frac{\lambda_i \lambda_j}{M_R^2}. \quad (2.18)$$

We will also encounter the matrix products

$$\left(Y^\nu Y^{\nu\dagger} Y^\nu Y^{\nu\dagger} \right)_{ij} \quad \left(Y^\nu Y^{\nu\dagger} \right)_{ij} \left(Y^\nu Y^{\nu\dagger} \right)_{kl}. \quad (2.19)$$

If we apply the parametrisation in Eq. (2.14) and set $M_{R,1} = M_{R,2} = M_R$, T_{ij} , we find

$$\left(Y^\nu Y^{\nu\dagger} Y^\nu Y^{\nu\dagger} \right)_{ij} = 4 \lambda_i \lambda_j \sum_{k \in \{e, \mu, \tau\}} \lambda_k^2 \quad (2.20)$$

$$\left(Y^\nu Y^{\nu\dagger} \right)_{ij} \left(Y^\nu Y^{\nu\dagger} \right)_{kl} = 4 \lambda_i \lambda_j \lambda_k \lambda_l. \quad (2.21)$$

If we take three sterile neutrinos with degenerate masses $M_{R,1} = M_{R,2} = M_R$, and the Yukawa matrix of Eq. (2.15), these matrix products take the form

$$T_{ij} = (1 + |z|^2 + |1 + z^2|) \frac{\lambda_i \lambda_j}{M_R^2}. \quad (2.22)$$

$$\left(Y^\nu Y^{\nu\dagger} Y^\nu Y^{\nu\dagger} \right)_{ij} = (1 + |z|^2 + |1 + z^2|)^2 \lambda_i \lambda_j \sum_{k \in \{e, \mu, \tau\}} \lambda_k^2 \quad (2.23)$$

$$\left(Y^\nu Y^{\nu\dagger} \right)_{ij} \left(Y^\nu Y^{\nu\dagger} \right)_{kl} = (1 + |z|^2 + |1 + z^2|)^2 \lambda_i \lambda_j \lambda_k \lambda_l. \quad (2.24)$$

The presence of active-sterile mixing leads to tree-level modifications of the gauge boson couplings to the SM neutrinos. Defining the covariant derivative as

$$D_\mu = \partial_\mu + ig_2 W_\mu^I \tau^I + ig_1 B_\mu Y, \quad (2.25)$$

where $\tau^I \equiv \sigma^I/2$ and σ^I denote the Pauli matrices, and introducing the Lagrangian of the neutral and charged current interactions after electroweak symmetry breaking,

$$\mathcal{L}_{W,Z}^{\ell,\nu} = \left(\bar{\ell}_i g_{ij}^{\ell\nu} \gamma^\mu P_L \nu_j W_\mu + \text{h.c.} \right) + \left[\bar{\ell}_i \gamma^\mu \left(g_{ij}^{\ell L} P_L + g_{ij}^{\ell R} P_R \right) \ell_j + \bar{\nu}_i g_{ij}^{\nu} \gamma^\mu P_L \nu_j \right] Z_\mu, \quad (2.26)$$

where i and j are flavour indices, we identify the couplings

$$\begin{aligned} g_{ij}^{\ell L} &= \frac{e}{2s_W c_W} (1 - 2s_W^2) \delta_{ij}, & g_{ij}^{\ell R} &= -\frac{es_W}{c_W} \delta_{ij}, \\ g_{ij}^{\nu} &= -\frac{e}{2s_W c_W} (\delta_{ij} - S_{ij}), & g_{ij}^{\ell\nu} &= -\frac{e}{\sqrt{2}s_W} \left(\delta_{ij} - \frac{1}{2} S_{ij} \right). \end{aligned} \quad (2.27)$$

In the following, we will use the notation

$$\begin{aligned} g_{\text{SM}}^{\ell L} &= \frac{e}{2s_W c_W} (1 - 2s_W^2), & g_{\text{SM}}^{\ell R} &= -\frac{es_W}{c_W}, \\ g_{\text{SM}}^{\nu} &= -\frac{e}{2s_W c_W}, & g_{\text{SM}}^{\ell\nu} &= -\frac{e}{\sqrt{2}s_W}. \end{aligned} \quad (2.28)$$

Note that the $Z\ell\ell$ couplings, $g_{ij}^{\ell L}$ and $g_{ij}^{\ell R}$, are not modified at tree-level, while the interactions of the EW gauge bosons with neutrinos receive contributions proportional to S_{ij} and can therefore be flavour off-diagonal. The interactions of the charged Goldstone bosons with neutrinos are modified in a similar way. All relevant Feynman rules are given in Table 1.

These (expanded) Feynman rules can be visualised in the Mass Insertion Approximation (MIA): Instead of working in the mass eigenbasis, one can remain in the interaction eigenbasis of Eq. (2.4), and treat off-diagonal mass terms as perturbative interactions. This approach leads to the same amplitudes as those derived in the mass eigenbasis and afterwards expanded in the seesaw limit. Figures 1a and 1b show how Eqs. (2.16) and (2.17) are represented or obtained diagrammatically.

3 Matching onto the SMEFT

In this section we calculate the matching onto the SMEFT. These results could be used as initial conditions of a renormalisation group improved computation of charged lepton flavour violating observables.¹ For the derivation of our results, we made extensive use of the **Mathematica** packages **FeynRules** [86], **FeynArts** [87] and **Package-X** [88, 89] in combination with **CollierLink**, a **Package-X** interface to the **Collier** library [90].

¹Our results agree with Ref. [83] (v3). We thank the authors for useful discussions.

Interaction	Expanded Feynman rule
$\bar{\ell}_i W_\mu^- n_{R,j}^{1,c}$	$-\frac{e}{\sqrt{2}s_W} \left(\delta_{ij} - \frac{S_{ij}}{2} \right) \gamma^\mu P_L$
$\bar{\ell}_i W_\mu^- n_{R,a}^{h,c}$	$-\frac{e}{\sqrt{2}s_W} (M_D M_R^{-1})_{ia} \gamma^\mu P_L$
$n_{R,i}^{1,c} Z_\mu n_{R,j}^{1,c}$	$-\frac{e}{2s_W c_W} (\delta_{ij} - S_{ij}) \gamma^\mu P_L$
$n_{R,i}^{1,c} Z_\mu n_{R,a}^{h,c}$	$-\frac{e}{2s_W c_W} (M_D M_R^{-1})_{ia} \gamma^\mu P_L$
$n_{R,a}^{h,c} Z_\mu n_{R,b}^{h,c}$	$-\frac{e}{2s_W c_W} (M_R^{-1} M_D^\dagger M_D M_R^{-1})_{ab} \gamma^\mu P_L$
$\bar{\ell}_i \varphi^- n_{R,j}^1$	0
$\bar{\ell}_i \varphi^- n_{R,a}^h$	$\frac{\sqrt{2}}{v} M_{D,ia} P_R$

Table 1: Feynman rules at leading order in the seesaw expansion, neglecting charged lepton masses. The active (light) states are denoted as n^l , the sterile (heavy) states as n^h . M_D is the $3 \times n$ Dirac mass matrix defined in Eq. (2.3), M_R is the $n \times n$ real and diagonal Majorana mass matrix introduced in Eq. (2.1) and S_{ij} the mass insertion defined in Eq. (2.16).

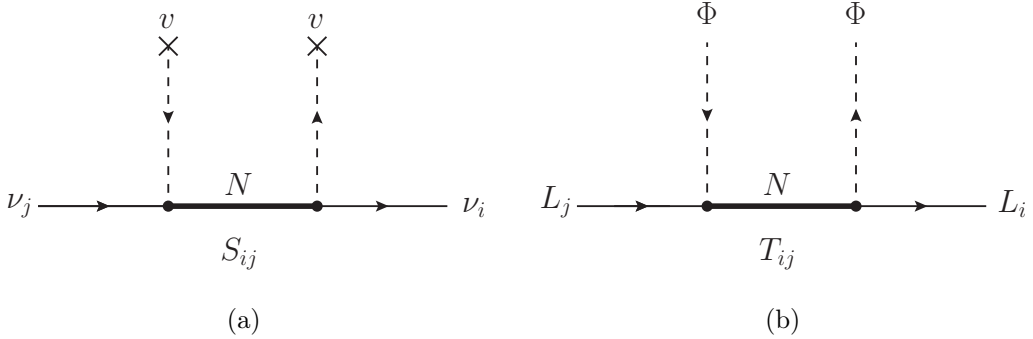


Figure 1: (a) Diagrammatic representation of the mass insertion S_{ij} in the broken theory (see Eq. (2.16)). ν_i and ν_j are SM-like left-handed neutrino gauge eigenstates, which can also interact with the SM gauge bosons, whereas N is the right-handed neutrino, which is a singlet under the SM gauge group. The dashed lines indicate the insertions of the Higgs vev v . (b) The related object, T_{ij} , defined in Eq. (2.17), which is relevant in the unbroken theory and enters the SMEFT matching relations. Here L_i and L_j are SM lepton doublets. N is the right-handed neutrino.

Interaction	Feynman rule in the EFT
$\bar{\ell}_i W_\mu^- n_{R,j}^{l,c}$	$-\frac{e}{\sqrt{2}s_W} \left(\delta_{ij} + v^2 C_{\varphi\ell,ij}^{(3)} \right) \gamma^\mu P_L$
$n_{R,i}^{l,c} Z_\mu n_{R,j}^{l,c}$	$-\frac{e}{2s_W c_W} \left(\delta_{ij} + v^2 X_{ij}^- \right) \gamma^\mu P_L$
$\varphi^+ \bar{\ell}_i n_{R,j}^{l,c}$	$\sqrt{2}v p_\mu^+ C_{\varphi\ell,ij}^{(3)} \gamma^\mu P_L$
$\varphi^-(p^-) \varphi^+(p^+) \bar{n}_{R,i}^{l,c} n_{R,j}^{l,c}$	$(p_\mu^+ - p_\mu^-) X_{ij}^+ \gamma^\mu P_L$
$\varphi^-(p^-) \varphi^+(p^+) \bar{\ell}_i \ell_j$	$-(p_\mu^+ - p_\mu^-) X_{ij}^- \gamma^\mu P_L$
$\varphi^-(p^-) W^+ \bar{n}_{R,i}^{l,c} n_{R,j}^{l,c}$	$-\frac{e}{s_W} v C_{\varphi\ell,ij}^{(1)} \gamma^\mu P_L$
$\varphi^-(p^-) W^+ \bar{\ell}_i \ell_j$	$-\frac{e}{s_W} v C_{\varphi\ell,ij}^{(1)} P_L \gamma^\mu$

Table 2: Feynman rules for the relevant operators of the SMEFT for vanishing charged lepton masses. The tree-level results for $C_{\varphi\ell,ij}^{(3)}$ and X_{ij}^- are given in Eqs. (3.9) and (3.11).

3.1 Conventions

The SMEFT extends the SM Lagrangian $\mathcal{L}_{\text{SM}}^{(4)}$ by higher dimensional operators, which are invariant under the full SM gauge group. Up to the dimension 6 level we write

$$\mathcal{L}_{\text{SMEFT}} = \mathcal{L}_{\text{SM}}^{(4)} + C^{(5)} \mathcal{O}^{(5)} + \sum_k C_k^{(6)} \mathcal{O}_k^{(6)}, \quad (3.1)$$

where $\mathcal{O}^{(5)}$ is the dimension Weinberg operator

$$\mathcal{L}^{(5)} \equiv C_{ij}^{(5)} \mathcal{O}_{ij}^{(5)} + \text{h.c.} \equiv C_{ij}^{(5)} \left(\bar{L}_i^c \tilde{\Phi}^* \right) \left(\tilde{\Phi}^\dagger L_j \right) + \text{h.c.} . \quad (3.2)$$

We will only consider the subset of dimension-six operators that can, at $\mathcal{O}(v^2/M_R^2)$ and for vanishing charged lepton masses, lead to direct contributions to lepton flavour violating observables. These are

$$\begin{aligned} \sum_k C_k^{(6)} Q_k^{(6)} &= C_{\varphi\ell}^{(1)} \mathcal{O}_{\varphi\ell}^{(1)} + C_{\varphi\ell}^{(3)} \mathcal{O}_{\varphi\ell}^{(3)} + (C_{eW} \mathcal{O}_{eW} + C_{eB} \mathcal{O}_{eB} + \text{h.c.}) \\ &+ C_{\ell\ell} \mathcal{O}_{\ell\ell} + C_{\ell e} \mathcal{O}_{\ell e} + C_{\ell q}^{(1)} \mathcal{O}_{\ell q}^{(1)} + C_{\ell q}^{(3)} \mathcal{O}_{\ell q}^{(3)} + C_{\ell u} \mathcal{O}_{\ell u} + C_{\ell d} \mathcal{O}_{\ell d}, \end{aligned} \quad (3.3)$$

	L	e	Q	u	d	Φ
hypercharge Y	$-\frac{1}{2}$	-1	$\frac{1}{6}$	$\frac{2}{3}$	$-\frac{1}{3}$	$\frac{1}{2}$

Table 3: Hypercharges for the SM fermions and Higgs field.

which are defined as [91]

$$\begin{aligned}
\mathcal{O}_{\varphi\ell,ij}^{(1)} &= \left(\Phi^\dagger i\overleftrightarrow{D}_\mu \Phi\right) (\bar{L}_i \gamma^\mu L_j) , \\
\mathcal{O}_{\varphi\ell,ij}^{(3)} &= \left(\Phi^\dagger i\overleftrightarrow{D}_\mu^I \Phi\right) (\bar{L}_i \sigma^I \gamma^\mu L_j) , \\
\mathcal{O}_{eW,ij} &= (\bar{L}_i \sigma_{\mu\nu} e_j) \sigma^I \Phi W^{I\mu\nu} , \\
\mathcal{O}_{eB,ij} &= (\bar{L}_i \sigma_{\mu\nu} e_j) \Phi B^{\mu\nu} . \\
(\mathcal{O}_{\ell\ell})_{ij,kl} &= (\bar{L}_i \gamma_\mu L_j) (\bar{L}_k \gamma_\mu L_l) , \\
(\mathcal{O}_{\ell e})_{ij,kl} &= (\bar{L}_i \gamma_\mu L_j) (\bar{e}_k \gamma_\mu e_l) , \\
\left(\mathcal{O}_{\ell q}^{(1)}\right)_{ij,kl} &\equiv (\bar{L}_i \gamma_\mu L_j) (\bar{Q}_k \gamma^\mu Q_l) , \\
\left(\mathcal{O}_{\ell q}^{(3)}\right)_{ij,kl} &\equiv (\bar{L}_i \gamma_\mu \sigma^I L_j) (\bar{Q}_k \gamma^\mu \sigma^I Q_l) , \\
(\mathcal{O}_{\ell u})_{ij,kl} &\equiv (\bar{L}_i \gamma_\mu L_j) (\bar{u}_k \gamma^\mu u_l) , \\
(\mathcal{O}_{\ell d})_{ij,kl} &\equiv (\bar{L}_i \gamma^\mu L_j) (\bar{d}_k \gamma_\mu d_l) .
\end{aligned} \tag{3.4}$$

Note that in all operators involving $SU(2)_L$ doublets, the $SU(2)_L$ indices are contracted within the fermion bilinears. We follow the hypercharge conventions of Ref. [91], given in Table 3. The covariant derivative is defined in Eq. (2.25). Using the short-hand notation $\Phi^\dagger \overleftrightarrow{D}_\mu \Phi \equiv (D_\mu \Phi)^\dagger \Phi$, we define the Hermitian derivative terms

$$\Phi^\dagger i\overleftrightarrow{D}_\mu \Phi \equiv i\Phi^\dagger \left(D_\mu - \overleftrightarrow{D}_\mu\right) \Phi , \quad \Phi^\dagger i\overleftrightarrow{D}_\mu^I \Phi \equiv i\Phi^\dagger \left(\sigma^I D_\mu - \overleftrightarrow{D}_\mu \sigma^I\right) \Phi , \tag{3.5}$$

which enter the operators $\mathcal{O}_{\varphi\ell}^{(1)}$ and $\mathcal{O}_{\varphi\ell}^{(3)}$. The field strength tensors $W_{\mu\nu}^I \equiv \partial_\mu W_\nu^I - \partial_\nu W_\mu^I - g_2 \epsilon^{IJK} W_\mu^J W_\nu^K$ and $B_{\mu\nu} \equiv \partial_\mu B_\nu - \partial_\nu B_\mu$, are associated to the $SU(2)_L$ and $U(1)_Y$ gauge fields W^I and B , respectively. We follow the convention of summation over all flavour indices in the Lagrangian. For the operators involving four leptons, this means that we write the corresponding terms as follows

$$C\mathcal{O} = \sum_{i,j,k,l} C_{ij,kl} \mathcal{O}_{ij,kl}, \quad i, j, k, l \in \{e, \mu, \tau\} . \tag{3.6}$$

For operators whose fields are distinguishable, i.e. $\mathcal{O}_{\ell e}$, $\mathcal{O}_{\ell q}^{(1)}$, $\mathcal{O}_{\ell q}^{(3)}$, $\mathcal{O}_{\ell u}$, $\mathcal{O}_{\ell d}$, and that thus cannot be fierzed into themselves, this summation convention has no impact. However, for $\mathcal{O}_{\ell\ell}$, which is invariant under the exchange of the two fermion bilinears, this leads to a

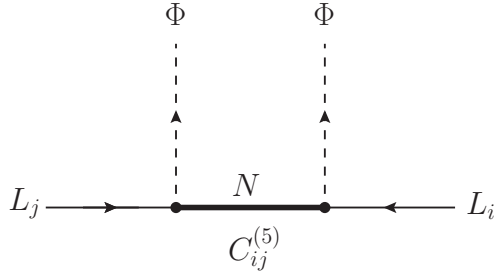


Figure 2: Feynman diagram in the type-I seesaw contributing to the Wilson coefficient of the Weinberg operator. In the inverse seesaw limit, the neutrino Yukawa matrices are chosen in such a way that this diagram vanishes and lepton number is conserved.

factor 2 at the amplitude level (the contraction of $SU(2)_L$ indices is taken into account):

$$\begin{aligned} & C_{ij,kl}^{\ell\ell} (\bar{L}_i^a \gamma_\mu L_j^a) (\bar{L}_k^b \gamma^\mu L_l^b) + C_{kl,ij}^{\ell\ell} (\bar{L}_k^a \gamma_\mu L_l^a) (\bar{L}_i^b \gamma^\mu L_j^b) \\ & + C_{kj,il}^{\ell\ell} (\bar{L}_k^a \gamma_\mu L_j^a) (\bar{L}_i^b \gamma^\mu L_l^b) + C_{il,kj}^{\ell\ell} (\bar{L}_i^a \gamma_\mu L_l^a) (\bar{L}_k^b \gamma^\mu L_j^b) \\ & \rightarrow 2 \left(C_{ij,kl}^{\ell\ell} (\bar{L}_i^a \gamma_\mu L_j^a) (\bar{L}_k^b \gamma^\mu L_l^b) + C_{ij,kl}^{\ell\ell} (\bar{L}_i^a \gamma_\mu L_j^b) (\bar{L}_k^b \gamma^\mu L_l^a) \right). \end{aligned} \quad (3.7)$$

Note that L on the left-handed side corresponds to a field, while on the right-handed side it denotes a spinor. a and b denote $SU(2)_L$ indices.

3.2 Tree Level Matching

The Feynman diagram in Figure 2 leads to the following Wilson coefficient of the Weinberg operator

$$C^{(5)} = \frac{1}{2} Y^{\nu*} M_R^{-1} Y^{\nu\dagger}. \quad (3.8)$$

After electroweak symmetry breaking, this can be expressed as $C^{(5)} = \frac{1}{v^2} M_D^* M_R^{-1} M_D^\dagger$, which features, by definition, the same combination of Dirac- and Majorana matrices as the active neutrino block of the neutrino mass matrix. In the inverse seesaw limit, this combination of matrices is set to zero.

At the dimension-6 level, the Wilson coefficients of the operators $\mathcal{O}_{\varphi\ell}^{(1)}$ and $\mathcal{O}_{\varphi\ell}^{(3)}$ receive tree-level contributions induced by the diagrams in Figure 3a:

$$C_{\varphi\ell,ij}^{(3)} = -C_{\varphi\ell,ij}^{(1)} = -\frac{1}{4} T_{ij}, \quad (3.9)$$

T_{ij} is defined in Eq. (2.17). The relation $C_{\varphi\ell}^{(3)} = -C_{\varphi\ell}^{(1)}$, which follows from the fact that only neutrino couplings, no charged lepton couplings, are modified, motivates a change of basis from $\{\mathcal{O}_{\varphi\ell}^{(1)}, \mathcal{O}_{\varphi\ell}^{(3)}\}$ to $\{\mathcal{O}^+, \mathcal{O}^-\}$,

$$\begin{aligned} \mathcal{O}_{ij}^+ &= \frac{1}{2} \left(\mathcal{O}_{\varphi\ell,ij}^{(3)} + \mathcal{O}_{\varphi\ell,ij}^{(1)} \right), & \mathcal{O}_{ij}^- &= \frac{1}{2} \left(\mathcal{O}_{\varphi\ell,ij}^{(3)} - \mathcal{O}_{\varphi\ell,ij}^{(1)} \right) \\ X_{ij}^+ &= C_{\varphi\ell,ij}^{(3)} + C_{\varphi\ell,ij}^{(1)}, & X_{ij}^- &= C_{\varphi\ell,ij}^{(3)} - C_{\varphi\ell,ij}^{(1)}, \end{aligned} \quad (3.10)$$

with

$$X_{ij}^+ = 0, \quad X_{ij}^- = -\frac{1}{2}T_{ij}. \quad (3.11)$$

The corresponding diagrams in the full and effective theory are shown in Figure 3a and Figure 3b, respectively.

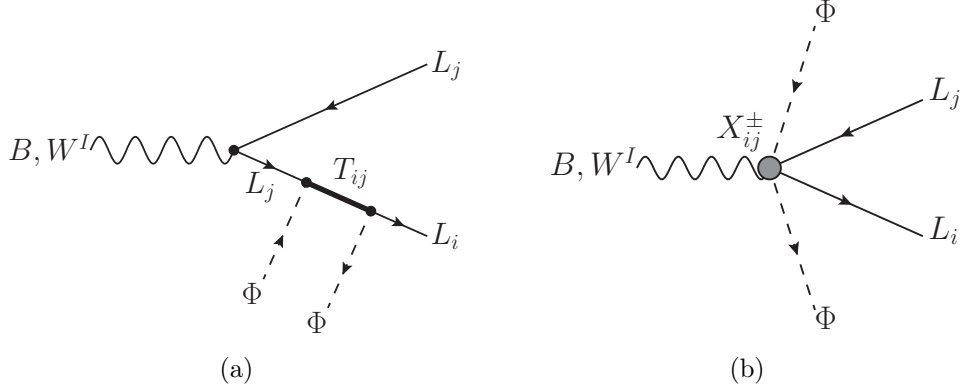


Figure 3: (a) Diagram giving rise to modifications of the lepton couplings to the $U(1)_Y$ and $SU(2)_L$ gauge bosons in the type-I seesaw. (b) Corresponding diagram in the effective theory.

3.3 One-Loop Matching

3.3.1 Modified Gauge-Boson Couplings ($\mathcal{O}_{\varphi\ell}^{(1)}$ and $\mathcal{O}_{\varphi\ell}^{(3)}$)

Note that since $X_{ij}^- \neq 0$ at tree-level, we will not calculate loop corrections to the corresponding operator, but rather focus on X_{ij}^+ , where finite corrections generate novel effects such as modified $Z\ell^+\ell^-$ couplings (after EW symmetry breaking). Indeed, at the one-loop level, the relation $C_{\varphi\ell,ij}^{(3)\alpha\beta} = -C_{\varphi\ell,ij}^{(1)}$ or, equivalently, $X^+ = 0$, is broken by the contributions of the diagrams shown in Figure 4. Performing an on-shell matching, we find

$$\begin{aligned} X_{ij}^+ &= \frac{1}{2304\pi^2} \sum_{a=1}^n Y_{ia}^\nu M_{R,a}^{-2} Y_{ja}^{\nu*} (g_1^2 + 17g_2^2) \left(11 + 6 \left(\frac{1}{\varepsilon} + \log \left(\frac{\mu^2}{M_{R,a}^2} \right) \right) \right) \\ &\quad - \frac{1}{32\pi^2} \sum_{a,b=1}^n Y_{ia}^\nu \left(\sum_{c=1}^3 Y_{ca}^{\nu*} Y_{cb}^\nu \right) Y_{jb}^{\nu*} \frac{1}{M_{R,a}^2 - M_{R,b}^2} \log \left(\frac{M_{R,a}^2}{M_{R,b}^2} \right) \\ &\quad - \frac{1}{128\pi^2} \sum_{a,b=1}^N Y_{ia}^\nu M_{R,a}^{-1} \left(\sum_{c=1}^3 Y_{ca}^\nu Y_{cb}^{\nu*} \right) M_{R,b}^{-1} Y_{jb}^{\nu*} \frac{M_{R,a}^2 + M_{R,b}^2}{M_{R,a}^2 - M_{R,b}^2} \log \left(\frac{M_{R,a}^2}{M_{R,b}^2} \right), \end{aligned} \quad (3.12)$$

where the $1/\varepsilon$ pole is cancelled by the renormalisation of the EFT operator, leading to the corresponding renormalisation group evolution (RGE) [92].

The third line of (3.12) originates from diagram given in Figure 4f, i.e. from penguins involving a combination of two $\Delta L = 2$ interactions. This term is only relevant in presence of large mass splitting between the sterile neutrinos, since it involves the same Yukawa

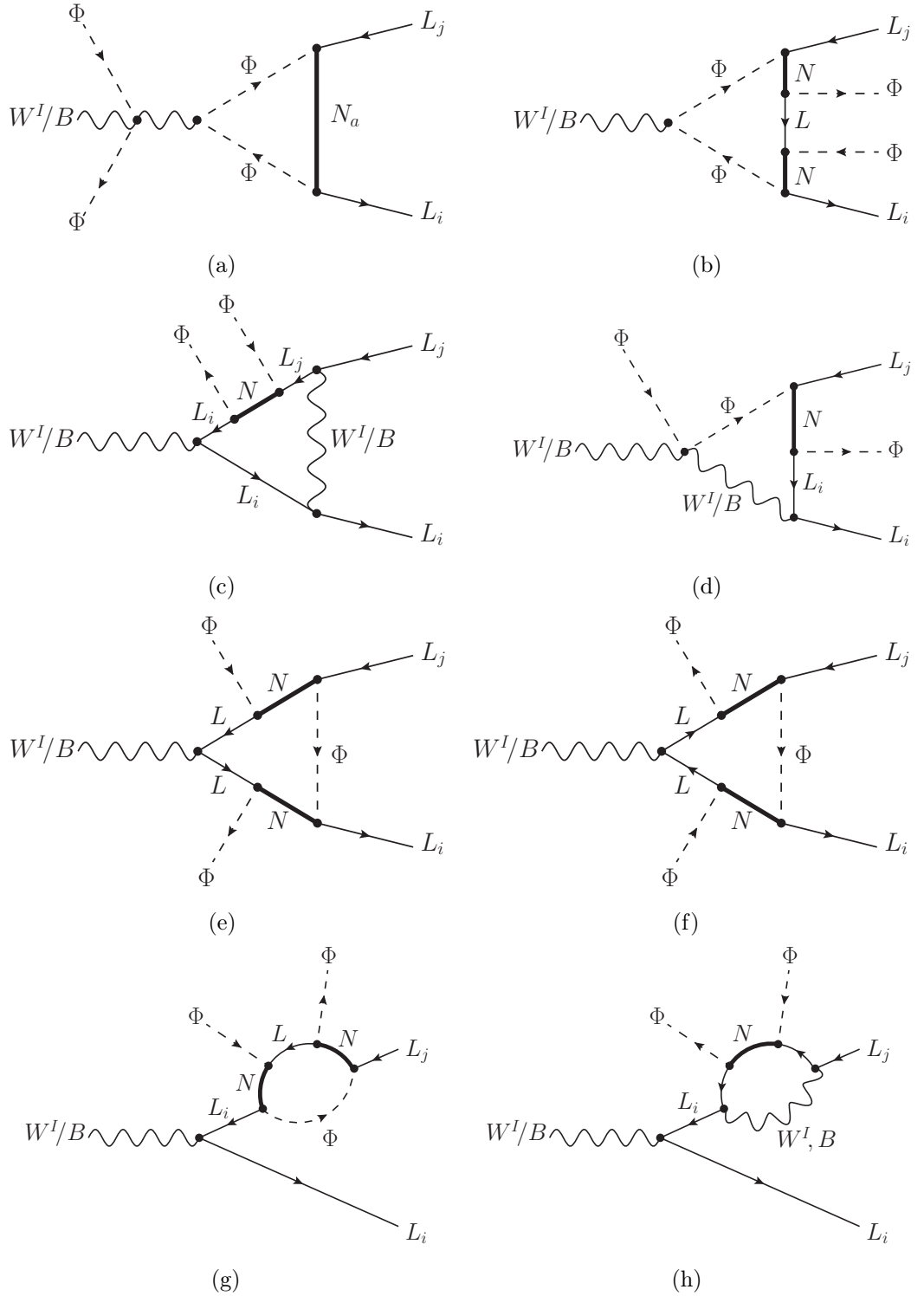


Figure 4: Diagrams contribution to the 1-loop matching onto $\mathcal{O}_{\varphi\ell}^{(1)}$ and $\mathcal{O}_{\varphi\ell}^{(3)}$ (see Figure 3b) or, equivalently, onto \mathcal{O}^+ and \mathcal{O}^- .

structure as the Wilson coefficient of the Weinberg operator and vanishes in the limit of degenerate heavy neutrino masses. See Appendices A and C.2 for a discussion of the identities we used for the derivation of this result.

3.3.2 Four-Lepton Operators ($\mathcal{O}_{\ell\ell}$ and $\mathcal{O}_{\ell e}$)

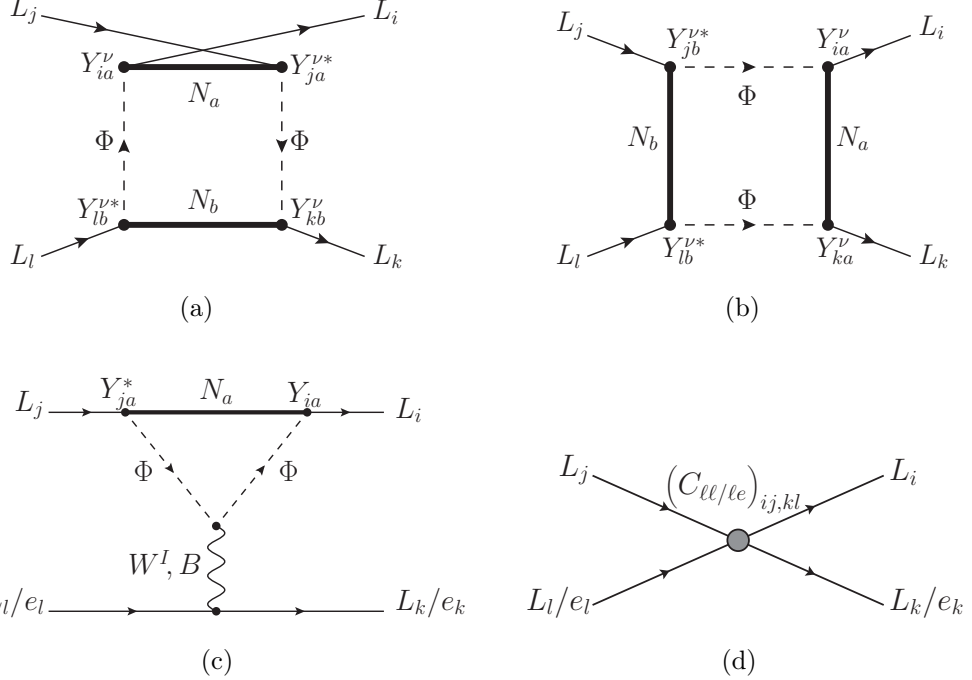


Figure 5: The double-Higgs boxes and the double-Higgs penguin are the only contributions to the loop-level matching onto $\mathcal{O}_{\ell\ell}$ and $\mathcal{O}_{\ell e}$.

The four-lepton operators $\mathcal{O}_{\ell\ell}$ and $\mathcal{O}_{\ell e}$ receive contributions from off-shell B and W penguins and Higgs-neutrino boxes (see Figure 5). The latter contribute only to $\mathcal{O}_{\ell\ell}$. We find the following (ξ -independent) Wilson coefficients:

$$(C_{\ell\ell})_{ij,kl} = \frac{g_1^2 + g_2^2}{4608\pi^2} \sum_{a=1}^n \left(Y_{ia}^{\nu} M_{R,a}^{-2} Y_{ja}^{\nu*} \delta_{kl} + Y_{ka}^{\nu} M_{R,a}^{-2} Y_{la}^{\nu*} \delta_{ij} \right) \left(11 + 6 \left(\frac{1}{\varepsilon} + \log \left(\frac{\mu^2}{M_{R,a}^2} \right) \right) \right) \\ + \frac{1}{128\pi^2} \sum_{a,b=1}^n Y_{ia}^{\nu} Y_{ja}^{\nu*} Y_{kb}^{\nu} Y_{lb}^{\nu*} \frac{1}{M_{R,a}^2 - M_{R,b}^2} \log \left(\frac{M_{R,a}^2}{M_{R,b}^2} \right) \\ + \frac{1}{128\pi^2} \sum_{a=1}^N \left(Y_{ia}^{\nu} M_{R,a}^{-1} Y_{ka}^{\nu} \right) \left(Y_{jb}^{\nu*} M_{R,b}^{-1} Y_{lb}^{\nu*} \right) \frac{M_{R,a}^2 + M_{R,b}^2}{M_{R,a}^2 - M_{R,b}^2} \log \left(\frac{M_{R,a}^2}{M_{R,b}^2} \right) \quad (3.13)$$

$$(C_{\ell e})_{ij,kl} = \frac{g_1^2}{1152\pi^2} \sum_{a=1}^n Y_{ia}^{\nu} M_{R,a}^{-2} Y_{ja}^{\nu*} \delta_{kl} \left(11 + 6 \left(\frac{1}{\varepsilon} + \log \left(\frac{\mu^2}{M_{R,a}^2} \right) \right) \right). \quad (3.14)$$

The third line of Eq. (3.13) corresponds to the contribution of the diagram in Figure 5b, which can only arise if Majorana particles are in the loop, since it features two lepton

number violating interactions. Given that we are imposing the inverse seesaw condition of Eq. (2.12), these diagrams only contribute in presence of sterile neutrino mass splitting.

3.3.3 Two-Lepton-Two-Quark Operators ($\mathcal{O}_{\ell q}^{(1)}$, $\mathcal{O}_{\ell q}^{(3)}$, $\mathcal{O}_{\ell u}$ and $\mathcal{O}_{\ell d}$)

Next we consider contributions to the two-lepton-two-quark operators $\mathcal{O}_{\ell q}^{(1)}$, $\mathcal{O}_{\ell q}^{(3)}$, $\mathcal{O}_{\ell u}$ and $\mathcal{O}_{\ell d}$, defined in Eq. (3.4), which receive contributions from W^I and B penguins similar to the ones shown in Figure 5c. Here we find the Wilson coefficients

$$C_{\ell q,ij}^{(1)} = -\frac{g_1^2}{6912\pi^2} \sum_{a=1}^n Y_{ia}^\nu M_{R,a}^{-2} Y_{ja}^{\nu*} \left(11 + 6 \left(\frac{1}{\varepsilon} + \log \left(\frac{\mu^2}{M_{R,a}^2} \right) \right) \right) \quad (3.15)$$

$$C_{\ell q,ij}^{(3)} = -\frac{g_2^2}{2304\pi^2} \sum_{a=1}^n Y_{ia}^\nu M_{R,a}^{-2} Y_{ja}^{\nu*} \left(11 + 6 \left(\frac{1}{\varepsilon} + \log \left(\frac{\mu^2}{M_{R,a}^2} \right) \right) \right) \quad (3.16)$$

$$C_{\ell u,ij}^{VLR} = -\frac{g_1^2}{1728\pi^2} \sum_{a=1}^n Y_{ia}^\nu M_{R,a}^{-2} Y_{ja}^{\nu*} \left(11 + 6 \left(\frac{1}{\varepsilon} + \log \left(\frac{\mu^2}{M_{R,a}^2} \right) \right) \right) \quad (3.17)$$

$$C_{\ell d,ij}^{VLR} = -\frac{g_1^2}{3456\pi^2} \sum_{a=1}^n Y_{ia}^\nu M_{R,a}^{-2} Y_{ja}^{\nu*} \left(11 + 6 \left(\frac{1}{\varepsilon} + \log \left(\frac{\mu^2}{M_{R,a}^2} \right) \right) \right). \quad (3.18)$$

Note that the box contributions vanish in the limit of zero quark Yukawa couplings. Only the box involving the top quark could be sizeable, which, however, is not relevant for charged lepton flavour violating processes, such as $\mu \rightarrow e$ conversion in nuclei.

3.3.4 Magnetic Operators (\mathcal{O}_{eW} and \mathcal{O}_{eB})

The diagrams contributing to the matching onto the magnetic operators are shown in Figure 6. These result in

$$C_{eW,ij} = -\frac{5g_2}{384\pi^2} T_{ij} Y_j^\ell, \quad (3.19)$$

$$C_{eB,ij} = -\frac{g_1}{384\pi^2} T_{ij} Y_j^\ell, \quad (3.20)$$

where Y_j^ℓ is the Yukawa coupling of the charged lepton ℓ_j . These matching conditions agree with the results in Ref. [72]. Note the absence of logarithms, which can be explained by the fact that, in the lepton number conserving limit, the type-I seesaw introduces purely left-handed, i.e. chirality conserving, new physics, resulting in the absence of operator mixing in the EFT at the one-loop level.

4 Observables

In the last section we calculated the matching of the type-I seesaw onto the SMEFT at the scale M_R . However, these results are not sufficient for a phenomenological analysis of charged lepton flavour violating observables. For this, the running from M_R to the EW scale, the matching at this scale onto the Low-Energy Effective Field Theory (LEFT) [93], as well as the RGE from the weak scale to the charged lepton scale [94, 95] and the evaluation

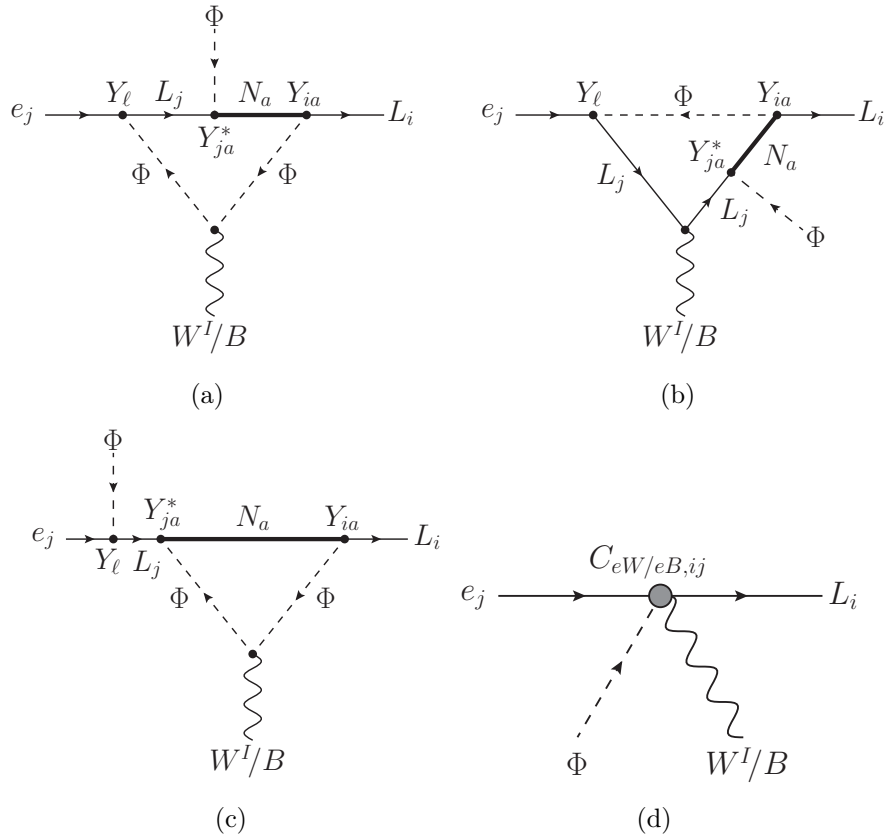


Figure 6: (a-c) Diagrams contributing to the matching onto the magnetic operators \mathcal{O}_{eW} and \mathcal{O}_{eB} . (d) Diagram in the effective theory originating from the magnetic operators.

of the matrix elements at the tau or muon scale would be required. As these results are not fully available, in particular, because even the calculation of 2-loop effects would be necessary for a consistent treatment, we naively calculate in this section the relevant diagrams without scale separation (i.e. without resumming the logarithms). Note that these formulae nonetheless include the (potential) leading logarithm as well as the finite scheme independent terms, which correspond to the sum of any hard and soft contributions to the amplitudes. We will then use these results in our phenomenological analysis in Section 5.

4.1 Lepton Flavour Universality Tests

The $W\ell\nu$ couplings, which are modified at tree-level by the neutrino mixing, lead to effects in processes such as $\ell \rightarrow \ell'\nu\nu$ (see Figure 7), $\tau \rightarrow \pi\nu$, $\pi \rightarrow \ell\bar{\nu}$, $\tau \rightarrow K\nu$ or $K \rightarrow \ell\bar{\nu}$. For these decays, LFU ratios can be formed, which we compare to the HFLAV fit results [96, 97] for the coupling fractions $(g_i/g_j)_\tau$, which are obtained using pure leptonic processes, and

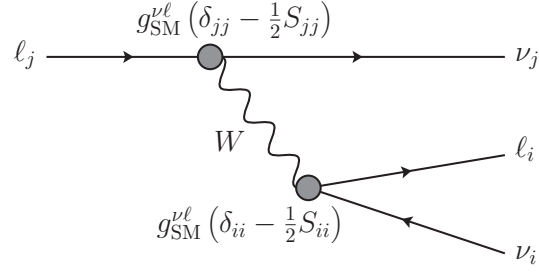


Figure 7: Tree-level diagrams generating $\ell \rightarrow \ell' \nu \nu$, in the type-I seesaw. $g_{\text{SM}}^{\nu \ell}$ is the SM $W \ell \nu$ coupling defined in Eq. (2.28) and S_{ii} the new physics modification of Eq. (2.16).

$(g_i/g_j)_P$, $P \in \{\pi, K\}$, which are defined as [96, 97]

$$\left| \frac{g_\tau}{g_\mu} \right|_P^2 = \frac{\text{Br}(\tau \rightarrow P \nu_\tau)}{\text{Br}(P \rightarrow \mu \bar{\nu}_\mu)} \frac{\tau_P}{\tau_\tau} \frac{2m_P m_\mu^2}{m_\tau^3} \left(\frac{1 - m_\mu^2/m_P^2}{1 - m_P^2/m_\tau^2} \right)^2 \frac{1}{1 + \delta R_{\tau/P}}, \quad (4.1)$$

where $\delta R_{\tau/P}$ accounts for the radiative corrections to $\Gamma(\tau \rightarrow P \nu_\tau)/\Gamma(P \rightarrow \mu \bar{\nu}_\mu)$, $P \in \{\pi, K\}$, which have been estimated as [98–102]

$$\delta R_{\tau/\pi} = (0.16 \pm 0.14)\%, \quad \delta R_{\tau/K} = (0.90 \pm 0.22)\%. \quad (4.2)$$

We identify the new physics amplitude fractions directly with the current HFLAV fit results [96, 97] for the coupling fractions g_i/g_j , $i, j \in \{e, \mu, \tau\}$.

$$\begin{aligned} \frac{\mathcal{M}(\tau \rightarrow e \bar{\nu} \nu)}{\mathcal{M}(\mu \rightarrow e \bar{\nu} \nu)} &\simeq 1 - \frac{1}{2} (S_{\tau\tau} - S_{\mu\mu}) \equiv \left| \frac{g_\tau}{g_\mu} \right|_\tau = 1.0009(14) \\ \frac{\mathcal{M}(\tau \rightarrow \mu \bar{\nu} \nu)}{\mathcal{M}(\mu \rightarrow e \bar{\nu} \nu)} &\simeq 1 - \frac{1}{2} (S_{\tau\tau} - S_{ee}) \equiv \left| \frac{g_\tau}{g_e} \right|_\tau = 1.0027(14) \\ \frac{\mathcal{M}(\tau \rightarrow \mu \bar{\nu} \nu)}{\mathcal{M}(\tau \rightarrow e \bar{\nu} \nu)} &\simeq 1 - \frac{1}{2} (S_{\mu\mu} - S_{ee}) \equiv \left| \frac{g_\mu}{g_e} \right|_\tau = 1.0019(14) \\ \frac{\mathcal{M}(\tau \rightarrow K \nu_\tau)}{\mathcal{M}(K \rightarrow \mu \bar{\nu}_\mu)} &\simeq 1 - \frac{1}{2} (S_{\tau\tau} - S_{\mu\mu}) \equiv \left| \frac{g_\tau}{g_\mu} \right|_K = 0.9855(75) \\ \frac{\mathcal{M}(\tau \rightarrow \pi \nu_\tau)}{\mathcal{M}(\pi \rightarrow \mu \bar{\nu}_\mu)} &= 1 - \frac{1}{2} (S_{\tau\tau} - S_{\mu\mu}) \equiv \left| \frac{g_\tau}{g_\mu} \right|_\pi = 0.9959(38) \end{aligned} \quad (4.3)$$

The HFLAV fit results come with the correlation matrix [96, 97]

$$\begin{array}{c}
\left| \frac{g_\tau}{g_\mu} \right|_\tau \quad \left| \frac{g_\tau}{g_e} \right|_\tau \quad \left| \frac{g_\mu}{g_e} \right|_\tau \quad \left| \frac{g_\tau}{g_\mu} \right|_\pi \quad \left| \frac{g_\tau}{g_\mu} \right|_K \\
\left(\begin{array}{ccccc} 1 & 0.51 & -0.49 & 2 & 0.16 \\ 0.51 & 1 & 0.49 & 0.18 & 0.11 \\ -0.49 & 0.49 & 1 & 0.01 & -0.01 \\ 0.16 & 0.18 & 0.01 & 1 & 0.07 \\ 0.12 & 0.11 & -0.01 & 0.07 & 1 \end{array} \right) \quad \left| g_\tau/g_\mu \right|_\tau \\
\left| g_\tau/g_e \right|_\tau \\
\left| g_\mu/g_e \right|_\tau \\
\left| g_\tau/g_\mu \right|_\pi \\
\left| g_\tau/g_\mu \right|_K
\end{array}$$

Belle II, which will produce approximately ten times more tauons than Belle or BaBar, is expected to improve the measurements of $\tau \rightarrow \mu\nu\bar{\nu}$ and $\tau \rightarrow e\nu\bar{\nu}$ [103].

Further LFU ratios that are relevant in this context are [102]

$$\left| \frac{g_\mu}{g_e} \right|_{P \rightarrow e/\mu}^2 = \frac{\text{Br}(P^- \rightarrow \mu\bar{\nu}_\mu(\gamma))}{\text{Br}(P^- \rightarrow e\bar{\nu}_e(\gamma))} \frac{m_e^2}{m_\mu^2} \left(\frac{1 - m_e^2/m_P^2}{1 - m_\mu^2/m_P^2} \right)^2 (1 + \delta R_{P \rightarrow e/\mu}), \quad (4.4)$$

where $\delta R_{P \rightarrow e/\mu}$ denotes the radiative corrections, including a summation of the leading QED logarithms $\alpha^n \log(m_\mu/m_e)$ [101, 104], and a two-loop calculation of $\mathcal{O}(e^2 p^4)$ effects within chiral perturbation theory [105]. Comparing the SM predictions [105] with the experimental results [106, 107] for $K \rightarrow e/\nu$, for $\pi \rightarrow e/\nu$, one obtains [102]

$$\frac{\mathcal{M}(K \rightarrow \mu\nu)}{\mathcal{M}(K \rightarrow e\nu)} \simeq 1 - \frac{1}{2} (S_{\mu\mu} - S_{ee}) \equiv \left| \frac{g_\mu}{g_e} \right|_{K \rightarrow e/\mu} = 0.9978(20). \quad (4.5)$$

This measurement will also be performed by J-PARC E36 [108]. Comparing the SM predictions [105] with the experimental results for $\pi \rightarrow e/\nu$ [109], one finds [102]

$$\frac{\mathcal{M}(\pi \rightarrow \mu\nu)}{\mathcal{M}(\pi \rightarrow e\nu)} \simeq 1 - \frac{1}{2} (S_{\mu\mu} - S_{ee}) \equiv \left| \frac{g_\mu}{g_e} \right|_{\pi \rightarrow e/\mu} = 1.0010(09). \quad (4.6)$$

The PEN experiment expects to improve the sensitivity to $\pi \rightarrow \mu\nu/\pi \rightarrow e\nu$ by more than a factor three [110].

Decays of the form $K \rightarrow \pi\ell\bar{\nu}_\ell$ [111] are not helicity suppressed and are used for the determination of the Cabibbo angle. Comparing the values for the CKM element V_{us} from $K \rightarrow \pi\mu\bar{\nu}_\mu$ with the V_{us} from $K \rightarrow \pi e\bar{\nu}_e$ allows for a further test of LFU: [102, 111, 112],

$$\frac{\mathcal{M}(K \rightarrow \pi\mu\bar{\nu})}{\mathcal{M}(K \rightarrow \pi e\bar{\nu})} \simeq 1 - \frac{1}{2} (S_{\mu\mu} - S_{ee}) \equiv \left| \frac{g_\mu}{g_e} \right|_{K \rightarrow \pi(\mu/e)} = 1.0010(25). \quad (4.7)$$

²The HFLAV collaboration reports -0.50 due to numerical limitations, however, we use -0.49 in order to have a positive semi-definite correlation matrix.

LFU can also be tested directly in leptonic W boson decays, however, these channels are statistically limited [102, 113–115] and the resulting bounds are not competitive with the ones from tau, kaon and pion decays. However, future e^+e^- colliders such as the International Linear Collider (ILC) [116], the Compact Linear Collider (CLIC) [117] or the Future Circular Collider (FCC-ee) [118, 119] could improve these bounds.

4.2 $Z \rightarrow \nu\nu$

Also $Z \rightarrow \nu_i \bar{\nu}_j$ receives corrections at tree-level in presence of neutrino mixing. The corresponding amplitude

$$\mathcal{M}(Z \rightarrow \nu_j \bar{\nu}_i) = -\frac{e}{2s_W c_W} (\delta_{ij} - S_{ij}) \bar{\nu}_i \gamma^\mu P_L \nu_j Z_\mu \quad (4.8)$$

affects the effective number of light neutrino species [120, 121]

$$N_\nu^{\text{eff.}} = 2.9840 \pm 0.0082. \quad (4.9)$$

Considering Eq. (4.8), we can approximate $N_\nu \sim 3 - 2 \sum_i S_{ii}$ in the type-I seesaw model if we neglect effects that do not interfere with the SM contribution.

4.3 $Z \rightarrow \ell\ell'$

Z decays into charged leptons $Z \rightarrow \bar{\ell}_i \ell_j$ only receive corrections at loop-level in the type-I seesaw model. Expanding the diagrams shown in Figure 8 in v^2/M_R^2 , we find

$$\mathcal{M}(Z \rightarrow \bar{\ell}_i \ell_j) = -\frac{e^3}{16\pi^2 c_W s_W^3} \bar{\mathcal{Z}}_{ij}^{\text{VL}}(q_Z^2) \bar{\ell}_i(p_i) \not{Z} P_L \ell_j(p_j), \quad (4.10)$$

with

$$\begin{aligned} \bar{\mathcal{Z}}_{ij}^{\text{VL}}(M_Z^2) &= \sum_{a=1}^n M_{D,ia} M_{R,a}^{-2} M_{D,ja}^* \left(f(c_W^2) + g(c_W^2) \log \left(\frac{M_W^2}{M_{R,a}^2} \right) \right) \\ &\quad + \frac{1}{4M_W^2} \sum_{a,b=1}^n M_{D,ia} \left(\sum_{c=1}^3 M_{D,ca}^* M_{D,cb} \right) M_{D,jb} h(M_{R,a}^2, M_{R,b}^2) \\ &\quad + \frac{1}{8M_W^2} \sum_{a,b=1}^n M_{D,ia} M_{R,a}^{-1} \left(\sum_{k=1}^3 M_{D,ka} M_{D,kb}^* \right) M_{R,b}^{-1} M_{D,jb}^* k(M_{R,a}^2, M_{R,b}^2), \end{aligned} \quad (4.11)$$

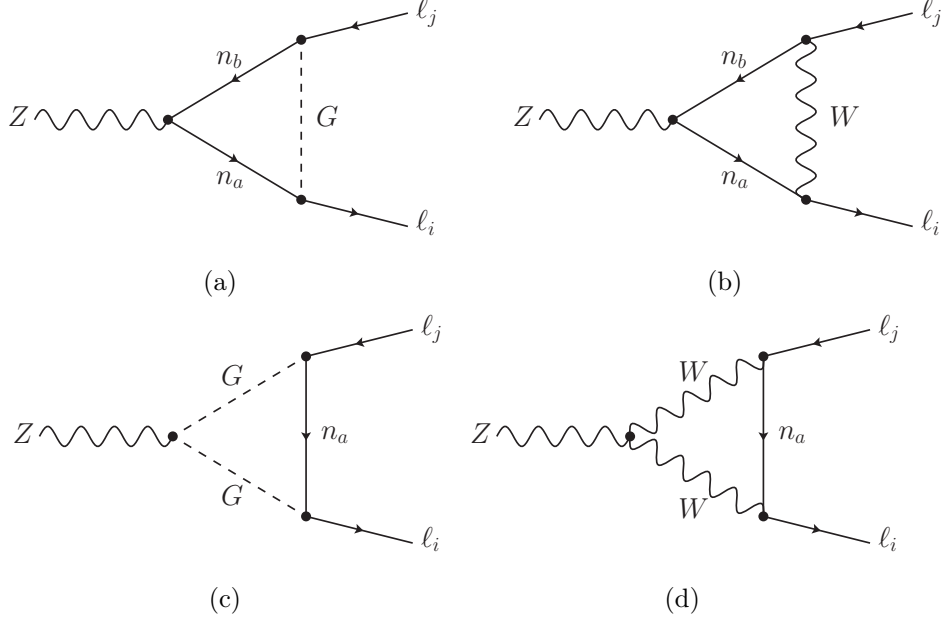


Figure 8: Diagrams contributing to the $Z\ell\ell'$ coupling at the one-loop level. Here n_a and n_b correspond to neutrino mass eigenstates. The formulae in the main text are obtained by expanding the amplitudes corresponding to these diagrams in v^2/M_R^2 , i.e. they are given in the seesaw limit. The unexpanded results are given in Appendix C.

where

$$\begin{aligned} f(x) = & \frac{13}{6} + \frac{5}{144x} (1 - 2x) + \frac{11}{12}x - x^2 - \frac{1}{3}\pi^2(1+x)^2 \\ & + \frac{1}{2}\log(x) \left(3 + 2x + (1+x)^2\log(x) \right) \\ & + (1+x)^2 \text{Li}_2(1+x) + i\pi \left(\frac{3}{2} + x + (1+x)^2\log(x) \right) \\ & - 4x^2(2+x)\arctan^2((4x-1)^{-1/2}) \\ & + \sqrt{4x-1} \left(-\frac{1}{12x} - \frac{3}{2} + \frac{7}{3}x + 2x^2 \right) \arctan((4x-1)^{-1/2}), \end{aligned} \quad (4.12)$$

$$g(x) = -\frac{2}{3} \left(1 + \frac{1}{16x} \right) \quad (4.13)$$

$$h(M_{R,a}^2, M_{R,b}^2) = \frac{1}{M_{R,a}^2 - M_{R,b}^2} \log \left(\frac{M_{R,a}^2}{M_{R,b}^2} \right), \quad (4.14)$$

$$k(M_{R,a}^2, M_{R,b}^2) = \frac{1}{2} \frac{M_{R,a}^2 + M_{R,b}^2}{M_{R,a}^2 - M_{R,b}^2} \log \left(\frac{M_{R,a}^2}{M_{R,b}^2} \right). \quad (4.15)$$

Note that while the first two terms of Eq. (4.11) agree with Ref. [69], the third term, which is only present for Majorana neutrinos, was not included there.

$\text{Br}[Z \rightarrow e^\pm \mu^\mp]$	$< 7.5 \times 10^{-7}$ (95% CL)	ATLAS: [122]
$\text{Br}[Z \rightarrow e^\pm \tau^\mp]$	$< 5.0 \times 10^{-6}$ (95% CL)	ATLAS: [123]
$\text{Br}[Z \rightarrow \mu^\pm \tau^\mp]$	$< 6.5 \times 10^{-6}$ (95% CL)	ATLAS: [123]

Table 4: Bounds on $\text{Br}(Z \rightarrow \ell\ell')$.

$\text{Br}[Z \rightarrow e^\pm \mu^\mp]$	$10^{-7} - 10^{-8}$	FCC-ee: [119, 124]
$\text{Br}[Z \rightarrow e^\pm \mu^\mp]$	3.0×10^{-9}	CEPC: [125]
$\text{Br}[Z \rightarrow e^\pm \tau^\mp]$	10^{-9}	FCC-ee: [119, 124]
$\text{Br}[Z \rightarrow e^\pm \tau^\mp]$	2.0×10^{-8}	CEPC: [125]
$\text{Br}[Z \rightarrow \mu^\pm \tau^\mp]$	10^{-9}	FCC-ee: [119, 124]
$\text{Br}[Z \rightarrow \mu^\pm \tau^\mp]$	2.0×10^{-8}	CEPC: [125]

Table 5: Future sensitivities to $\text{Br}(Z \rightarrow \ell\ell')$

The branching ratio of $Z \rightarrow \ell_i \ell_j$, for $i \neq j$ is given by

$$\begin{aligned} \text{Br}(Z \rightarrow \ell_i^\pm \ell_j^\mp) &\equiv \text{Br}(Z \rightarrow \ell_i^+ \ell_j^-) + \text{Br}(Z \rightarrow \ell_i^- \ell_j^+) \\ &= \frac{1}{24\pi} \frac{M_Z}{\Gamma_Z} \left(\frac{e^3}{16\pi^2 c_W s_W^3} \right)^2 \left(|\overline{\mathcal{Z}}_{ij}(M_Z^2)|^2 + |\overline{\mathcal{Z}}_{ji}(M_Z^2)|^2 \right) \end{aligned} \quad (4.16)$$

We compare this result with the ATLAS and LEP measurements given in Table 4 and to the future sensitivities in Table 5.

4.4 $\ell \rightarrow \ell' \gamma$

Defining the effective Lagrangian in broken $SU(2)_L$,

$$\mathcal{L}_{\text{eff}} = \mathcal{A}_{ij}^M \bar{\ell}_i \sigma_{\mu\nu} P_R \ell_j F^{\mu\nu} + \text{h.c.}, \quad (4.17)$$

where $F^{\mu\nu} = \partial^\mu A^\nu - \partial^\nu A^\mu$ is the electromagnetic field strength tensor, we find

$$\mathcal{A}_{ij}^M = \frac{e^3 m_{\ell_j}}{128\pi^2 s_W^2 M_W^2} \sum_{a=4}^n U_{ia} U_{ja}^* \approx \frac{e^3 m_{\ell_j}}{128\pi^2 s_W^2 M_W^2} S_{ij}, \quad (4.18)$$

in the seesaw limit, $v \ll M_R$, with S_{ij} as defined in Eq. (2.16). The absence of a logarithm involving a sterile neutrino mass can be understood as a consequence of the purely left-handed new physics effect in this model. This avoids chiral enhancement, and implies that the anomalous magnetic moments do not yield relevant bounds, and that electric dipole moments are absent [126].

4.5 $\ell \rightarrow 3\ell'$ and $\ell \rightarrow \ell' \ell'' \ell'''$

Processes of the type $\ell \rightarrow 3\ell'$ receive contributions from photon and Z penguins, as well as from box diagrams. In the seesaw limit, the sum of the off-shell photon penguins, the

$\text{Br} [\mu \rightarrow e\gamma]$	$< 4.2 \times 10^{-13}$	MEG: [127]
$\text{Br} [\tau \rightarrow e\gamma]$	$< 3.3 \times 10^{-8}$	BaBar: [128]
$\text{Br} [\tau \rightarrow \mu\gamma]$	$< 4.2 \times 10^{-8}$	Belle: [129]

Table 6: Current experimental upper bounds on $\text{Br}(\ell \rightarrow \ell'\gamma)$.

$\text{Br} [\mu \rightarrow e\gamma]$	6×10^{-14}	MEG II: [130]
$\text{Br} [\tau \rightarrow \mu\gamma]$	2.7×10^{-8}	Belle II: [103]

Table 7: Future sensitivities to $\text{Br}(\ell \rightarrow \ell'\gamma)$.

off-shell Z penguins and boxes, leads to

$$\begin{aligned}
\text{Br} [\tau^\mp \rightarrow e^\mp \mu^\pm \mu^\mp] &= -\frac{e^2 m_\tau^3}{48 \pi^3 \Gamma_\tau} \left(|\mathcal{A}_{e\tau}^M|^2 + |\mathcal{A}_{\tau e}^M|^2 \right) \left(3 + \log \left(\frac{m_\mu^2}{m_\tau^2} \right) \right) \\
&\quad + \frac{m_\tau^5}{1536 \pi^3 \Gamma_\tau} \left(|\mathcal{F}_{e\tau, \mu\mu}^{\text{VLL}} + \mathcal{F}_{\mu\tau, e\mu}^{\text{VLL}}|^2 + |\mathcal{F}_{e\tau, \mu\mu}^{\text{VLR}} + \mathcal{F}_{\mu\tau, e\mu}^{\text{VLR}}|^2 \right) \\
&\quad + \frac{e m_\tau^4}{192 \pi^3 \Gamma_\tau} \left(\text{Re} \left[\mathcal{A}_{e\tau}^{M*} \left(\mathcal{F}_{e\tau, \mu\mu}^{\text{VLL}} + \mathcal{F}_{\mu\tau, e\mu}^{\text{VLL}} + \mathcal{F}_{e\tau, \mu\mu}^{\text{VLR}} + \mathcal{F}_{\mu\tau, e\mu}^{\text{VLR}} \right) \right] \right), \\
\text{Br} [\tau \rightarrow 3\mu] &= -\frac{e^2 m_\tau^3}{192 \pi^3 \Gamma_\tau} \left(|\mathcal{A}_{\mu\tau}^M|^2 + |\mathcal{A}_{\tau\mu}^M|^2 \right) \left(11 + 4 \log \left(\frac{m_\mu^2}{m_\tau^2} \right) \right) \\
&\quad + \frac{m_\tau^5}{1536 \pi^3 \Gamma_\tau} \left(2 |\mathcal{F}_{\mu\tau, \mu\mu}^{\text{VLL}}|^2 + |\mathcal{F}_{\mu\tau, \mu\mu}^{\text{VLR}}|^2 \right) \\
&\quad + \frac{e m_\tau^4}{192 \pi^3 \Gamma_\tau} \left(\text{Re} \left[\mathcal{A}_{\mu\tau}^{M*} (2 \mathcal{F}_{\mu\tau, \mu\mu}^{\text{VLL}} + \mathcal{F}_{\mu\tau, \mu\mu}^{\text{VLR}}) \right] \right), \\
\text{Br} [\tau^\mp \rightarrow \mu^\mp e^\pm \mu^\mp] &= \frac{m_\tau^5}{1536 \pi^3 \Gamma_\tau} \left(2 |\mathcal{F}_{\mu\tau, \mu e}^{\text{VLL}}|^2 + |\mathcal{F}_{\mu\tau, \mu e}^{\text{VLR}}|^2 \right), \tag{4.19}
\end{aligned}$$

$\text{Br} [\mu^- \rightarrow e^- e^+ e^-]$, 90% C.L.	$\leq 1.0 \times 10^{-12}$	SINDRUM: [131]
$\text{Br} [\tau^- \rightarrow e^- e^+ e^-]$, 90% C.L.	$\leq 2.7 \times 10^{-8}$	Belle: [132]
$\text{Br} [\tau^- \rightarrow e^- \mu^+ \mu^-]$, 90% C.L.	$\leq 2.7 \times 10^{-8}$	Belle: [132]
$\text{Br} [\tau^- \rightarrow \mu^- e^+ \mu^-]$, 90% C.L.	$\leq 1.7 \times 10^{-8}$	Belle: [132]
$\text{Br} [\tau^- \rightarrow \mu^- e^+ e^-]$, 90% C.L.	$\leq 1.8 \times 10^{-8}$	Belle: [132]
$\text{Br} [\tau^- \rightarrow e^- \mu^+ e^-]$, 90% C.L.	$\leq 1.5 \times 10^{-8}$	Belle: [132]
$\text{Br} [\tau^- \rightarrow \mu^- \mu^+ \mu^-]$, 90% C.L.	$\leq 2.1 \times 10^{-8}$	Belle: [132]

Table 8: Current upper bounds on lepton flavour violating decays of the type $\ell \rightarrow 3\ell'$.

with

$$\begin{aligned} \mathcal{F}_{ij,kl}^{VLL} = & \frac{e^4}{384\pi^2 s_W^4 M_W^2} \left\{ \sum_{a=1}^n M_{D,ia} M_{R,a}^{-2} M_{D,ja}^* \delta_{kl} \left(9 - 37s_W^2 + (-9 + 16s_W^2) \log \left(\frac{M_{R,a}^2}{M_W^2} \right) \right) \right. \\ & + \frac{3}{M_W^2} \sum_{a,b=1}^n \left((-1 + 2s_W^2) \left(M_{D,ia} \left(\sum_{c=1}^3 M_{D,ca}^* M_{D,cb} \right) M_{D,jb}^* \right) \delta_{kl} \right. \\ & \quad \left. \left. + \frac{1}{2} (M_{D,ia} M_{D,ja}^*) (M_{D,kb} M_{D,lb}^*) \right) h(M_{R,a}^2, M_{R,b}^2) \right. \\ & + \frac{3}{2M_W^2} \sum_{a,b=1}^n \left((-1 + 2s_W^2) \left(M_{D,ia} \left(\sum_{c=1}^3 M_{D,ca}^* M_{D,cb} \right) M_{D,jb}^* \right) \delta_{kl} \right. \\ & \quad \left. \left. + 2 (M_{D,ia} M_{D,ja}^*) (M_{D,kb} M_{D,lb}^*) \right) k(M_{R,a}^2, M_{R,b}^2) \right\}, \end{aligned} \quad (4.20)$$

$$\begin{aligned} \mathcal{F}_{ij,kl}^{VLR} = & \frac{e^4}{384\pi^2 s_W^2 M_W^2} \left\{ \sum_{a=1}^n M_{D,ia} M_{R,a}^{-2} M_{D,ja}^* \delta_{kl} \left(-37 + 16 \log \left(\frac{M_{R,a}^2}{M_W^2} \right) \right) \right. \\ & + \frac{6}{M_W^2} \sum_{a,b=1}^n \left(M_{D,ia} \left(\sum_{c=1}^3 M_{D,ca}^* M_{D,cb} \right) M_{D,jb}^* \right) \delta_{kl} h(M_{R,a}^2, M_{R,b}^2) \left. \right\}, \end{aligned} \quad (4.21)$$

with the functions h and k given in Eq. (4.15) and Eq. (4.14), respectively. The corresponding formula for $\text{Br} [\tau \rightarrow 3e]$ and $\text{Br} [\mu \rightarrow 3e]$ can be obtained by the appropriate replacement of flavour indices.

4.6 $\mu \rightarrow e$ Conversion in Nuclei

Next we consider $\mu \rightarrow e$ conversion in nuclei and define

$$\mathcal{L}_{\text{eff}} = \sum_{q=u,d} (\mathcal{F}_{e\mu,qq}^{LL} \mathcal{O}_{e\mu,qq}^{LL} + \mathcal{F}_{e\mu,qq}^{LR} \mathcal{O}_{e\mu,qq}^{LR}) + (L \leftrightarrow R) + \text{h.c.}, \quad (4.22)$$

$\text{Br} [\mu \rightarrow 3e]$	10^{-15}	Mu3e, phase I: [133, 134]
$\text{Br} [\mu \rightarrow 3e]$	10^{-16}	Mu3e, phase II: [133, 134]
$\text{Br} [\tau \rightarrow 3e]$	10^{-9}	Belle-II: [103]
$\text{Br} [\tau \rightarrow 3\mu]$	$\mathcal{O}(10^{-9})$	CMS, ATLAS, LHCb at HL-LHC [135]
$\text{Br} [\tau \rightarrow 3\mu]$	3.3×10^{-10}	Belle-II: [103]

Table 9: Future sensitivities to $\text{Br}(\ell \rightarrow 3\ell')$.

with

$$\begin{aligned}\mathcal{O}_{ij,qq}^{\text{VLL}} &= (\bar{\ell}_i \gamma_\mu P_L \ell_j) (\bar{q} \gamma_\mu P_L q), \\ \mathcal{O}_{ij,qq}^{\text{VLR}} &= (\bar{\ell}_i \gamma_\mu P_L \ell_j) (\bar{q} \gamma_\mu P_R q).\end{aligned}\quad (4.23)$$

This process receives contributions from photon and Z penguins, as well as from box diagrams, resulting in

$$\begin{aligned}\mathcal{F}_{ij,uu}^{\text{VLL}} &= \frac{e^4}{384\pi^2 s_W^4 M_W^2} \left\{ \sum_{a=1}^n M_{D,ia} M_{R,a}^{-2} M_{D,ja}^* \frac{1}{3} \left(27 + 74s_W^2 + (27 - 32s_W^2) \log \left(\frac{M_{R,a}^2}{M_W^2} \right) \right) \right. \\ &\quad \left. + \frac{3 - 4s_W^2}{M_W^2} \sum_{a,b=1}^n M_{D,ia} \left(\sum_{c=1}^3 M_{D,ca}^* M_{D,cb} \right) M_{D,jb}^* h(M_{R,a}^2, M_{R,b}^2) \right\} \\ \mathcal{F}_{ij,uu}^{\text{VLR}} &= \frac{e^4}{384\pi^2 s_W^2 M_W^2} \left\{ \sum_{a=1}^n M_{D,ia} M_{R,a}^{-2} M_{D,ja}^* \frac{2}{3} \left(37 - 16 \log \left(\frac{M_{R,a}^2}{M_W^2} \right) \right) \right. \\ &\quad \left. - \frac{4}{M_W^2} \sum_{a,b=1}^n M_{D,ia} \left(\sum_{c=1}^3 M_{D,ca}^* M_{D,cb} \right) M_{D,jb}^* h(M_{R,a}^2, M_{R,b}^2) \right\} \\ \mathcal{F}_{ij,dd}^{\text{VLL}} &= \frac{e^4}{384\pi^2 s_W^4 M_W^2} \left\{ \sum_{a=1}^n M_{D,ia} M_{R,a}^{-2} M_{D,ja}^* \frac{1}{3} \left(27 - 37s_W^2 + (-27 + 16s_W^2) \log \left(\frac{M_{R,a}^2}{M_W^2} \right) \right) \right. \\ &\quad \left. - \frac{3 - 2s_W^2}{M_W^2} \sum_{a,b=1}^n M_{D,ia} \left(\sum_{c=1}^3 M_{D,ca}^* M_{D,cb} \right) M_{D,jb}^* h(M_{R,a}^2, M_{R,b}^2) \right\} \\ \mathcal{F}_{ij,dd}^{\text{VLR}} &= \frac{e^4}{384\pi^2 s_W^4 M_W^2} \left\{ \sum_{a=1}^n M_{D,ia} M_{R,a}^{-2} M_{D,ja}^* \frac{s_W^2}{3} \left(-37 + 16 \log \left(\frac{M_{R,a}^2}{M_W^2} \right) \right) \right. \\ &\quad \left. + \frac{2s_W^2}{M_W^2} \sum_{a,b=1}^n M_{D,ia} \left(\sum_{c=1}^3 M_{D,ca}^* M_{D,cb} \right) M_{D,jb}^* h(M_{R,a}^2, M_{R,b}^2) \right\} \\ \mathcal{F}_{ij,qq}^{\text{VRL}} &= 0, \quad \mathcal{F}_{ij,qq}^{\text{VRR}} = 0,\end{aligned}\quad (4.24)$$

with $q = u, d$ and h as given in Eq. (4.14). Here we neglected the quark masses and CKM-suppressed effects in the box diagrams by using $(V^{\text{CKM}} V^{\text{CKM}\dagger})_{kl} = \delta_{kl}$.

Together with \mathcal{A}_{ij}^M from the magnetic photon penguin (see Eq. (4.18)), the transition rate $\Gamma_{\mu \rightarrow e}^N \equiv \Gamma(\mu N \rightarrow e N)$ follows as

$$\Gamma_N^{\mu \rightarrow e} = \frac{m_\mu^5}{4} \left\{ \left| \frac{\mathcal{A}_{e\mu}^M}{m_\mu} D_N + 4 \sum_{q=u,d} (\mathcal{F}_{e\mu,qq}^{LL} + \mathcal{F}_{e\mu,qq}^{LR}) (f_{Vp}^{(q)} V_N^p + f_{Vn}^{(q)} V_N^n) \right|^2 + \left| \frac{\mathcal{A}_{\mu e}^M}{m_\mu} D_N \right|^2 \right\}. \quad (4.25)$$

For the overlap integrals between the muon and electron wave functions and the nucleon densities D_{Au} , V_{Au}^p and V_{Au}^n , we use the numerical values [136]

$$D_{\text{Au}} = 0.189, \quad V_{\text{Au}}^p = 0.0974, \quad V_{\text{Au}}^n = 0.146, \quad (4.26)$$

$$D_{\text{Al}} = 0.0362, \quad V_{\text{Al}}^p = 0.0161, \quad V_{\text{Al}}^n = 0.0173. \quad (4.27)$$

The nucleon form factors are given by

$$f_{Vp}^{(u)} = 2, \quad f_{Vn}^{(u)} = 1, \quad f_{Vp}^{(d)} = 1, \quad f_{Vn}^{(d)} = 2. \quad (4.28)$$

The $\mu \rightarrow e$ conversion rate is defined as the $\mu \rightarrow e$ transition rate divided by the μ capture rate, which depends on the nature of the target N

$$\text{Cr}[\mu \rightarrow e, N] = \frac{\Gamma_N^{\mu \rightarrow e}}{\Gamma_N^{\text{capt}}}. \quad (4.29)$$

For the capture rates for gold and aluminium, we use the values [137]

$$\Gamma_{\text{Au}}^{\text{capt}} = 8.7 \times 10^{-18} \text{ GeV}, \quad \Gamma_{\text{Al}}^{\text{capt}} = 4.6 \times 10^{-19} \text{ GeV}. \quad (4.30)$$

The current best experimental limit on $\mu \rightarrow e$ conversion comes from SINDRUM II [138] (see Table 10). The COMET and Mu2e collaborations will be probing $\text{Cr}[\mu \rightarrow e, \text{Al}]$ and expect to improve the upper limit on $\mu \rightarrow e$ conversion by three orders of magnitude in the coming years [139] (see Table 11).

$\text{Cr}[\mu \rightarrow e, \text{Au}] < 7.0 \times 10^{-13}$	SINDRUM II: [138]
---	-------------------

Table 10: Current experimental upper bound on $\mu \rightarrow e$ conversion in Gold.

$\text{Cr}[\mu \rightarrow e, \text{Al}]$	2.6×10^{-17}	COMET: [140]
$\text{Cr}[\mu \rightarrow e, \text{Al}]$	2.87×10^{-17}	Mu2e: [141]

Table 11: Future sensitivities to $\mu \rightarrow e$ conversion in Aluminium.

5 Phenomenology

In this section we study the phenomenology of charged lepton flavour violating processes in the symmetry protected type-I seesaw, taking into account the constraints from $Z \rightarrow \nu\nu$ and tests of lepton flavour universality from pion, kaon and tau decays.³ For this we use the expressions for the processes obtained in Sec. 4, and the structure of the neutrino Yukawa couplings given in Eq. (2.15). In addition, we assume the case of three right-handed neutrinos with degenerate masses.⁴

Let us start by showing the dependence of the $\mu \rightarrow e$ processes $\mu \rightarrow 3e$, $\mu \rightarrow e\gamma$, $\mu \rightarrow e$ conversion in nuclei, and $Z \rightarrow e\mu$ on the right-handed neutrino mass. For this we fix the ratio $\lambda_i = M_R/(10^6 \text{ GeV})$, which involves the (approximately) degenerate sterile neutrino mass M_R , such that T_{ij} (see Eq. (2.17)) becomes independent of M_R . Here and in the following, the complex number z in Eq. (2.15) is fixed to 1, however, as can be seen from Eqs. (2.22), (2.23) and (2.24), varying $|z|$ and $\text{Arg}(z)$ would not add anything to our discussion.

As we can see from Fig. 9, the $\mu \rightarrow e$ conversion rates show sharp dips for specific values of the sterile neutrino masses, whose positions depend on the target nucleus.⁵ For masses around these blind spots, $\mu \rightarrow e$ conversion leads to less stringent bounds on the neutrino Yukawa couplings, such that e.g. the bounds from $\mu \rightarrow 3e$ can be competitive. Note that $\text{Br}(Z \rightarrow e^\pm \mu^\mp)$ not only displays a blind spot, but that this branching ratio is generally inaccessible to current experiments, and even at future Z factories (taking into account the current limits from the other $\mu \rightarrow e$ processes).

Let us now consider correlations between the different charged lepton flavour violating processes. For this we again assume three mass degenerate right-handed neutrinos with masses of either $M_R = 10^3 \text{ GeV}$, $M_R = 10^4 \text{ GeV}$ or $M_R = 10^5 \text{ GeV}$, whereas the couplings λ_i , $i \in \{e, \mu, \tau\}$ are logarithmically sampled within the range $[10^{-6}, 1]$. The resulting rates are compared to the current experimental bounds and future sensitivities given in Tables 4, 6, 8 10 and in Tables 5, 7, 9, 11, respectively. In all plots we disregarded all points in parameter space that are disfavoured by the combined χ^2 function of $Z \rightarrow \nu\nu$ and tests of lepton flavour universality of the charged current (at the 95% CL), or that are excluded by any of the current upper bounds on charged lepton flavour violating observables that are not plotted on the axes.

In Figure 10 we show the three possible combinations of the $\mu \rightarrow e$ observables $\text{Br}(\mu \rightarrow 3e)$, $\text{Br}(\mu \rightarrow e\gamma)$ and $\text{Cr}(\mu \rightarrow e, \text{ Al})$. Here we do not consider $\text{Br}(Z \rightarrow \mu e)$,

³Even though also beta decays can be used as a probe of lepton flavour universality [142], we do not include them here, since the Cabibbo angle anomaly points towards an enhanced $W - \mu - \nu$ coupling [68, 143], which cannot be achieved in our model and increases the tensions in the EW fit [142]. Furthermore, such a modification would further increase the tension within the EW fit via its effect in the determination of the Fermi constant [144].

⁴Note that the phenomenological analysis would be the same if we were to supplement the SM with two mass degenerate sterile neutrinos, given that Eqs. (2.22), (2.23) and (2.21) are obtained by a simple rescaling of Eqs. (2.22), (2.23) and (2.21).

⁵This behaviour was already observed in Ref. [55] and is due to a cancellation between u -quark and d -quark contributions which enter the $\mu \rightarrow e$ conversion rate with opposite sign.

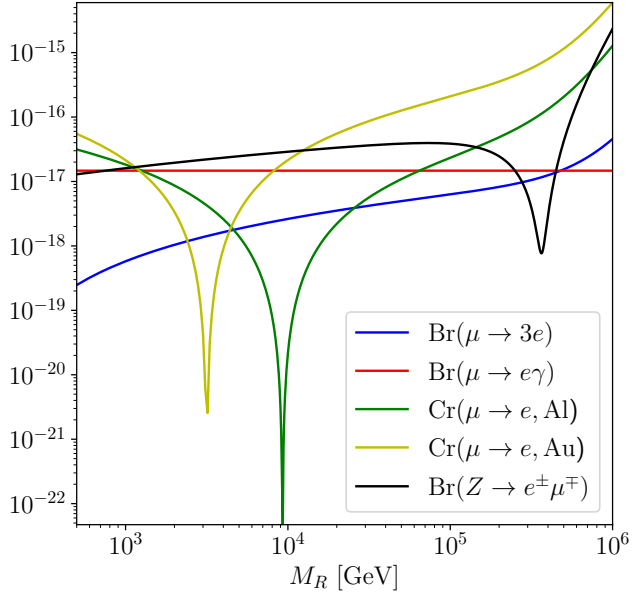


Figure 9: Branching ratios and conversion rates of processes involving $\mu \rightarrow e$ transitions for degenerate sterile neutrinos of mass M_R , and with the Yukawa coupling structure given in Eq. (2.15), corresponding to the symmetry protected type-I seesaw. For this plot we set $\lambda_i = M_R/(10^6 \text{ GeV})$, $i \in \{e, \mu, \tau\}$, such that T_{ij} is constant. Therefore, also $\text{Br}(\mu \rightarrow e\gamma)$, which is proportional to T_{ij} , is independent of M_R , whereas the amplitudes entering $\text{Br}(\mu \rightarrow 3e)$, $\text{Cr}(\mu \rightarrow e)$ and $\text{Br}(Z \rightarrow e\mu)$ involve terms with four Yukawa couplings in addition. Furthermore, $\text{Cr}(\mu \rightarrow e, \text{Au})$ and $\text{Cr}(\mu \rightarrow e, \text{Al})$ feature target dependent blind spots.

since it does not give relevant bounds, even once future prospects are taken into account (see Fig. 9). We see that, apart from in the regions of parameter space around the blind spots shown in Fig. 9, $\mu \rightarrow e$ conversion in nuclei is currently more constraining than $\mu \rightarrow 3e$, which is phase space suppressed. Furthermore, as Fig. 9 shows, the branching ratio of $\mu \rightarrow e\gamma$ is larger than that of $\mu \rightarrow 3e$ in the range of sterile neutrino masses considered here. Consequently, $\mu \rightarrow 3e$ can only lead to more stringent bounds than $\mu \rightarrow e\gamma$ if the corresponding experimental limit is more precise. This is currently not the case, however, the future Mu3e limits on the branching ratio will be lower than that of MEG II.

The spread of the points in Fig. 10a can be explained by the terms proportional to four powers of the neutrino Yukawa couplings. Indeed, if one disregarded these Y^4 terms, the predicted points in parameter space would converge to the upper left boundary of the current region, and we would obtain direct correlations between the two observables $\text{Br}(\mu \rightarrow 3e)$ and $\text{Br}(\mu \rightarrow e\gamma)$. In particular, the smaller the sterile neutrino mass, the stronger the bounds on the couplings and the smaller the Y^4 terms w.r.t. the quadratic ones. Consequently, larger values of $\text{Br}(\mu \rightarrow 3e)$ and $\text{Br}(\mu \rightarrow e\gamma)$ can be attained by

$\mathcal{O}(10^3)$ GeV and $\mathcal{O}(10^4)$ GeV sterile neutrinos than by $\mathcal{O}(10^5)$ GeV sterile neutrinos. For $\mathcal{O}(10^3)$ GeV and $\mathcal{O}(10^4)$ GeV sterile neutrinos, even the current bound on $\text{Br}(\mu \rightarrow e\gamma)$ is constraining.

Fig. 11 (Fig. 12) depicts the $\tau \rightarrow e(\mu)$ observables $\text{Br}(\tau \rightarrow e(\mu)\gamma)$, $\text{Br}(\tau \rightarrow 3e(\mu))$ and $\text{Br}(Z \rightarrow e(\mu)\tau)$. Fig. 11a implies that Belle II will probe a part of the parameter space of sterile neutrinos with masses $\sim \mathcal{O}(10^4) - \mathcal{O}(10^5)$ GeV, via $\text{Br}(\tau \rightarrow 3e)$, however, $\text{Br}(Z \rightarrow e\tau)$, seems to be more sensitive to sterile neutrinos with masses $\sim \mathcal{O}(10^5)$ GeV (see also Figs. 11b and 11c), since it can exclude a part of the parameter space lying below the current experimental bound on $\text{Br}(\tau \rightarrow 3e)$. Furthermore, FCC-ee promises a substantial improvement in sensitivity to the $Z \rightarrow e\tau$ channel. The spread of the points can be understood in the same way as for $\mu \rightarrow e$ transitions.

Similar results are obtained for $\tau \rightarrow \mu$ processes, as can be seen in Figure 12. Among them, $Z \rightarrow \mu\tau$ is the observable most sensitive to sterile neutrinos with masses in the range of $\sim \mathcal{O}(10^5)$ GeV, however, future searches for $\tau \rightarrow 3\mu$ will also be able to probe the parameter space for $\sim \mathcal{O}(10^4) - \mathcal{O}(10^5)$ GeV sterile neutrinos. Note that the largest possible values for the branching ratios $\text{Br}(\tau \rightarrow e\mu e)$ and $\text{Br}(\tau \rightarrow \mu e \mu)$, which feature two flavour changes, lie approximately eight orders of magnitude below their current bounds. For this reason, we do not study these two observables in more detail. We expect a similar behaviour for muonium-antimuonium oscillations, since also these feature two flavour transitions.

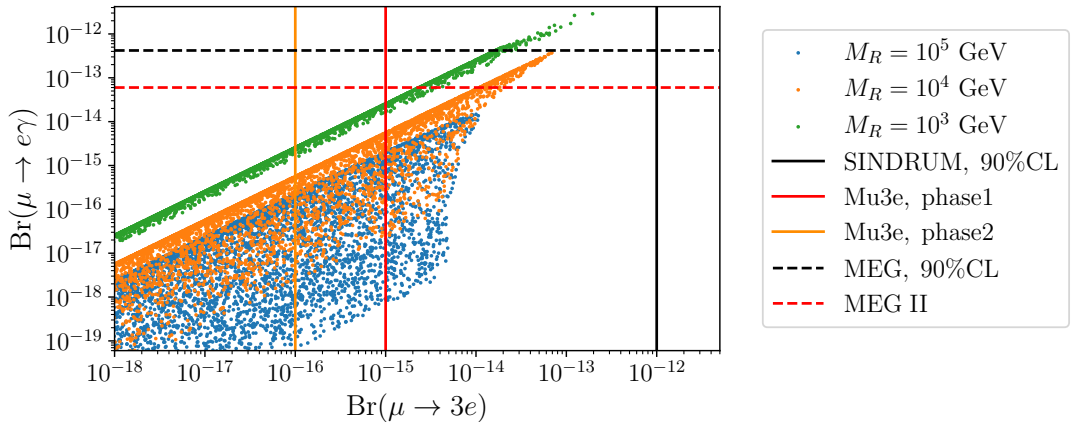
6 Conclusions

The type-I seesaw is a natural mechanism to generate the observed smallness of the active neutrino masses. In general, this requires the corresponding neutrino Yukawa couplings to be tiny for TeV scale right-handed neutrinos. However, the Wilson coefficient of the Weinberg operator can be protected from a non-zero contribution by a symmetry, as in the inverse seesaw model. We refer to this setup as the symmetry protected type-I seesaw, and to the corresponding limit as the inverse seesaw limit. In the inverse seesaw limit, the neutrino Yukawa couplings can be sizeable (for TeV scale sterile neutrinos), such that observable effects in tests of lepton flavour (universality) violation are possible.

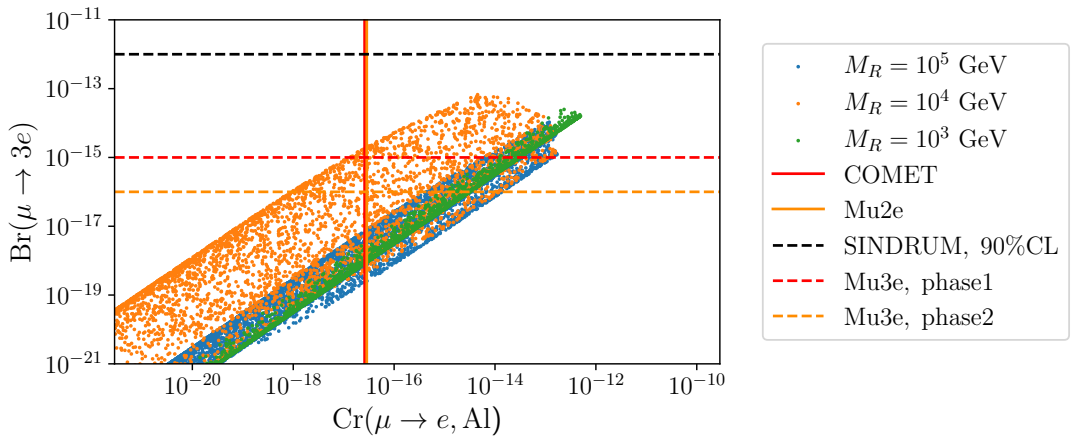
Within this setup, we performed a complete and comprehensive analysis of charged lepton flavour violation. In particular, we calculated the matching of the type-I seesaw on the SMEFT at the dim-6 level, as well as the 1-loop contributions to the processes

- $Z \rightarrow \ell\ell'$
- $\ell \rightarrow \ell'\gamma$
- $\ell \rightarrow 3\ell'$
- $\mu \rightarrow e$ conversion in nuclei

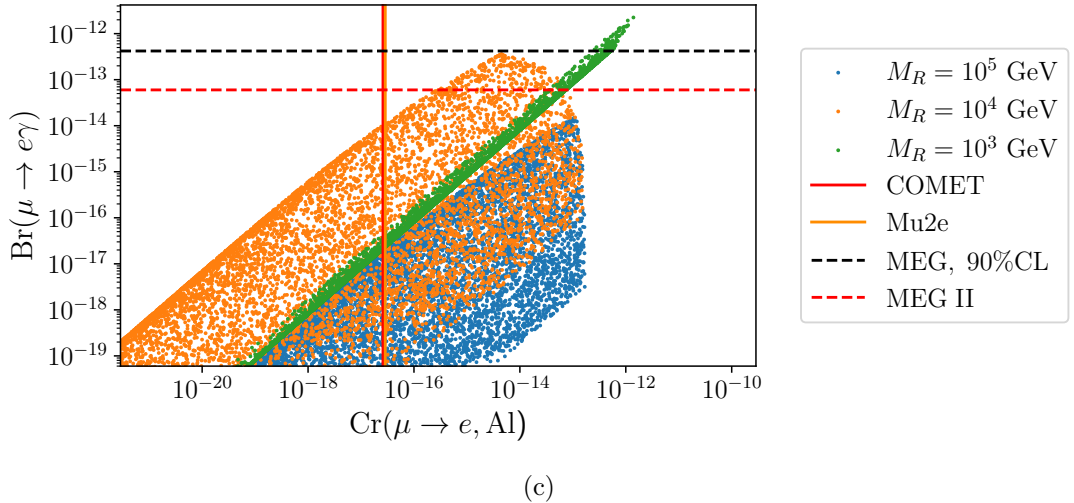
in the seesaw limit, i.e. at leading order in v^2/M_R^2 . In the appendix we also provide the corresponding expressions in a general R_ξ gauge using exact diagonalisation of the neutrino mass matrix.



(a)

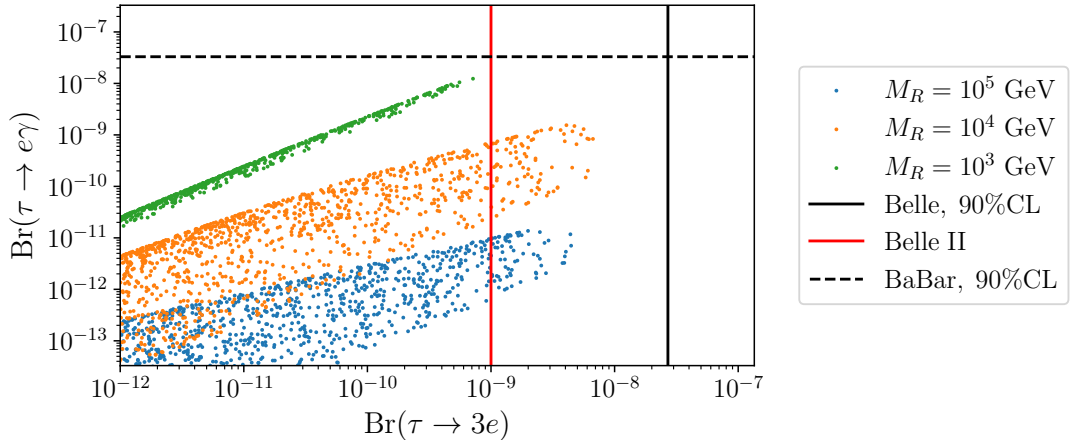


(b)

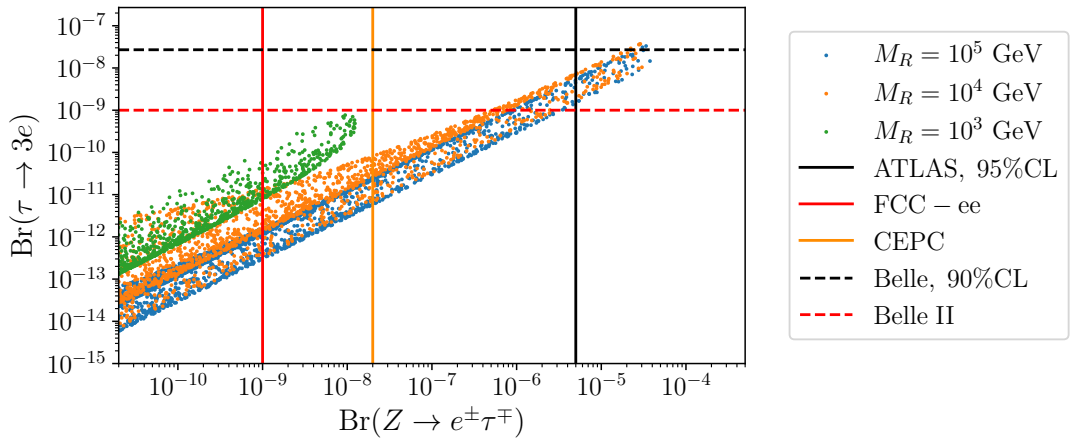


(c)

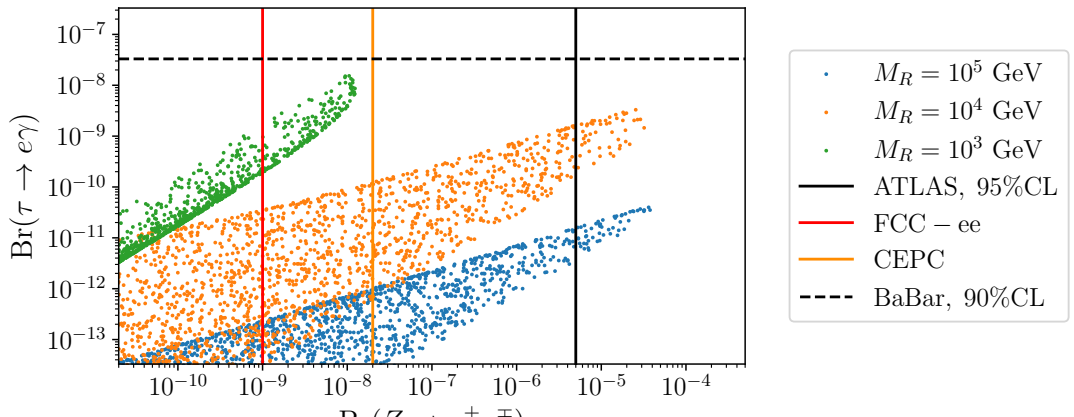
Figure 10: Correlations between the processes $\mu \rightarrow 3e$, $\mu \rightarrow e\gamma$ and $\mu \rightarrow e$ conversion in aluminium nuclei. The current experimental upper limits are indicated by the black lines while the future sensitivities are shown in red and orange.



(a)

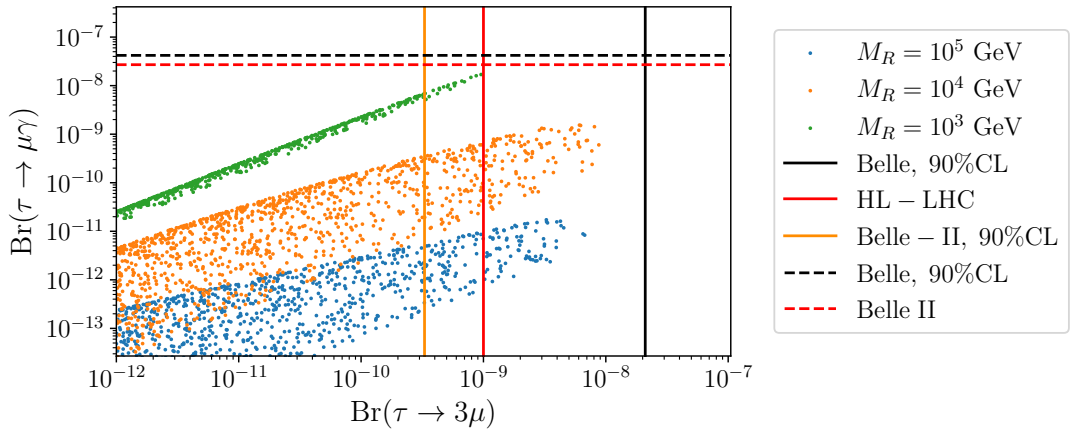


(b)

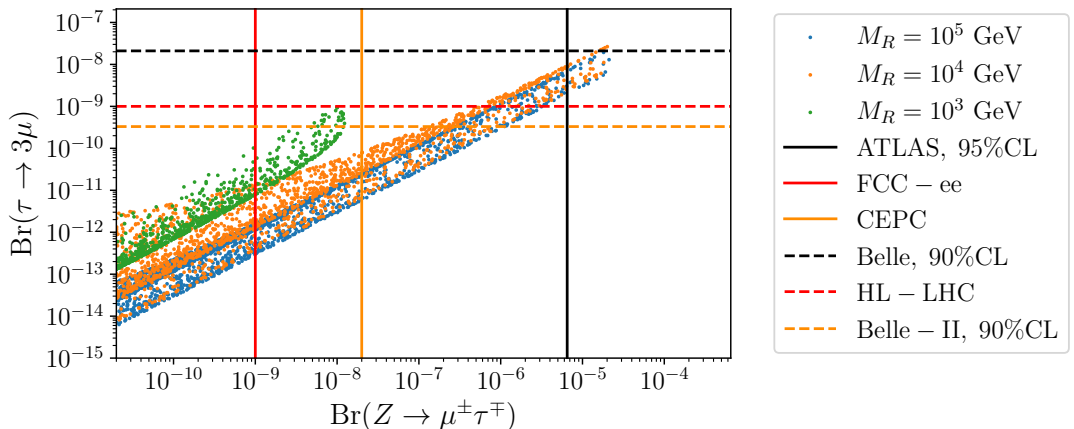


(c)

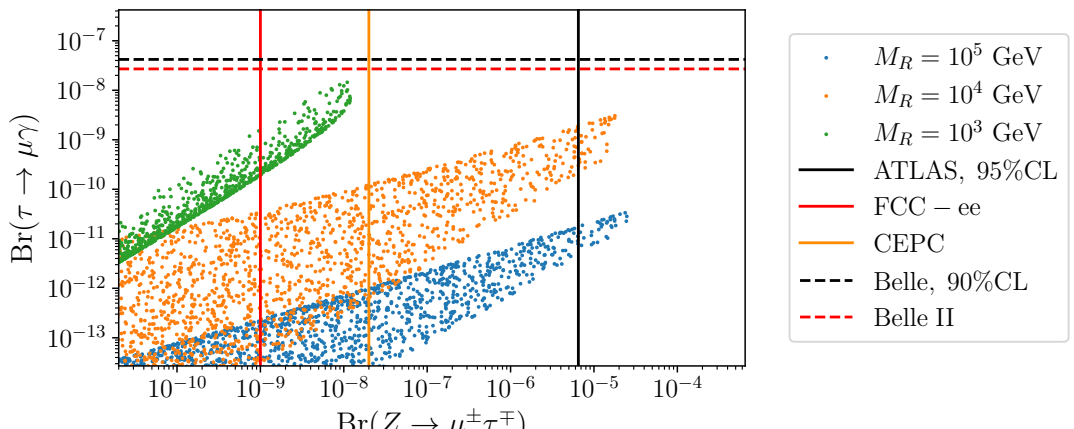
Figure 11: Correlations between the processes $\tau \rightarrow 3e$, $\tau \rightarrow e\gamma$ and $Z \rightarrow e\tau$. The current experimental upper limits are indicated by the black lines while the future sensitivities are shown in red and orange.



(a)



(b)



(c)

Figure 12: Correlations between the lepton flavour violating processes $\tau \rightarrow 3\mu$, $\tau \rightarrow \mu\gamma$ and $Z \rightarrow \mu\tau$. The current experimental upper limits are indicated by the black lines while the future sensitivities are shown in red and in orange.

In our phenomenological analysis, we correlated $\mu \rightarrow e\gamma$ to $\mu \rightarrow 3e$ and $\mu \rightarrow e$ conversion, as well as $\tau \rightarrow e(\mu)\gamma$ to $\tau \rightarrow 3e(\mu)$ and $Z \rightarrow \tau e(\mu)$. Taking into account the bounds from lepton flavour universality violation in tau, kaon and pion decays, and the limit on $\text{Br}(Z \rightarrow \nu\nu)$, we found that, while for sterile neutrino masses of the order of 1 TeV, the correlation between any two $\ell \rightarrow \ell'$ processes is direct, i.e. showing a linear correlation, the allowed parameter space significantly broadens for heavier right-handed neutrinos. The reason for this behaviour is that for heavier right-handed neutrino masses, the neutrino Yukawa couplings Y^ν can be larger, while still respecting experimental bounds, such that the $(Y^\nu)^4$ effects in $\ell \rightarrow \ell'$ and $Z \rightarrow \ell\ell'$ can be (relatively) more important. In particular, we observed that

- Mu3e and future $\mu \rightarrow e$ conversion experiments have the capability of covering a large portion of the so-far unexplored (i.e. unconstrained) parameter space.
- The lepton flavour violating Z decays, $Z \rightarrow e\tau$ and $Z \rightarrow \mu\tau$ can have sizeable branching ratios and could be observed at future e^+e^- colliders such as FCC-ee or CEPC.

While we performed the phenomenological analysis without resummation of potentially large logarithms between the right-handed neutrino scale and the EW scale, the formulae for the matching on the SMEFT can in the future be used for an automated computation. However, for this both a (at least partial) two-loop renormalisation group evolution, as well as the inclusion of the (finite) loop contributions to the relevant observables within LEFT, i.e. the contributions of the operators at the low scale to the matrix elements of the processes, would be necessary.

Acknowledgments

We would like to thank Peter Stoffer and Zhang Di for useful discussions. This work is supported by the Swiss National Science Foundation, under Project No. PP00P21_76884.

A Neutrino Mixing Matrix

For the derivation of the results for the amplitudes with exact diagonalisation of the neutrino mass matrix (see Appendix C), it is useful (as was already noticed in Ref. [6]) to define the $3 \times (3 + n)$ mixing matrix

$$U \equiv V^{\ell L, \dagger} \begin{pmatrix} \mathbb{1}_3 & \mathbb{O}_3 \end{pmatrix} V, \\ U_{is} \equiv \sum_{j=1}^3 V_{ij}^{\ell L*} V_{js}, \quad (\text{A.1})$$

where i and j are lepton flavour indices that run from 1 to 3, whereas s is a neutrino index which runs from 1 to $3 + n$. V is the $(3 + n) \times (3 + n)$ neutrino mixing matrix introduced

in Eqs. (2.6)-(2.7) and $V^{\ell L}$ is one of the two 3×3 matrices $V^{\ell L}$ and $V^{\ell R}$ that diagonalise the charged lepton Yukawa as in

$$Y^{\ell, \text{diag}} = V^{\ell L, \dagger} Y^\ell V^{\ell R}. \quad (\text{A.2})$$

Note that U is a semi-unitary matrix, since $UU^\dagger = \mathbb{1}_3$, but $U^\dagger U \neq \mathbb{1}_{3+n}$. At leading order in v/M_R , U is given by

$$U \approx \begin{pmatrix} \mathbb{1}_3 - \frac{1}{2} M_D M_R^{-2} M_D^\dagger & M_D M_R^{-1} \end{pmatrix}, \quad (\text{A.3})$$

which corresponds to the upper $3 \times (3+n)$ block of the seesaw-expanded neutrino mixing matrix V , given in Eq. (2.9).

The Feynman rules for the type-I seesaw can be expressed in terms of the neutrino mixing matrix U . These are listed in Table 12. Expanding them in powers of v/M_R , we recover the Feynman rules given in Table 1.

Interaction	Exact Feynman rule
$\bar{\ell}_i W_\mu^- n_{R,s}^c$	$-\frac{e}{\sqrt{2}s_W} \gamma^\mu U_{is} P_L$
$n_{R,s}^c Z_\mu n_{R,t}^c$	$-\frac{e}{2s_W c_W} (U^\dagger \gamma^\mu U)_{st} P_L$
$\bar{\ell}_i \varphi^- n_{R,s}^c$	$-\frac{\sqrt{2}}{v} (m_\ell^{\text{diag}} U)_{is} P_L$
$\bar{\ell}_i \varphi^- n_{R,s}$	$\frac{\sqrt{2}}{v} (U M_\nu^{\text{diag}})_{is} P_R$

Table 12: Feynman rules for Majorana neutrinos in the mass eigenbasis, without applying the seesaw approximation. The lepton flavour index i runs from 1 to 3, the neutrino indices s and t run from 1 to $3+n$. m_ℓ^{diag} is the diagonal mass matrix of the charged leptons.

In the derivation of the results given in Appendix C we use

$$\begin{aligned} U M_\nu^{\text{diag}} U^T &= V^{\ell L, \dagger} \left(\mathbb{1}_3 \otimes_3 \right) V M_\nu^{\text{diag}} \left(V^{\ell L, \dagger} \left(\mathbb{1}_3 \otimes_3 \right) V \right)^T \\ &= \left(\mathbb{1}_3 \otimes_3 \right) \begin{pmatrix} \mathbb{O}_3 & M_D \\ M_D^T & M_R \end{pmatrix} \begin{pmatrix} \mathbb{1}_3 \\ \mathbb{O}_3 \end{pmatrix} = \mathbb{O}_3, \end{aligned} \quad (\text{A.4})$$

relating the mixing matrix U , defined in Eq. (A.1), with the active and sterile neutrino masses. This identity is simply an extension of Eq. (2.7).

B Contributions to charged lepton flavour violating processes within the EFT

By definition, the Wilson coefficients, obtained from a matching at a high scale, contain only the hard part of the corresponding amplitudes of the full theory (i.e. the SM with right-handed neutrinos in our case). However, when calculating physical processes at fixed order, as is done in Sec. 4, the full amplitudes, i.e. the sum of the hard and the soft part of the amplitudes, enters. Therefore, the SMEFT matching of Sec. 3.3 would be insufficient to calculate physical processes because the soft part of the amplitudes, corresponding to the loop-contributions to the respective processes within the EFT, would be missing. In this section we obtain these soft parts of the amplitudes by calculating the loop diagrams with the insertions of the modified tree-level couplings of neutrinos with Z and W bosons resulting from Eq. (3.9).

B.1 $\ell \rightarrow \ell' \gamma$

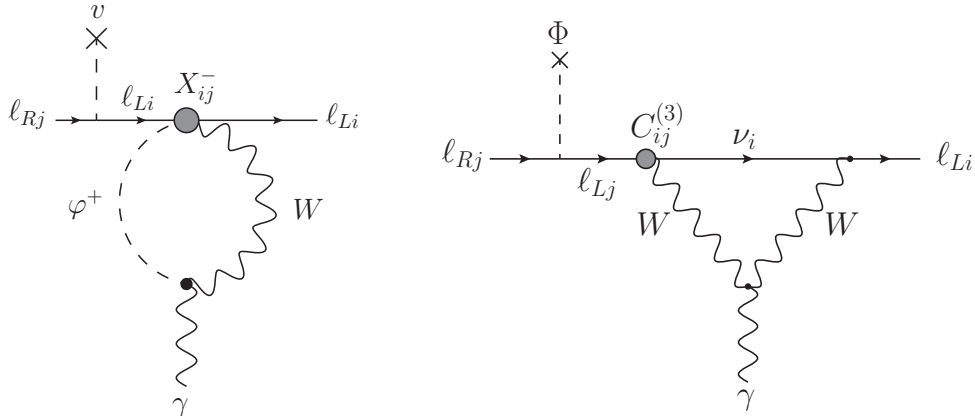


Figure 13: Diagrams with the insertions of the SMEFT operator modified at tree-level, contributing to $\ell \rightarrow \ell' \gamma$.

Defining

$$\mathcal{L}_{\text{eff}} = a_{ij}^M \bar{\ell}_{Li} \sigma_{\mu\nu} \ell_{Rj} F^{\mu\nu} + \text{h.c.}, \quad (\text{B.1})$$

where $F^{\mu\nu} = \partial^\mu A^\nu - \partial^\nu A^\mu$ is the electromagnetic field strength tensor, we find the contributions to $\ell \rightarrow \ell' \gamma$, shown in Figure 13, to be given by

$$a_{ij}^M = - \frac{5e^3 m_{\ell_j}}{384\pi^2 s_W^2 M_W^2} S_{ij}. \quad (\text{B.2})$$

Together with the contribution to the Wilson coefficients from the one-loop matching of the full theory onto SMEFT, reported in Eqs. (3.20) and (3.19), this combines to the full $\ell \rightarrow \ell' \gamma$ amplitude given in Eq. (4.18).

B.2 Four Lepton Amplitudes

The amplitudes of $\ell_j \ell_l \rightarrow \ell_i \ell_k$ processes, can be decomposed as

$$\begin{aligned} \mathcal{M} = & (a_{ij,kl}^{\text{VLL}} + \tilde{z}_{ij,kl}^{\text{VLL}} + d_{ij,kl}^{\text{VLL}}) (\bar{\ell}_i \gamma_\mu P_L \ell_j) (\bar{\ell}_k \gamma_\mu P_L \ell_l) \\ & + (a_{ij,kl}^{\text{VLR}} + \tilde{z}_{ij,kl}^{\text{VLR}}) (\bar{\ell}_i \gamma_\mu P_L \ell_j) (\bar{\ell}_k \gamma_\mu P_R \ell_l), \end{aligned} \quad (\text{B.3})$$

where $a_{ij,kl}^{\text{VAB}}$ denotes the off-shell photon penguin contributions, $\tilde{z}_{ij,kl}^{\text{VAB}}$ the Z penguin, and $d_{ij,kl}^{\text{VAB}}$ the box contributions.

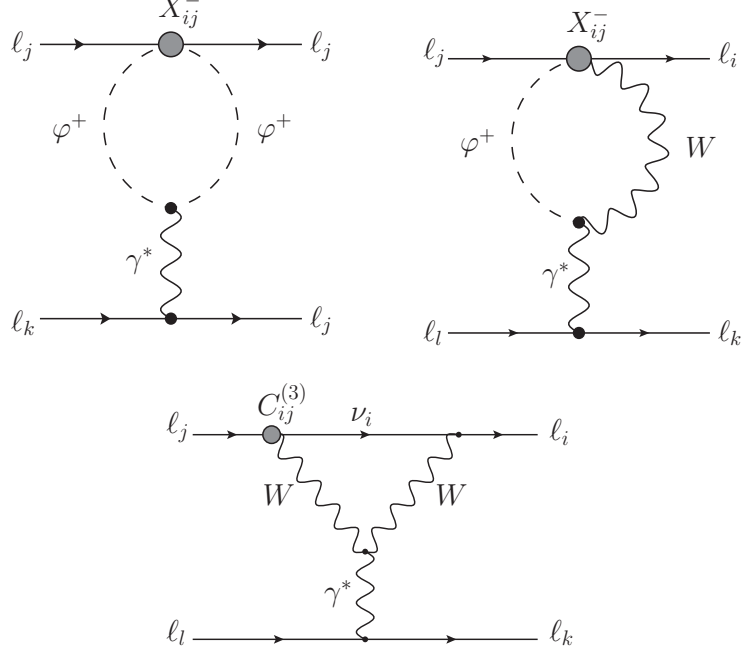


Figure 14: Off-shell photon penguins contributing to four-lepton processes

There are three classes of diagrams with an off-shell photon exchange, as shown in Figure 14):

- Diagrams with two Goldstone bosons in the loop
- Diagrams with a Goldstone and W boson in the loop
- Diagrams with two W bosons and a light neutrino in the loop

Due to the vectorial nature of the photon coupling, $a_{ij,kl}^{\text{VLL}} = a_{ij,kl}^{\text{VLR}}$ and we find

$$a_{ij,kl}^{\text{VLL}} = a_{ij,kl}^{\text{VLR}} = -e Q_e a_{ij}^V \delta_{kl} = e, a_{ij}^V \delta_{kl} \quad (\text{B.4})$$

with a_{ij}^V given in R_ξ -gauge by

$$a_{ij}^V = -\frac{e^3}{576\pi^2 s_W^2 M_W^2} \sum_{a=1}^n M_{D,ia} M_{R,a}^{-2} M_{D,ja}^* \frac{1}{2} \left(95 - 9\xi + 54 \frac{\xi \log \xi}{1-\xi} + 6 \log \left(\frac{\mu^2}{M_W^2} \right) \right). \quad (\text{B.5})$$

Together with the result of the one-loop matching, the Z-penguin and box contributions, this leads to the results in Eqs. (4.20) and (4.21).

Below the electroweak scale, the diagrams with an off-shell Z boson exchange are the ones shown in Figure 16, with a fermion line attached to the Z boson. They give

$$\begin{aligned} \tilde{z}_{ij,kl}^{VLL} &= g_{\text{SM}}^{\ell L} \delta_{kl} \tilde{z}_{ij}^L \\ \tilde{z}_{ij,kl}^{VLR} &= g_{\text{SM}}^{\ell R} \delta_{kl} \tilde{z}_{ij}^L, \end{aligned} \quad (\text{B.6})$$

with

$$\tilde{z}_{ij}^L = -\frac{e^3 c_W}{128\pi^2 s_W^3 M_W^2} \left\{ \sum_{a=1}^n M_{D,ia} M_{R,a}^{-2} M_{D,ja}^* \left(8 - \xi + \frac{6\xi \log \xi}{1-\xi} + 6 \log \left(\frac{\mu^2}{M_W^2} \right) \right) \right\}$$

in R_ξ gauge, and

$$\tilde{z}_{ij}^L = -\frac{e^3 c_W}{128\pi^2 s_W^3 M_W^2} \left\{ \sum_{a=1}^n M_{D,ia} M_{R,a}^{-2} M_{D,ja}^* \left(1 + 6 \log \left(\frac{\mu^2}{M_W^2} \right) \right) \right\}.$$

in Feynman gauge.

The box diagram with two W bosons in the loop (see Figure 15) contributes as follows in the R_ξ -gauge:

$$d_{ij,kl}^{VLL} = -\frac{e^4}{64\pi^2 s_W^4 M_W^2} \sum_{a=1}^n M_{D,ia} M_{R,a}^{-2} M_{D,ja}^* \delta_{kl} \frac{1}{4} \left(-3 + \xi - \frac{6\xi \log \xi}{1-\xi} \right), \quad (\text{B.7})$$

In Feynman-gauge we have

$$d_{ij,kl}^{VLL} = -\frac{e^4}{64\pi^2 s_W^4 M_W^2} \sum_{a=1}^n M_{D,ia} M_{R,a}^{-2} M_{D,ja}^* \delta_{kl}. \quad (\text{B.8})$$

B.3 Two-Lepton-Two-Quark Interactions

Next we consider $\mu \rightarrow e$ conversion in nuclei, whose amplitude can be written as

$$\begin{aligned} \mathcal{M}_{\text{eff}} &= (a_{ij,qq}^{VLL} + z_{ij,qq}^{VLL} + d_{ij,qq}^{VLL}) (\bar{\ell}_i \gamma_\mu P_L \ell_j) (\bar{q} \gamma_\mu P_L q) \\ &\quad + (a_{ij,qq}^{VLR} + z_{ij,qq}^{VLR}) (\bar{\ell}_i \gamma_\mu P_L \ell_j) (\bar{q} \gamma_\mu P_R q). \end{aligned} \quad (\text{B.9})$$

with $q = u, d$.

The photon penguin contributions are of the same form of those given in (B.4).

$$\begin{aligned} a_{ij,uu}^{VLL} &= a_{ij,uu}^{VLR} = -e Q_u a_{ij}^V = -\frac{2}{3} e a_{ij}^V, \\ a_{ij,dd}^{VLL} &= a_{ij,dd}^{VLR} = -e Q_d a_{ij}^V = \frac{1}{3} e a_{ij}^V. \end{aligned} \quad (\text{B.10})$$

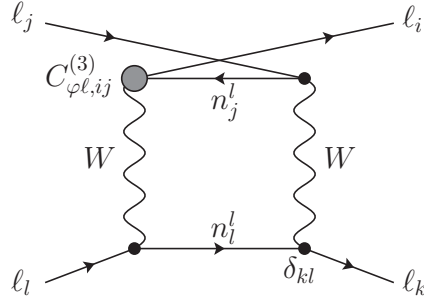


Figure 15: Box diagram contributing to four lepton processes with an (tree-level) operator insertion.

Similarly, the Z boson penguins lead to

$$\begin{aligned}\tilde{z}_{ij,qq}^{\text{VLL}} &= \tilde{z}_{ij}^L g_{\text{SM}}^{qL}, \\ \tilde{z}_{ij,qq}^{\text{VLR}} &= \tilde{z}_{ij}^L g_{\text{SM}}^{qR},\end{aligned}\tag{B.11}$$

where g_{SM}^{qL} , and g_{SM}^{qR} , $q = u, d$, are the SM Z boson couplings to left- and right-handed up- and down-type quarks,

$$\begin{aligned}g_{\text{SM}}^{uL} &= -\frac{e}{2s_{\text{WCW}}} \left(1 - \frac{4}{3}s_{\text{W}}^2\right), \\ g_{\text{SM}}^{uR} &= \frac{2es_{\text{W}}}{3c_{\text{W}}}, \\ g_{\text{SM}}^{dL} &= \frac{e}{2s_{\text{WCW}}} \left(1 - \frac{2}{3}s_{\text{W}}^2\right), \\ g_{\text{SM}}^{dR} &= -\frac{es_{\text{W}}}{3c_{\text{W}}},\end{aligned}\tag{B.12}$$

and \tilde{z}_{ij}^L is as defined in Eq. (B.6).

In R_ξ -gauge we obtain the following box contributions:

$$\begin{aligned}
d_{ij,u_k u_l}^{VLL} &= - \frac{e^4}{256\pi^2 s_W^4 M_W^2} \left\{ \sum_{a=1}^n \sum_{g=1}^3 M_{D,ia} M_{R,a}^{-2} M_{D,ja}^* V_{kg}^{\text{CKM}} V_{lg}^{\text{CKM}*} \right. \\
&\quad \left(\frac{-(-9 + 8\xi + \xi^2 + 6\xi \log \xi) M_W^2 + \xi (-1 + \xi + 6 \log \xi) m_{d_g}^2}{(-1 + \xi)(M_W^2 - m_{d_g}^2)} \right. \\
&\quad \left. + \frac{m_{d_g}^2}{M_W^2} \log \left(\frac{M_{R,a}^2}{M_W^2} \right) + \frac{m_{d_g}^2 (4M_W^2 - m_{d_g}^2)^2}{M_W^2 (M_W^2 - m_{d_g}^2)^2} \log \left(\frac{M_W^2}{m_{d_g}^2} \right) \right) \Big\} \\
d_{ij,d_k d_l}^{VLL} &= - \frac{e^4}{256\pi^2 s_W^4 M_W^2} \left\{ \sum_{a=1}^n \sum_{g=1}^3 M_{D,ia} M_{R,a}^{-2} M_{D,ja}^* V_{gk}^{\text{CKM}*} V_{gl}^{\text{CKM}} \right. \\
&\quad \left(\frac{(3 - 4\xi + \xi^2 + 6\xi \log \xi) M_W^2 - \xi (-1 + \xi + 6 \log \xi) m_{u_g}^2}{(-1 + \xi)(M_W^2 - m_{u_g}^2)} \right. \\
&\quad \left. - \frac{m_{u_g}^2}{M_W^2} \log \left(\frac{M_{R,a}^2}{M_W^2} \right) - \frac{m_{u_g}^2 (4M_W^2 - 8m_{u_g}^2 M_W^2 + m_{u_g}^4)}{M_W^2 (M_W^2 - m_{u_g}^2)^2} \log \left(\frac{M_W^2}{m_{u_g}^2} \right) \cdot \right) \Big\} \\
\end{aligned} \tag{B.13}$$

The terms with two Dirac mass matrices are generated by double W boson boxes, whereas the terms with four Dirac mass matrices are generated by double-Goldstone boxes. In the following, we neglect the possibility of having a flavour transition in the quark line, since this effect is CKM-suppressed (when summing the contributions we set $(V^{\text{CKM}} V^{\text{CKM}\dagger})_{kl} = \delta_{kl}$).

C Exact diagonalisation and/or R_ξ Dependence

In the following, we give the full results, i.e. the sum of the soft and hard parts of the amplitudes, for the processes of interest in our work, with exact diagonalization of the neutrino mixing matrix (as described in Appendix A) and in the R_ξ gauge. We sum over the flavour indices a, b and c , which denote, respectively, internal neutrinos and charged leptons, while the indices i, j, k, l denote external leptons, which are fixed. For the sake of simplicity, we express the result in terms of master integrals, reported in Appendix D.

C.1 Anomalous Magnetic Moments and Radiative Leptonic Decays

Defining

$$\mathcal{L}_{\text{eff}} = \mathcal{A}_{ij}^M \bar{\ell}_i \sigma_{\mu\nu} P_R \ell_j F^{\mu\nu} + \text{h.c.} \tag{C.1}$$

where $F^{\mu\nu} = \partial^\mu A^\nu - \partial^\nu A^\mu$ is the electromagnetic field strength tensor, we find

$$\mathcal{A}_{ij}^M = \frac{e^3 m_{\ell_j}}{256\pi^2 s_W^2} \sum_{a=1}^n U_{ia} U_{ja}^* f^M(M_{\nu,a}, M_W), \tag{C.2}$$

where

$$f^M(M_{\nu,a}, M_W) = \frac{M_{\nu,a}^2}{M_W^2 (M_{\nu,a}^2 - M_W^2)^4} \left(6M_{\nu,a}^2 M_W^2 (A_0(M_{\nu,a}) - M_W^2) - 3M_{\nu,a}^4 (2A_0(M_W) - M_W^2) + 2M_{\nu,a}^6 + M_W^6 \right). \quad (\text{C.3})$$

C.2 $Z \rightarrow \ell\ell'$

The $Z \rightarrow \ell_i \bar{\ell}_j$ amplitude can be cast into the form

$$\mathcal{M}(Z \rightarrow \ell_i \bar{\ell}_j) = -\frac{e^3}{16\pi^2 c_W s_W^3} \overline{\mathcal{Z}}_{ij}^{VL} \bar{\ell}_j \not{Z} P_L \ell_i,$$

with

$$\begin{aligned} \overline{\mathcal{Z}}_{ij}^{VL} &= U_{ia} U_{ja}^* f_A^V(M_{\nu,a}^2) + U_{ia} \left(\sum_{k=1}^3 U_{ka}^* U_{kb} \right) U_{jb}^* f_B^V(M_{\nu,a}^2, M_{\nu,b}^2) \\ &\quad + U_{ia} U_{ka} U_{kb}^* U_{jb}^* f_C^V(M_{\nu,a}^2, M_{\nu,b}^2), \end{aligned} \quad (\text{C.4})$$

$$\begin{aligned} f_A^V(M_{\nu,a}^2) &= \left\{ \frac{-2(2M_W^2 - M_Z^2)}{M_Z^4 (M_{\nu,a}^2 - M_W^2)^2} \left(4M_W^4 (M_W^2 + 2M_Z^2) - 3M_W^2 (2M_W^2 + 3M_Z^2) M_{\nu,a}^2 \right. \right. \\ &\quad \left. \left. + 4M_Z^2 M_{\nu,a}^4 + 2M_{\nu,a}^6 \right) A_0(M_W) \right. \\ &\quad \left. + \frac{2(2M_W^2 - M_Z^2)}{M_Z^4 (M_{\nu,a}^2 - M_W^2)^2} \left(4M_W^4 (M_W^2 + 2M_Z^2) - 6M_W^2 (M_W^2 + M_Z^2) M_{\nu,a}^2 \right. \right. \\ &\quad \left. \left. + M_Z^2 M_{\nu,a}^4 + 2M_{\nu,a}^6 \right) A_0(M_{\nu,a}) \right. \\ &\quad \left. - \frac{2}{M_Z^4} \left((4M_W^2 M_Z^2 + 4M_W^4 - M_Z^4) M_{\nu,a}^2 \right. \right. \\ &\quad \left. \left. + 2(2M_W^2 - M_Z^2) M_{\nu,a}^4 \right) B_0(M_Z^2; M_W, M_W) \right. \\ &\quad \left. - \frac{4}{M_Z^4} \left(4M_W^6 (M_W^2 + 2M_Z^2) + M_W^2 (4M_Z^4 - 5M_W^2 M_Z^2 - 6M_W^4) M_{\nu,a}^2 \right. \right. \\ &\quad \left. \left. + M_Z^2 (4M_W^2 - M_Z^2) M_{\nu,a}^4 + (2M_W^2 - M_Z^2) M_{\nu,a}^6 \right) \right. \\ &\quad \left. \times C_0(0, 0, M_Z^2; M_W, M_{\nu,a}, M_W) \right. \\ &\quad \left. + \frac{2M_W^2 - M_Z^2}{M_Z^2 (M_{\nu,a}^2 - M_W^2)} (2M_W^4 + 5M_{\nu,a}^2 M_W^2 - M_{\nu,a}^4) \right\} \frac{1}{16M_W^2}, \end{aligned} \quad (\text{C.5})$$

$$\begin{aligned}
f_B^V(M_{\nu,a}^2, M_{\nu,b}^2) = & \left\{ M_W^2 (-2M_W^2 - 3M_Z^2 + M_{\nu,a}^2 + M_{\nu,b}^2) B_0(M_Z^2; M_{\nu,a}, M_{\nu,b}) \right. \\
& + \left(-2M_W^2 (M_W^2 + M_Z^2)^2 + 2M_W^2 (M_W^2 + M_Z^2) (M_{\nu,a}^2 + M_{\nu,b}^2) \right. \\
& \quad \left. \left. - (2M_W^2 + M_Z^2) M_{\nu,a}^2 M_{\nu,b}^2 \right) \right. \\
& \times C_0(0, 0, M_Z^2; M_{\nu,a}, M_W, M_{\nu,b}) \left. \right\} \frac{1}{4M_W^2 M_Z^2}, \\
\end{aligned} \tag{C.6}$$

and

$$\begin{aligned}
f_C^V(M_{\nu,a}^2, M_{\nu,b}^2) = & \left\{ \left(-2M_W^2 + M_Z^2 + M_{\nu,a}^2 + M_{\nu,b}^2 \right) B_0(M_Z^2; M_{\nu,a}, M_{\nu,b}) \right. \\
& - 2 \left(M_{\nu,a}^2 M_{\nu,b}^2 - M_W^2 (M_{\nu,a}^2 + M_{\nu,b}^2) + M_W^2 (M_W^2 + 2M_Z^2) \right) \\
& \times C_0(0, 0, M_Z^2; M_{\nu,a}, M_W, M_{\nu,b}) \left. \right\} \frac{-M_{\nu,a} M_{\nu,b}}{8M_W^2 M_Z^2}. \\
\end{aligned} \tag{C.7}$$

Note that all three structures are both ξ -independent and UV-finite after taking into account the unitarity of the neutrino mixing matrix and Eq. (A.4).

Performing the seesaw expansion (see Eqs. (2.9)-(2.11)), Eq. (C.4) simplifies to Eq. (C.9). The structure $U_{ia} U_{ca} U_{cb}^* U_{jb}^*$ vanishes by virtue of the inverse seesaw condition, Eq. (2.12). Terms with this structure survive only in presence of sterile neutrino mass splitting and can be simplified as follows. Using the notation $Y^4|_{\mathcal{L}} = \sum_{a,b=1}^N Y_{ia}^\nu M_{R,a}^{-1} \left(\sum_{c=1}^3 Y_{ca}^\nu Y_{cb}^{\nu*} \right) M_{R,b}^{-1} Y_{jb}^{\nu*}$, we find

$$\begin{aligned}
Y^4|_{\mathcal{L}} \times \left\{ -\frac{M_{R,a}^2}{M_{R,a}^2 - M_{R,b}^2} \log \left(\frac{\mu^2}{M_{R,a}^2} \right) + \frac{M_{R,b}^2}{M_{R,a}^2 - M_{R,b}^2} \log \left(\frac{\mu^2}{M_{R,b}^2} \right) \right\} = \\
Y^4|_{\mathcal{L}} \times \left\{ +\frac{M_{R,a}^2}{M_{R,a}^2 - M_{R,b}^2} \log(M_{R,a}^2) - \frac{M_{R,b}^2}{M_{R,a}^2 - M_{R,b}^2} \log(M_{R,b}^2) \right\} = \\
Y^4|_{\mathcal{L}} \times \left\{ \frac{1}{2} \frac{M_{R,a}^2 - M_{R,b}^2}{M_{R,a}^2 - M_{R,b}^2} \log(M_{R,a}^2) + \frac{M_{R,a}^2}{M_{R,a}^2 - M_{R,b}^2} \log(M_{R,a}^2) \right. \\
\left. - \frac{1}{2} \frac{M_{R,a}^2 - M_{R,b}^2}{M_{R,a}^2 - M_{R,b}^2} \log(M_{R,b}^2) - \frac{M_{R,b}^2}{M_{R,a}^2 - M_{R,b}^2} \log(M_{R,b}^2) \right\} = \\
Y^4|_{\mathcal{L}} \times \left\{ \frac{1}{2} \frac{M_{R,a}^2 + M_{R,b}^2}{M_{R,a}^2 - M_{R,b}^2} \log \left(\frac{M_{R,a}^2}{M_{R,b}^2} \right) \right\} = Y^4|_{\mathcal{L}} \times k(M_{R,a}^2, M_{R,b}^2), \\
\end{aligned} \tag{C.8}$$

with the function k , as defined in Eq. (4.15).

$$\begin{aligned}
\overline{\mathcal{Z}}_{ij}^{\text{VL}}(q_Z^2) = & \sum_{a=1}^n M_{D,ia} M_{R,a}^{-2} M_{D,ja}^* f_2(M_{R,a}^2) \\
& + \sum_{a,b=1}^n M_{D,ia} \left(\sum_{k=1}^3 M_{D,ka}^* M_{D,kb} \right) M_{D,jb} f_{4A}(M_{R,a}^2, M_{R,b}^2) \\
& + \sum_{a,b=1}^n M_{D,ia} M_{R,a}^{-1} \left(\sum_{k=1}^3 M_{D,ka} M_{D,kb}^* \right) M_{R,b}^{-1} M_{D,jb}^* f_{4B}(M_{R,a}^2, M_{R,b}^2), \quad (\text{C.9})
\end{aligned}$$

The loop functions f_2 and f_{4A} and f_{4B} , reduced to master integrals, are given by

$$\begin{aligned}
f_2(M_R^2) = & - (1 - 2c_W^2) \frac{2M_R^6 + M_R^4 q_Z^2 - 6M_R^2 M_W^2 (M_W^2 + q_Z^2) + 4M_W^4 (M_W^2 + 2q_Z^2)}{8M_W^2 q_Z^2 (M_R^2 - M_W^2)^2} A_0(M_R) \\
& + (1 - 2c_W^2) \frac{M_R^2 (2M_R^4 - 4M_R^2 (M_W^2 + q_Z^2) + 7M_W^2 q_Z^2 + 2M_W^4)}{8M_W^2 q_Z^2 (M_R^2 - M_W^2)^2} A_0(M_W) \\
& + \frac{1}{2q_Z^2} (M_R^2 - 2M_W^2 - 3q_Z^2) B_0(q_Z^2; 0, M_R) \\
& + \frac{M_R^2}{8M_W^2 q_Z^2} (2(1 - 2c_W^2) M_R^2 - 2(1 + 2c_W^2) M_W^2 + (1 - 2c_W^2) q_Z^2) B_0(q_Z^2; M_W, M_W) \\
& + \frac{1}{q_Z^2} (M_W^2 + q_Z^2) (M_R^2 - M_W^2 - q_Z^2) C_0(0, 0, q_Z^2, M_R, M_W, 0) \\
& + \frac{1}{4M_W^2 q_Z^2} \left((1 - 2c_W^2) M_R^6 - M_R^4 (2M_W^2 - (1 - 2c_W^2) q_Z^2) \right. \\
& \quad \left. + M_R^2 M_W^2 ((1 + 6c_W^2) M_W^2 - 4(1 - c_W^2) q_Z^2) \right. \\
& \quad \left. - 4c_W^2 M_W^4 (M_W^2 + 2q_Z^2) \right) C_0(0, 0, q_Z^2, M_W, M_R, M_W) \\
& + \frac{(1 - 2c_W^2) M_R^2 (M_R^2 - 7M_W^2)}{16M_W^2 (M_R^2 - M_W^2)}, \quad (\text{C.10})
\end{aligned}$$

and

$$f_{4A}(M_{R,a}, M_{R,b}) = - \frac{1}{4M_W^2} C_0(0, 0, q_Z^2, M_{R,a}, M_W, M_{R,b}) \quad (\text{C.11})$$

$$\begin{aligned}
f_{4B}(M_{R,a}^2, M_{R,b}^2) = & - \frac{1}{8M_W^2 q_Z^2 M_{R,a} M_{R,b}} \\
& \times \left\{ \left(M_{R,a}^2 + M_{R,b}^2 - 2M_W^2 + q_Z^2 \right) B_0(q_Z^2; M_{R,a}, M_{R,b}) \right. \\
& \quad \left. - 2 \left(M_{R,a}^2 M_{R,b}^2 - M_W^2 (M_{R,a}^2 + M_{R,b}^2) + M_W^2 (M_W^2 + 2q_Z^2) \right) \right. \\
& \quad \left. \times C_0(0, 0, q_Z^2; M_{R,a}, M_W, M_{R,b}) \right\} \quad (\text{C.12})
\end{aligned}$$

q_Z^2 corresponds to the momentum squared of the Z boson. For on-shell Z , q_Z^2 is to be substituted with M_Z^2 .

C.3 $\ell \rightarrow \ell' \bar{\ell}' \ell'''$

The amplitudes of $\ell \rightarrow 3\ell'$ processes can be cast into the form

$$\begin{aligned} \mathcal{M}(\ell_j \rightarrow \ell_i \ell_k \bar{\ell}_l) &= (\mathcal{A}_{ij,kl}^{VLR} + \mathcal{Z}_{ij,kl}^{VLR}) (\bar{\ell}_i \gamma_\mu P_L \ell_j) (\bar{\ell}_k \gamma_\mu P_R \ell_l) \\ &\quad + [(\mathcal{A}_{ij,kl}^{VLL} + \mathcal{Z}_{ij,kl}^{VLL} + \mathcal{D}_{ij,kl}^{VLL}) (\bar{\ell}_i \gamma_\mu P_L \ell_j) (\bar{\ell}_k \gamma_\mu P_L \ell_l) \\ &\quad + ((ij, kl) \rightarrow (kl, ij)) \\ &\quad + ((ij, kl) \rightarrow (kj, il)) \\ &\quad + ((ij, kl) \rightarrow (il, kj))] \\ &\quad + \mathcal{D}_{jl,ik}^{SLR} (\bar{\ell}_i P_L \ell_k) (\bar{\ell}_j P_R \ell_l). \end{aligned} \quad (\text{C.13})$$

with $\mathcal{A}_{ij,kl}^{VL(L/R)}$, $\mathcal{Z}_{ij,kl}^{VL(L/R)}$, $\mathcal{D}_{ij,kl}^{VLL}$ and $\mathcal{D}_{ij,kl}^{SLR}$ as defined in the following subsections.

C.3.1 Photon Penguin Contributions

From the photon penguins, we obtain

$$\mathcal{A}_{ij,kl}^{VL} = \frac{e^3}{384\pi^2 M_W^2 s_W^2} U_{ia} M_{\nu,a}^2 U_{ja}^* \delta_{kl} \left\{ \frac{3\xi (6M_{\nu,a}^2 - (7-\xi)\xi M_W^2)}{(1-\xi)(M_{\nu,a}^2 - \xi M_W^2)^2} \log \left(\frac{M_{\nu,a}^2}{\xi M_W^2} \right) \right. \quad (\text{C.14})$$

$$\begin{aligned} &- \frac{(28-3\xi)M_{\nu,a}^6 - (43+19\xi)M_W^2 M_{\nu,a}^4 + (34\xi+9)M_W^4 M_{\nu,a}^2 - 6\xi M_W^6}{(M_{\nu,a}^2 - M_W^2)^3 (M_{\nu,a}^2 - \xi M_W^2)} \\ &+ \left. \frac{2(8\xi+1)M_{\nu,a}^6 - (41+13\xi)M_W^2 M_{\nu,a}^4 + 6(11-2\xi)M_W^4 M_{\nu,a}^2 - 3(7-\xi)M_W^6}{(1-\xi)(M_{\nu,a}^2 - M_W^2)^4} \log \left(\frac{M_{\nu,a}^2}{M_W^2} \right) \right\}. \end{aligned} \quad (\text{C.15})$$

C.3.2 Z Penguin Contributions

The Z penguin contributions give

$$\begin{aligned} \mathcal{Z}_{ij,kl}^{VLR} &= g_{\text{SM}}^{\ell L} \mathcal{Z}_{ij}^{VL} \delta_{kl}, \\ \mathcal{Z}_{ij,kl}^{VLL} &= g_{\text{SM}}^{\ell R} \mathcal{Z}_{ij}^{VL} \delta_{kl}, \end{aligned} \quad (\text{C.16})$$

with the couplings $g_{\text{SM}}^{\ell L}$ and $g_{\text{SM}}^{\ell R}$, as defined in Eq. (2.28), and

$$\mathcal{Z}_{ij,kl}^{VL}|_{R_\xi} = \mathcal{Z}_{ij,kl}^{VL}|_{\text{FG}} + \mathcal{Z}_{ij,kl}^{VL}|_\xi, \quad (\text{C.17})$$

where $\mathcal{Z}_{ij,kl}^{VL}\Big|_{R_\xi}$ denotes the result in R_ξ gauge, $\mathcal{Z}_{ij,kl}^{VL}\Big|_{\text{FG}}$ is the result in Feynman gauge and $\mathcal{Z}_{ij,kl}^{VL}\Big|_\xi$ collects the ξ -dependent terms:

$$\begin{aligned} \mathcal{Z}_{ij}^{VL}\Big|_{\text{FG}} &= \frac{e^3 c_W}{128\pi^2 s_W^3 M_W^2} \frac{U_{ia} U_{ja}^*}{(M_{\nu,a}^2 - M_W^2)^2} \left\{ M_{\nu,a}^4 \left(9 - 10 \log \left(\frac{M_{\nu,a}^2}{M_W^2} \right) \right) - 8 M_W^2 M_{\nu,a}^2 - M_W^4 \right\} \\ &\quad - \frac{e^3 c_W}{64\pi^2 s_W^3 M_W^2} U_{ia} U_{ma}^* U_{mb} U_{jb}^* \\ &\quad \times \frac{M_{\nu,a}^4 (M_{\nu,b}^2 - M_W^2)^2 \log \left(\frac{M_{\nu,a}^2}{M_W^2} \right) - M_{\nu,b}^4 (M_{\nu,a}^2 - M_W^2)^2 \log \left(\frac{M_{\nu,b}^2}{M_W^2} \right)}{M_W^2 (M_{\nu,a}^2 - M_{\nu,b}^2) (M_{\nu,a}^2 - M_W^2) (M_{\nu,b}^2 - M_W^2)} \\ &\quad - \frac{e^3 c_W}{128\pi^2 s_W^3 M_W^2} U_{ia} U_{ma} U_{mb} U_{jb}^* \\ &\quad \times \left\{ \frac{M_{\nu,a}^3 M_{\nu,b} (M_{\nu,a}^2 - 4M_W^2) \log \left(\frac{M_{\nu,a}^2}{M_W^2} \right)}{M_W^2 (M_{\nu,a}^2 - M_{\nu,b}^2) (M_{\nu,a}^2 - M_W^2)} - \frac{M_{\nu,a} M_{\nu,b}^3 (M_{\nu,b}^2 - 4M_W^2) \log \left(\frac{M_{\nu,b}^2}{M_W^2} \right)}{M_W^2 (M_{\nu,a}^2 - M_{\nu,b}^2) (M_{\nu,b}^2 - M_W^2)} \right\}, \end{aligned} \tag{C.18}$$

and

$$\begin{aligned} \mathcal{Z}_{ij}^{VL}\Big|_\xi &= \frac{e^3 c_W}{128\pi^2 s_W^3} U_{ia} U_{ja}^* \\ &\quad \times \left\{ \frac{7}{M_{\nu,a}^2 - M_W^2} - \frac{\xi^2}{M_{\nu,a}^2 - \xi M_W^2} \right. \\ &\quad + \left(\frac{\xi^2 M_{\nu,a}^2}{(M_{\nu,a}^2 - \xi M_W^2)^2} - \frac{2\xi^2(1+2\xi)}{(1-\xi)(M_{\nu,a}^2 - \xi M_W^2)} \right) \log \left(\frac{M_{\nu,a}^2}{\xi M_W^2} \right) \\ &\quad - \left(\frac{3(5-9\xi)}{2(1-\xi)(M_{\nu,a}^2 - M_W^2)} + \frac{7(M_{\nu,a}^2 + M_W^2)}{2(M_{\nu,a}^2 - M_W^2)^2} + \frac{4(1-\xi)}{M_W^2} \right) \log \left(\frac{M_{\nu,a}^2}{M_W^2} \right) \right\} \\ &\quad + \frac{e^3 c_W}{64\pi^2 s_W^3} U_{ia} U_{ka}^* U_{kb} U_{jb}^* \\ &\quad \times \left\{ \frac{M_{\nu,a}^2}{M_W^2} \left(\frac{\xi \log \left(\frac{M_{\nu,a}^2}{\xi M_W^2} \right)}{M_{\nu,a}^2 - \xi M_W^2} - \frac{\log \left(\frac{M_{\nu,a}^2}{M_W^2} \right)}{M_{\nu,a}^2 - M_W^2} \right) + \frac{M_{\nu,b}^2}{M_W^2} \left(\frac{\xi \log \left(\frac{M_{\nu,b}^2}{\xi M_W^2} \right)}{M_{\nu,b}^2 - \xi M_W^2} - \frac{\log \left(\frac{M_{\nu,b}^2}{M_W^2} \right)}{M_{\nu,b}^2 - M_W^2} \right) \right\} \end{aligned} \tag{C.19}$$

C.3.3 Box Contributions

For general neutrino mixing matrices, we find two different classes of box contributions: vectorial, lepton number conserving boxes that we will denote $\mathcal{D}_{ij,kl}^{VLL}$, as well as scalar, lepton number violating boxes, which we denote $\mathcal{D}_{ij,kl}^{SLR}$ and vanish in the inverse seesaw

limit in presence of degenerate sterile neutrinos. The full box contributions in the R_ξ gauge can be split into the result in Feynman gauge and the ξ -dependent terms:

$$\begin{aligned}\mathcal{D}_{ij,kl}^{VLL}|_{R_\xi} &= \mathcal{D}_{ij,kl}^{VLL}|_{\text{FG}} + \mathcal{D}_{ij,kl}^{VLL}|_\xi, \\ \mathcal{D}_{ij,kl}^{SLR}|_{R_\xi} &= \mathcal{D}_{ij,kl}^{SLR}|_{\text{FG}} + \mathcal{D}_{ij,kl}^{SLR}|_\xi.\end{aligned}\quad (\text{C.20})$$

(C.21)

We find

$$\begin{aligned}\mathcal{D}_{ij,kl}^{VLL}|_{\text{FG}} &= \frac{e^4}{256\pi^2 s_W^4 M_W^4} \sum_{a,b=1}^n U_{ia} U_{ja}^* U_{kb} U_{lb}^* \frac{1}{(M_{\nu,a}^2 - M_{\nu,b}^2)(M_{\nu,a}^2 - M_W^2)^2(M_{\nu,b}^2 - M_W^2)^2} \\ &\times \left\{ M_{\nu,a}^6 M_{\nu,b}^6 \log \left(\frac{M_{\nu,a}^2}{M_{\nu,b}^2} \right) \right. \\ &- M_W^2 M_{\nu,a}^6 M_{\nu,b}^4 \left(7 + 2 \log \left(\frac{M_{\nu,a}^2}{M_W^2} \right) - 8 \log \left(\frac{M_{\nu,b}^2}{M_W^2} \right) \right) \\ &+ M_W^2 M_{\nu,a}^4 M_{\nu,b}^6 \left(7 + 2 \log \left(\frac{M_{\nu,b}^2}{M_W^2} \right) - 8 \log \left(\frac{M_{\nu,a}^2}{M_W^2} \right) \right) \\ &+ 20 M_W^4 M_{\nu,a}^4 M_{\nu,b}^4 \log \left(\frac{M_{\nu,a}^2}{M_{\nu,b}^2} \right) \\ &+ M_W^4 M_{\nu,a}^2 M_{\nu,b}^2 \left(M_{\nu,a}^4 \left(7 + \log \left(\frac{M_{\nu,a}^2}{M_W^2} \right) \right) - M_{\nu,b}^4 \left(7 + \log \left(\frac{M_{\nu,b}^2}{M_W^2} \right) \right) \right) \\ &- M_W^6 M_{\nu,a}^2 M_{\nu,b}^2 \left(M_{\nu,a}^2 \left(3 + 16 \log \left(\frac{M_{\nu,a}^2}{M_W^2} \right) \right) - M_{\nu,b}^2 \left(3 + 16 \log \left(\frac{M_{\nu,b}^2}{M_W^2} \right) \right) \right) \\ &- 4 M_W^8 \left(M_{\nu,a}^4 \left(1 - \log \left(\frac{M_{\nu,a}^2}{M_W^2} \right) \right) - M_{\nu,b}^4 \left(1 - \log \left(\frac{M_{\nu,b}^2}{M_W^2} \right) \right) \right) \\ &\left. + 4 M_W^{10} (M_{\nu,a}^2 - M_{\nu,b}^2) \right\},\end{aligned}\quad (\text{C.22})$$

$$\begin{aligned}
\mathcal{D}_{ij,kl}^{\text{VLL}}|_{\xi} = & \frac{e^4}{1024\pi^2 s_W^4} \sum_{a,b=1}^n U_{ia} U_{ja}^* U_{kb} U_{lb}^* \\
& \times \left\{ -\frac{4\xi^2 \left(1 - \xi + 6 \log \left(\frac{M_{\nu,a}^2}{\xi M_W^2} \right) \right)}{(1-\xi)(M_{\nu,a}^2 - \xi M_W^2)} - \frac{4\xi^2 \left(1 - \xi + 6 \log \left(\frac{M_{\nu,b}^2}{\xi M_W^2} \right) \right)}{(1-\xi)(M_{\nu,b}^2 - \xi M_W^2)} \right. \\
& + \frac{4\xi^2 M_{\nu,a}^2}{(M_{\nu,a}^2 - \xi M_W^2)^2} \log \left(\frac{M_{\nu,a}^2}{\xi M_W^2} \right) + \frac{4\xi^2 M_{\nu,b}^2}{(M_{\nu,b}^2 - \xi M_W^2)^2} \log \left(\frac{M_{\nu,b}^2}{\xi M_W^2} \right) \\
& - \frac{(7 - 19\xi) \log \left(\frac{M_{\nu,a}^2}{M_W^2} \right) - 14(1-\xi)}{(1-\xi)M_{\nu,a}(M_{\nu,a} - M_W)} - \frac{(7 - 19\xi) \log \left(\frac{M_{\nu,b}^2}{M_W^2} \right) - 14(1-\xi)}{(1-\xi)M_{\nu,b}(M_{\nu,b} - M_W)} \\
& - \frac{(7 - 19\xi) \log \left(\frac{M_{\nu,a}^2}{M_W^2} \right) - 14(1-\xi)}{(1-\xi)M_{\nu,a}(M_{\nu,a} + M_W)} - \frac{(7 - 19\xi) \log \left(\frac{M_{\nu,b}^2}{M_W^2} \right) - 14(1-\xi)}{(1-\xi)M_{\nu,b}(M_{\nu,b} + M_W)} \\
& \left. - \frac{7 \log \left(\frac{M_{\nu,a}^2}{M_W^2} \right)}{(M_{\nu,a} - M_W)^2} - \frac{7 \log \left(\frac{M_{\nu,b}^2}{M_W^2} \right)}{(M_{\nu,b} - M_W)^2} - \frac{7 \log \left(\frac{M_{\nu,a}^2}{M_W^2} \right)}{(M_{\nu,a} + M_W)^2} - \frac{7 \log \left(\frac{M_{\nu,b}^2}{M_W^2} \right)}{(M_{\nu,b} + M_W)^2} \right\}, \tag{C.23}
\end{aligned}$$

$$\begin{aligned}
\mathcal{D}_{jl,ik}^{\text{SLR}}|_{\text{FG}} = & -\frac{e^4}{32\pi^2 s_W^4 M_W^4} \sum_{a,b=1}^n U_{ja}^* U_{la}^* U_{ib} U_{kb} \frac{M_{\nu,a} M_{\nu,b}}{(M_{\nu,a}^2 - M_{\nu,b}^2)(M_{\nu,a}^2 - M_W^2)^2(M_{\nu,b}^2 - M_W^2)^2} \\
& \times \left\{ M_{\nu,a}^6 M_{\nu,b}^4 \left(1 - \log \left(\frac{M_{\nu,b}^2}{M_W^2} \right) \right) - M_{\nu,a}^4 M_{\nu,b}^6 \left(1 - \log \left(\frac{M_{\nu,a}^2}{M_W^2} \right) \right) \right. \\
& - M_W^2 M_{\nu,a}^2 M_{\nu,b}^2 \left(M_{\nu,a}^4 + 4M_{\nu,a}^2 M_{\nu,b}^2 \log \left(\frac{M_{\nu,a}^2}{M_{\nu,b}^2} \right) - M_{\nu,b}^4 \right) \\
& + M_W^4 M_{\nu,a}^4 M_{\nu,b}^2 \left(3 + 5 \log \left(\frac{M_{\nu,a}^2}{M_W^2} \right) - 4 \log \left(\frac{M_{\nu,b}^2}{M_W^2} \right) \right) \\
& - M_W^4 M_{\nu,a}^2 M_{\nu,b}^4 \left(3 + 5 \log \left(\frac{M_{\nu,b}^2}{M_W^2} \right) - 4 \log \left(\frac{M_{\nu,a}^2}{M_W^2} \right) \right) \\
& - 8M_W^6 M_{\nu,a}^2 M_{\nu,b}^2 \log \left(\frac{M_{\nu,a}^2}{M_{\nu,b}^2} \right) \\
& - 2M_W^6 \left(M_{\nu,a}^4 \left(1 + \log \left(\frac{M_{\nu,a}^2}{M_W^2} \right) \right) - M_{\nu,b}^4 \left(1 + \log \left(\frac{M_{\nu,b}^2}{M_W^2} \right) \right) \right) \\
& \left. + 2M_W^8 \left(M_{\nu,a}^2 \left(1 + 2 \log \left(\frac{M_{\nu,a}^2}{M_W^2} \right) \right) - M_{\nu,b}^2 \left(1 + 2 \log \left(\frac{M_{\nu,b}^2}{M_W^2} \right) \right) \right) \right\}, \tag{C.24}
\end{aligned}$$

and

$$\begin{aligned} \mathcal{D}_{jl,ik}^{\text{SLR}}|_{\xi} = & \frac{e^4}{128\pi^2 s_W^4} \sum_{a,b=1}^n U_{ja}^* M_{\nu,a} U_{la}^* U_{ib} M_{\nu,b} U_{kb} & (\text{C.25}) \\ & \times \left\{ -\frac{4\xi^2 \left(1 - 2 \log \left(\frac{M_{\nu,a}^2}{\xi M_W^2} \right) \right)}{M_{\nu,a}^4 - \xi M_{\nu,a}^2 M_W^2} - \frac{4\xi^2 \left(1 - 2 \log \left(\frac{M_{\nu,b}^2}{\xi M_W^2} \right) \right)}{M_{\nu,b}^4 - \xi M_{\nu,b}^2 M_W^2} \right. \\ & + \frac{4\xi^2}{(M_{\nu,a}^2 - \xi M_W^2)^2} \log \left(\frac{M_{\nu,a}^2}{\xi M_W^2} \right) + \frac{4\xi^2}{(M_{\nu,b}^2 - \xi M_W^2)^2} \log \left(\frac{M_{\nu,b}^2}{\xi M_W^2} \right) \\ & + \frac{4}{M_{\nu,a}^2 M_W^2} \left(1 - \xi + 2\xi \log \left(\frac{M_{\nu,a}^2}{\xi M_W^2} \right) - 2 \log \left(\frac{M_{\nu,a}^2}{M_W^2} \right) \right) \\ & + \frac{4}{M_{\nu,b}^2 M_W^2} \left(1 - \xi + 2\xi \log \left(\frac{M_{\nu,b}^2}{\xi M_W^2} \right) - 2 \log \left(\frac{M_{\nu,b}^2}{M_W^2} \right) \right) \\ & + \frac{2 - 5 \log \left(\frac{M_{\nu,a}^2}{M_W^2} \right)}{M_{\nu,a}^3 (M_{\nu,a} + M_W)} + \frac{2 - 5 \log \left(\frac{M_{\nu,b}^2}{M_W^2} \right)}{M_{\nu,b}^3 (M_{\nu,b} + M_W)} \\ & + \frac{2 - 5 \log \left(\frac{M_{\nu,a}^2}{M_W^2} \right)}{M_{\nu,a}^3 (M_{\nu,a} - M_W)} + \frac{2 - 5 \log \left(\frac{M_{\nu,b}^2}{M_W^2} \right)}{M_{\nu,b}^3 (M_{\nu,b} - M_W)} \\ & - \frac{1}{M_{\nu,a}^2 (M_{\nu,a} - M_W)^2} \log \left(\frac{M_{\nu,a}^2}{M_W^2} \right) - \frac{1}{M_{\nu,b}^2 (M_{\nu,b} + M_W)^2} \log \left(\frac{M_{\nu,b}^2}{M_W^2} \right) \\ & - \frac{1}{M_{\nu,b}^2 (M_{\nu,b} - M_W)^2} \log \left(\frac{M_{\nu,b}^2}{M_W^2} \right) - \frac{1}{M_{\nu,a}^2 (M_{\nu,a} + M_W)^2} \log \left(\frac{M_{\nu,a}^2}{M_W^2} \right) \Big\}. & (\text{C.26}) \end{aligned}$$

In the sums $(\mathcal{A}_{ij,kl}^{\text{VLR}} + \mathcal{Z}_{ij,kl}^{\text{VLR}})$ and $(\mathcal{A}_{ij,kl}^{\text{VLL}} + \mathcal{Z}_{ij,kl}^{\text{VLL}} + \mathcal{D}_{ij,kl}^{\text{VLL}})$, which are the relevant contributions to $\ell \rightarrow 3\ell'$ processes in the case of lepton number conservation, the ξ dependence drops out by unitarity of the neutrino mixing matrix ($UU^\dagger = \mathbb{1}$). In \mathcal{D}^{SLR} , the ξ dependence drops out by virtue of Eq. (A.4), which is a consequence of the $SU(2)_L$ invariance of the Lagrangian (see Eq. (2.1)). Note that the structure $U_{ia} U_{ma} U_{mb}^* U_{jb}^*$ in the Z penguin contribution, Eq. (C.18), and the structure $U_{ja}^* U_{la}^* U_{ib} U_{kb}$ in the scalar boxes, Eq. (C.24), arise from lepton number violating contributions. These structures vanish in the inverse seesaw limit (see Eqs. (2.14) and (2.15)) if the sterile neutrino mass splitting is small.

C.4 $\mu \rightarrow e$ Conversion in Nuclei

Next we consider $\mu \rightarrow e$ conversion in nuclei. We define

$$\begin{aligned} \mathcal{M}_{\text{eff}} = & \sum_{q=u,d} (\mathcal{A}_{ij,qq}^{\text{VLR}} + \mathcal{Z}_{ij,qq}^{\text{VLR}}) (\bar{\ell}_i \gamma_\mu P_L \ell_j) (\bar{q} \gamma_\mu P_L q) \\ & + (\mathcal{A}_{ij,qq}^{\text{VLL}} + \mathcal{Z}_{ij,qq}^{\text{VLL}} + \mathcal{D}_{ij,qq}^{\text{VLL}}) (\bar{\ell}_i \gamma_\mu P_L \ell_j) (\bar{q} \gamma_\mu P_R q). & (\text{C.27}) \end{aligned}$$

with $\mathcal{A}_{ij,qq}^{\text{VLL/LR}}$, $\mathcal{Z}_{ij,qq}^{\text{VLL/LR}}$ and $\mathcal{D}_{ij,qq}^{\text{VLL}}$ as defined in the following subsections.

Taking the sum in Eq. (C.27) and the quark flavour-diagonal limit of the box contributions, $\mathcal{D}_{ij,qq}^{\text{VAB}} \equiv \mathcal{D}_{ij,q_k q_l}^{\text{VAB}} \delta_{kl}$, where $q = u, d$, we obtain the leading contribution to $\mu \rightarrow e$ conversion, which is given in Eq. (4.24).

C.4.1 Photon Penguin Contributions

The photon penguin contributions to $\mu \rightarrow e$ conversion in nuclei are of the same form as those contributing four lepton processes.

$$\begin{aligned}\mathcal{A}_{ij,uu}^{\text{VLL}} &= \mathcal{A}_{ij,uu}^{\text{VLR}} = Q_u \mathcal{A}_{ij}^{\text{VL}} = \frac{2}{3} \mathcal{A}_{ij}^{\text{VL}} \\ \mathcal{A}_{ij,dd}^{\text{VLL}} &= \mathcal{A}_{ij,dd}^{\text{VLR}} = Q_d \mathcal{A}_{ij}^{\text{VL}} = -\frac{1}{3} \mathcal{A}_{ij}^{\text{VL}}\end{aligned}\quad (\text{C.28})$$

with the form factor $\mathcal{A}_{ij}^{\text{VL}}$ given in Eq. (C.15).

C.4.2 Z Penguin Contributions

Similarly, the Z boson penguins lead to the contributions

$$\begin{aligned}\mathcal{Z}_{ij,qq}^{\text{VLL}} &= \mathcal{Z}_{ij}^L g_{\text{SM}}^{qL} \\ \mathcal{Z}_{ij,qq}^{\text{VLR}} &= \mathcal{Z}_{ij}^L g_{\text{SM}}^{qR}\end{aligned}\quad (\text{C.29})$$

where g_{SM}^{qL} , and g_{SM}^{qR} , $q = u, d$, are the SM Z boson couplings to left- and right-handed up- and down-type quarks, which are given in Eq. (B.12), and \mathcal{Z}_{ij}^L is the form factor given in Eq. (C.16).

C.4.3 Box Contributions

Since to order v^2/M_R^2 there are no box diagrams contributing to the matching onto $\mathcal{O}_{\ell q}^{(1)}$ and $\mathcal{O}_{\ell q}^{(3)}$, the only contributions are those given in Eq. (B.13). Neglecting the possible flavour effects on the quark line, we define

$$\mathcal{D}_{ij,qq}^{\text{VAB}} \equiv \mathcal{D}_{ij,q_k q_l}^{\text{VAB}} \delta_{kl} = d_{ij,q_k q_l}^{\text{VAB}} \delta_{kl}, \quad q = u, d. \quad (\text{C.30})$$

D Integrals

Assuming the hierarchy $M_W^2, M_Z^2, q_Z^2 \sim v^2 \ll M_R^2$, $|M_{R,a} - M_{R,b}| \ll |M_{R,a} + M_{R,b}|$, we can use the following expansions of the master integrals:

$$\begin{aligned}
B_0(q_Z^2; 0, M_R) &= 1 + \frac{q_Z^2}{2M_R^2} + \frac{1}{\varepsilon} + \log\left(\frac{\mu^2}{M_R^2}\right) \\
B_0(q_Z^2; M_W, M_W) &= 2 + \frac{1}{\varepsilon} + \log\left(\frac{\mu^2}{M_W^2}\right) - \arctan\left(\frac{\sqrt{q_Z^2(4M_W^2 - q_Z^2)}}{2M_W^2 - q_Z^2}\right) \sqrt{4\frac{M_W^2}{q_Z^2} - 1} \\
B_0(q_Z^2; M_{R,a}, M_{R,b}) &= 1 + \frac{1}{\varepsilon} + \frac{1}{2} \log\left(\frac{\mu^2}{M_{R,a}^2}\right) + \frac{1}{2} \log\left(\frac{\mu^2}{M_{R,b}^2}\right) - \frac{M_{R,a}^2 + M_{\nu,b}^2}{2(M_{R,a}^2 - M_{\nu,b}^2)} \log\left(\frac{M_{R,a}^2}{M_{R,b}^2}\right) \\
C_0(0, 0, q_Z^2, M_R, M_W, 0) &= -\frac{1}{2M_R^4} \left(M_W^2 - q_Z^2 + (2(M_R^2 + M_W^2) + q_Z^2) \log\left(\frac{M_R^2}{M_W^2}\right) \right) \\
C_0(0, 0, q_Z^2, M_W, M_R, M_W) &= \\
&= -\frac{1}{36M_R^6} \left\{ 36M_R^4 - 9M_R^2(q_Z^2 - 4M_W^2) + 4(q_Z^2 - 3M_W^2)^2 \right. \\
&\quad - 6(6M_R^4 + 3M_R^2(4M_W^2 - q_Z^2) + 2(q_Z^2 - 3M_W^2)^2) \log\left(\frac{M_R^2}{M_W^2}\right) \\
&\quad + \left(6(M_R^4 + M_R^2M_W^2 + M_W^4) - q_Z^2(3M_R^2 + 8M_W^2) + 2q_Z^4 \right) \\
&\quad \times 6 \arctan\left(\frac{\sqrt{q_Z^2(4M_W^2 - q_Z^2)}}{2M_W^2 - q_Z^2}\right) \sqrt{\frac{4M_W^2}{q_Z^2} - 1} \Big\} \\
C_0(0, 0, q_Z^2, M_{R,a}, M_W, M_{R,b}) &= -\frac{1}{M_{R,a}^2 - M_{R,b}^2} \log\left(\frac{M_{R,a}^2}{M_{R,b}^2}\right)
\end{aligned} \tag{D.1}$$

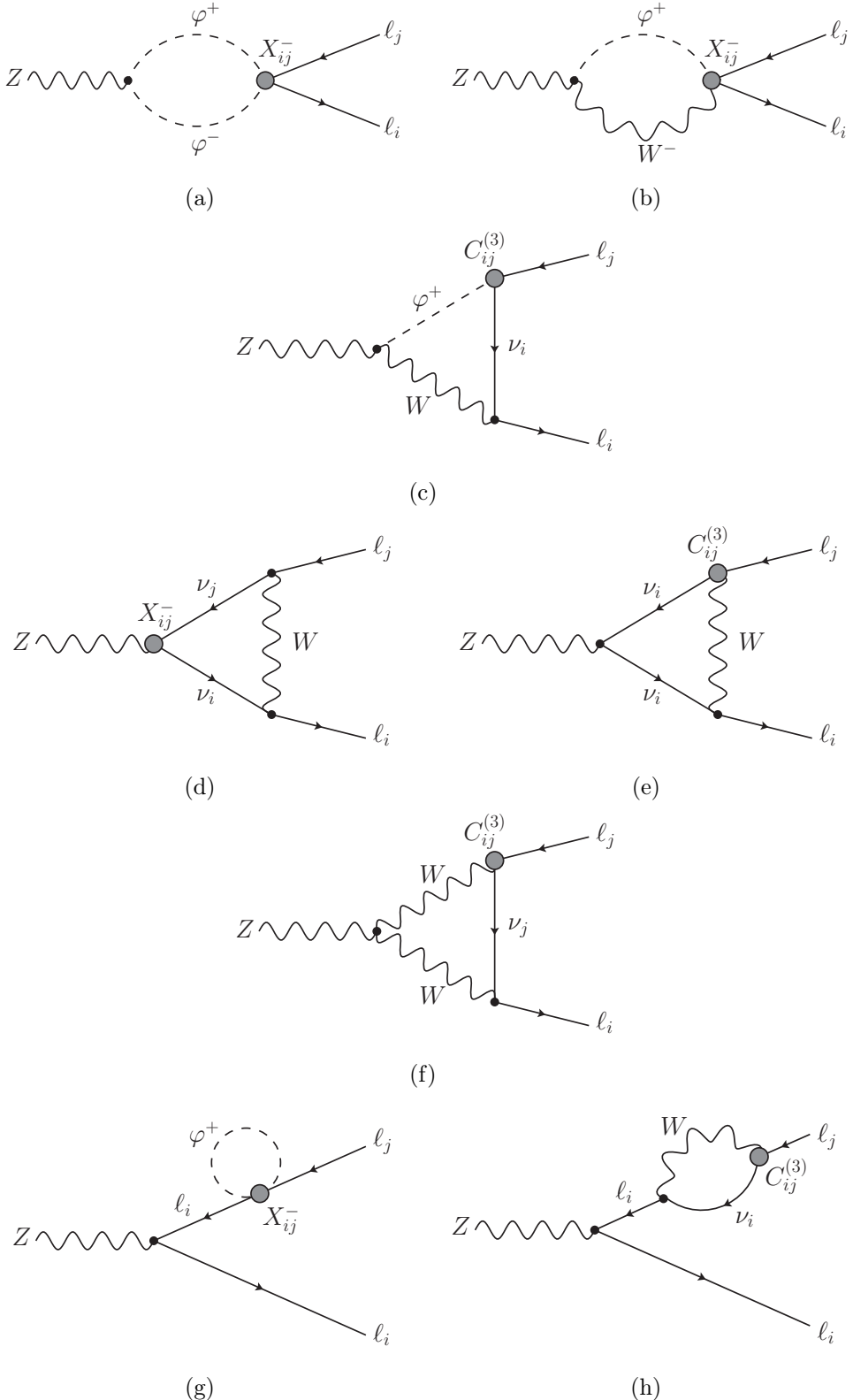


Figure 16: Insertions of X_{ij}^+ , X_{ij}^- and $C_{\varphi\ell,ij}^{(3)}$ in loop diagrams contributing to the process $Z \rightarrow \ell\ell'$.

References

- [1] R. N. Mohapatra and P. B. Pal, *Massive neutrinos in physics and astrophysics. Second edition*, vol. 60. 1998.
- [2] P. Minkowski, $\mu \rightarrow e\gamma$ at a Rate of One Out of 10^9 Muon Decays?, *Phys. Lett. B* **67** (1977) 421.
- [3] M. Gell-Mann, P. Ramond and R. Slansky, *Complex Spinors and Unified Theories*, *Conf. Proc. C* **790927** (1979) 315 [[1306.4669](#)].
- [4] T. Yanagida, *Horizontal gauge symmetry and masses of neutrinos*, *Conf. Proc. C* **7902131** (1979) 95.
- [5] R. N. Mohapatra and G. Senjanovic, *Neutrino Mass and Spontaneous Parity Nonconservation*, *Phys. Rev. Lett.* **44** (1980) 912.
- [6] J. Schechter and J. W. F. Valle, *Neutrino Masses in $SU(2) \times U(1)$ Theories*, *Phys. Rev. D* **22** (1980) 2227.
- [7] F. del Aguila, J. A. Aguilar-Saavedra and R. Pittau, *Heavy neutrino signals at large hadron colliders*, *JHEP* **10** (2007) 047 [[hep-ph/0703261](#)].
- [8] J. Kersten and A. Y. Smirnov, *Right-Handed Neutrinos at CERN LHC and the Mechanism of Neutrino Mass Generation*, *Phys. Rev. D* **76** (2007) 073005 [[0705.3221](#)].
- [9] F. F. Deppisch, P. S. Bhupal Dev and A. Pilaftsis, *Neutrinos and Collider Physics*, *New J. Phys.* **17** (2015) 075019 [[1502.06541](#)].
- [10] A. Atre, T. Han, S. Pascoli and B. Zhang, *The Search for Heavy Majorana Neutrinos*, *JHEP* **05** (2009) 030 [[0901.3589](#)].
- [11] S. Antusch and O. Fischer, *Non-unitarity of the leptonic mixing matrix: Present bounds and future sensitivities*, *JHEP* **10** (2014) 094 [[1407.6607](#)].
- [12] S. Banerjee, P. S. B. Dev, A. Ibarra, T. Mandal and M. Mitra, *Prospects of Heavy Neutrino Searches at Future Lepton Colliders*, *Phys. Rev. D* **92** (2015) 075002 [[1503.05491](#)].
- [13] S. Antusch, E. Cazzato and O. Fischer, *Displaced vertex searches for sterile neutrinos at future lepton colliders*, *JHEP* **12** (2016) 007 [[1604.02420](#)].
- [14] S. Pascoli, R. Ruiz and C. Weiland, *Heavy neutrinos with dynamic jet vetoes: multilepton searches at $\sqrt{s} = 14, 27$, and 100 TeV*, *JHEP* **06** (2019) 049 [[1812.08750](#)].
- [15] S. Chakraborty, M. Mitra and S. Shil, *Fat Jet Signature of a Heavy Neutrino at Lepton Collider*, *Phys. Rev. D* **100** (2019) 015012 [[1810.08970](#)].
- [16] A. Das, S. Jana, S. Mandal and S. Nandi, *Probing right handed neutrinos at the LHeC and lepton colliders using fat jet signatures*, *Phys. Rev. D* **99** (2019) 055030 [[1811.04291](#)].
- [17] K. Mękała, J. Reuter and A. F. Żarnecki, *Heavy neutrinos at future linear e^+e^- colliders*, *JHEP* **06** (2022) 010 [[2202.06703](#)].
- [18] M. Fukugita and T. Yanagida, *Baryogenesis Without Grand Unification*, *Phys. Lett. B* **174** (1986) 45.
- [19] S. Davidson, E. Nardi and Y. Nir, *Leptogenesis*, *Phys. Rept.* **466** (2008) 105 [[0802.2962](#)].
- [20] A. Boyarsky, O. Ruchayskiy and M. Shaposhnikov, *The Role of sterile neutrinos in cosmology and astrophysics*, *Ann. Rev. Nucl. Part. Sci.* **59** (2009) 191 [[0901.0011](#)].

- [21] S. Antusch, E. Cazzato, M. Drewes, O. Fischer, B. Garbrecht, D. Gueter et al., *Probing Leptogenesis at Future Colliders*, *JHEP* **09** (2018) 124 [[1710.03744](#)].
- [22] S. Dodelson and L. M. Widrow, *Sterile-neutrinos as dark matter*, *Phys. Rev. Lett.* **72** (1994) 17 [[hep-ph/9303287](#)].
- [23] X.-D. Shi and G. M. Fuller, *A New dark matter candidate: Nonthermal sterile neutrinos*, *Phys. Rev. Lett.* **82** (1999) 2832 [[astro-ph/9810076](#)].
- [24] T. Asaka, S. Blanchet and M. Shaposhnikov, *The nuMSM, dark matter and neutrino masses*, *Phys. Lett. B* **631** (2005) 151 [[hep-ph/0503065](#)].
- [25] M. Shaposhnikov and I. Tkachev, *The nuMSM, inflation, and dark matter*, *Phys. Lett. B* **639** (2006) 414 [[hep-ph/0604236](#)].
- [26] A. Ilakovac and A. Pilaftsis, *Flavor violating charged lepton decays in seesaw-type models*, *Nucl. Phys. B* **437** (1995) 491 [[hep-ph/9403398](#)].
- [27] D. Wyler and L. Wolfenstein, *Massless Neutrinos in Left-Right Symmetric Models*, *Nucl. Phys. B* **218** (1983) 205.
- [28] R. N. Mohapatra and J. W. F. Valle, *Neutrino Mass and Baryon Number Nonconservation in Superstring Models*, *Phys. Rev. D* **34** (1986) 1642.
- [29] G. C. Branco, W. Grimus and L. Lavoura, *The Seesaw Mechanism in the Presence of a Conserved Lepton Number*, *Nucl. Phys. B* **312** (1989) 492.
- [30] M. C. Gonzalez-Garcia and J. W. F. Valle, *Fast Decaying Neutrinos and Observable Flavor Violation in a New Class of Majoron Models*, *Phys. Lett. B* **216** (1989) 360.
- [31] R. Barbieri, T. Hambye and A. Romanino, *Natural relations among physical observables in the neutrino mass matrix*, *JHEP* **03** (2003) 017 [[hep-ph/0302118](#)].
- [32] M. Raidal, A. Strumia and K. Turzynski, *Low-scale standard supersymmetric leptogenesis*, *Phys. Lett. B* **609** (2005) 351 [[hep-ph/0408015](#)].
- [33] M. Shaposhnikov, *A Possible symmetry of the nuMSM*, *Nucl. Phys. B* **763** (2007) 49 [[hep-ph/0605047](#)].
- [34] A. Abada, C. Biggio, F. Bonnet, M. B. Gavela and T. Hambye, *Low energy effects of neutrino masses*, *JHEP* **12** (2007) 061 [[0707.4058](#)].
- [35] T. Asaka and S. Blanchet, *Leptogenesis with an almost conserved lepton number*, *Phys. Rev. D* **78** (2008) 123527 [[0810.3015](#)].
- [36] M. B. Gavela, T. Hambye, D. Hernandez and P. Hernandez, *Minimal Flavour Seesaw Models*, *JHEP* **09** (2009) 038 [[0906.1461](#)].
- [37] S. Weinberg, *Baryon and Lepton Nonconserving Processes*, *Phys. Rev. Lett.* **43** (1979) 1566.
- [38] R. N. Mohapatra, *Mechanism for Understanding Small Neutrino Mass in Superstring Theories*, *Phys. Rev. Lett.* **56** (1986) 561.
- [39] J. Bernabeu, A. Santamaria, J. Vidal, A. Mendez and J. W. F. Valle, *Lepton Flavor Nonconservation at High-Energies in a Superstring Inspired Standard Model*, *Phys. Lett. B* **187** (1987) 303.
- [40] B. W. Lee and R. E. Shrock, *Natural Suppression of Symmetry Violation in Gauge Theories: Muon - Lepton and Electron Lepton Number Nonconservation*, *Phys. Rev. D* **16** (1977) 1444.

- [41] R. E. Shrock, *New Tests For, and Bounds On, Neutrino Masses and Lepton Mixing*, *Phys. Lett. B* **96** (1980) 159.
- [42] R. E. Shrock, *General Theory of Weak Leptonic and Semileptonic Decays. 1. Leptonic Pseudoscalar Meson Decays, with Associated Tests For, and Bounds on, Neutrino Masses and Lepton Mixing*, *Phys. Rev. D* **24** (1981) 1232.
- [43] R. E. Shrock, *General Theory of Weak Processes Involving Neutrinos. 2. Pure Leptonic Decays*, *Phys. Rev. D* **24** (1981) 1275.
- [44] P. Langacker and D. London, *Mixing Between Ordinary and Exotic Fermions*, *Phys. Rev. D* **38** (1988) 886.
- [45] S. M. Bilenky and C. Giunti, *Seesaw type mixing and muon-neutrino \rightarrow tau-neutrino oscillations*, *Phys. Lett. B* **300** (1993) 137 [[hep-ph/9211269](#)].
- [46] E. Nardi, E. Roulet and D. Tommasini, *Limits on neutrino mixing with new heavy particles*, *Phys. Lett. B* **327** (1994) 319 [[hep-ph/9402224](#)].
- [47] D. Tommasini, G. Barenboim, J. Bernabeu and C. Jarlskog, *Nondecoupling of heavy neutrinos and lepton flavor violation*, *Nucl. Phys. B* **444** (1995) 451 [[hep-ph/9503228](#)].
- [48] S. Bergmann and A. Kagan, *Z - induced FCNCs and their effects on neutrino oscillations*, *Nucl. Phys. B* **538** (1999) 368 [[hep-ph/9803305](#)].
- [49] W. Loinaz, N. Okamura, T. Takeuchi and L. C. R. Wijewardhana, *The NuTeV anomaly, neutrino mixing, and a heavy Higgs boson*, *Phys. Rev. D* **67** (2003) 073012 [[hep-ph/0210193](#)].
- [50] W. Loinaz, N. Okamura, S. Rayyan, T. Takeuchi and L. C. R. Wijewardhana, *Quark lepton unification and lepton flavor nonconservation from a TeV scale seesaw neutrino mass texture*, *Phys. Rev. D* **68** (2003) 073001 [[hep-ph/0304004](#)].
- [51] W. Loinaz, N. Okamura, S. Rayyan, T. Takeuchi and L. C. R. Wijewardhana, *The NuTeV anomaly, lepton universality, and nonuniversal neutrino gauge couplings*, *Phys. Rev. D* **70** (2004) 113004 [[hep-ph/0403306](#)].
- [52] S. Antusch, C. Biggio, E. Fernandez-Martinez, M. B. Gavela and J. Lopez-Pavon, *Unitarity of the Leptonic Mixing Matrix*, *JHEP* **10** (2006) 084 [[hep-ph/0607020](#)].
- [53] S. Antusch, J. P. Baumann and E. Fernandez-Martinez, *Non-Standard Neutrino Interactions with Matter from Physics Beyond the Standard Model*, *Nucl. Phys. B* **810** (2009) 369 [[0807.1003](#)].
- [54] C. Biggio, *The Contribution of fermionic seesaws to the anomalous magnetic moment of leptons*, *Phys. Lett. B* **668** (2008) 378 [[0806.2558](#)].
- [55] R. Alonso, M. Dhen, M. B. Gavela and T. Hambye, *Muon conversion to electron in nuclei in type-I seesaw models*, *JHEP* **01** (2013) 118 [[1209.2679](#)].
- [56] A. Abada, D. Das, A. M. Teixeira, A. Vicente and C. Weiland, *Tree-level lepton universality violation in the presence of sterile neutrinos: impact for R_K and R_π* , *JHEP* **02** (2013) 048 [[1211.3052](#)].
- [57] E. Akhmedov, A. Kartavtsev, M. Lindner, L. Michaels and J. Smirnov, *Improving Electro-Weak Fits with TeV-scale Sterile Neutrinos*, *JHEP* **05** (2013) 081 [[1302.1872](#)].
- [58] L. Basso, O. Fischer and J. J. van der Bij, *Precision tests of unitarity in leptonic mixing*, *EPL* **105** (2014) 11001 [[1310.2057](#)].

- [59] A. Abada, A. M. Teixeira, A. Vicente and C. Weiland, *Sterile neutrinos in leptonic and semileptonic decays*, *JHEP* **02** (2014) 091 [[1311.2830](#)].
- [60] S. Antusch and O. Fischer, *Testing sterile neutrino extensions of the Standard Model at future lepton colliders*, *JHEP* **05** (2015) 053 [[1502.05915](#)].
- [61] A. Abada, V. De Romeri and A. M. Teixeira, *Impact of sterile neutrinos on nuclear-assisted CLFV processes*, *JHEP* **02** (2016) 083 [[1510.06657](#)].
- [62] E. Fernandez-Martinez, J. Hernandez-Garcia and J. Lopez-Pavon, *Global constraints on heavy neutrino mixing*, *JHEP* **08** (2016) 033 [[1605.08774](#)].
- [63] M. Chrzaszcz, M. Drewes, T. E. Gonzalo, J. Harz, S. Krishnamurthy and C. Weniger, *A frequentist analysis of three right-handed neutrinos with GAMBIT*, *Eur. Phys. J. C* **80** (2020) 569 [[1908.02302](#)].
- [64] A. Abada and T. Toma, *Electric Dipole Moments of Charged Leptons with Sterile Fermions*, *JHEP* **02** (2016) 174 [[1511.03265](#)].
- [65] A. Abada and T. Toma, *Electron electric dipole moment in Inverse Seesaw models*, *JHEP* **08** (2016) 079 [[1605.07643](#)].
- [66] P. D. Bolton, F. F. Deppisch and P. S. Bhupal Dev, *Neutrinoless double beta decay versus other probes of heavy sterile neutrinos*, *JHEP* **03** (2020) 170 [[1912.03058](#)].
- [67] A. M. Coutinho, A. Crivellin and C. A. Manzari, *Global Fit to Modified Neutrino Couplings and the Cabibbo-Angle Anomaly*, *Phys. Rev. Lett.* **125** (2020) 071802 [[1912.08823](#)].
- [68] A. Crivellin, F. Kirk, C. A. Manzari and M. Montull, *Global Electroweak Fit and Vector-Like Leptons in Light of the Cabibbo Angle Anomaly*, *JHEP* **12** (2020) 166 [[2008.01113](#)].
- [69] M. J. Herrero, X. Marcano, R. Morales and A. Szynkman, *One-loop effective LFV $Zl_k l_m$ vertex from heavy neutrinos within the mass insertion approximation*, *Eur. Phys. J. C* **78** (2018) 815 [[1807.01698](#)].
- [70] R. Coy and M. Frigerio, *Effective approach to lepton observables: the seesaw case*, *Phys. Rev. D* **99** (2019) 095040 [[1812.03165](#)].
- [71] C. Hagedorn, J. Kriewald, J. Orloff and A. M. Teixeira, *Flavour and CP symmetries in the inverse seesaw*, *Eur. Phys. J. C* **82** (2022) 194 [[2107.07537](#)].
- [72] D. Zhang and S. Zhou, *Radiative decays of charged leptons in the seesaw effective field theory with one-loop matching*, *Phys. Lett. B* **819** (2021) 136463 [[2102.04954](#)].
- [73] A. Abada, J. Kriewald and A. M. Teixeira, *On the role of leptonic CPV phases in cLFV observables*, *Eur. Phys. J. C* **81** (2021) 1016 [[2107.06313](#)].
- [74] A. Abada, J. Kriewald, E. Pinsard, S. Rosauro-Alcaraz and A. M. Teixeira, *LFV Higgs and Z-boson decays: leptonic CPV phases and CP asymmetries*, [2207.10109](#).
- [75] K. A. U. Calderón, I. Timiryasov and O. Ruchayskiy, *Improved constraints and the prospects of detecting TeV to PeV scale Heavy Neutral Leptons*, [2206.04540](#).
- [76] A. Broncano, M. B. Gavela and E. E. Jenkins, *The Effective Lagrangian for the seesaw model of neutrino mass and leptogenesis*, *Phys. Lett. B* **552** (2003) 177 [[hep-ph/0210271](#)].
- [77] V. Cirigliano, B. Grinstein, G. Isidori and M. B. Wise, *Minimal flavor violation in the lepton sector*, *Nucl. Phys. B* **728** (2005) 121 [[hep-ph/0507001](#)].

- [78] S. Antusch, J. Kersten, M. Lindner, M. Ratz and M. A. Schmidt, *Running neutrino mass parameters in see-saw scenarios*, *JHEP* **03** (2005) 024 [[hep-ph/0501272](#)].
- [79] A. de Gouvea and J. Jenkins, *A Survey of Lepton Number Violation Via Effective Operators*, *Phys. Rev. D* **77** (2008) 013008 [[0708.1344](#)].
- [80] J. Alcaide, S. Banerjee, M. Chala and A. Titov, *Probes of the Standard Model effective field theory extended with a right-handed neutrino*, *JHEP* **08** (2019) 031 [[1905.11375](#)].
- [81] J. De Vries, H. K. Dreiner, J. Y. Günther, Z. S. Wang and G. Zhou, *Long-lived Sterile Neutrinos at the LHC in Effective Field Theory*, *JHEP* **03** (2021) 148 [[2010.07305](#)].
- [82] A. Aparici, K. Kim, A. Santamaria and J. Wudka, *Right-handed neutrino magnetic moments*, *Phys. Rev. D* **80** (2009) 013010 [[0904.3244](#)].
- [83] D. Zhang and S. Zhou, *Complete one-loop matching of the type-I seesaw model onto the Standard Model effective field theory*, *JHEP* **09** (2021) 163 [[2107.12133](#)].
- [84] X. Li, D. Zhang and S. Zhou, *One-loop matching of the type-II seesaw model onto the Standard Model effective field theory*, *JHEP* **04** (2022) 038 [[2201.05082](#)].
- [85] B. Wolff, *Mesure du rapport $|\nu_{00}|e^{i\phi_{00}}$ des amplitudes de désintégration du K_L^0 et du K_S^0 dans le mode $2\pi^0$, du rapport de branchemet du K_L^0 en 2γ et d'une limite supérieure du rapport de branchemet du K_S^0 en 2γ* , other thesis, Paris U., 1971.
- [86] N. D. Christensen and C. Duhr, *FeynRules - Feynman rules made easy*, *Comput. Phys. Commun.* **180** (2009) 1614 [[0806.4194](#)].
- [87] T. Hahn, *Generating Feynman diagrams and amplitudes with FeynArts 3*, *Comput. Phys. Commun.* **140** (2001) 418 [[hep-ph/0012260](#)].
- [88] H. H. Patel, *Package-X: A Mathematica package for the analytic calculation of one-loop integrals*, *Comput. Phys. Commun.* **197** (2015) 276 [[1503.01469](#)].
- [89] H. H. Patel, *Package-X 2.0: A Mathematica package for the analytic calculation of one-loop integrals*, *Comput. Phys. Commun.* **218** (2017) 66 [[1612.00009](#)].
- [90] A. Denner, S. Dittmaier and L. Hofer, *Collier: a fortran-based Complex One-Loop Library in Extended Regularizations*, *Comput. Phys. Commun.* **212** (2017) 220 [[1604.06792](#)].
- [91] B. Grzadkowski, M. Iskrzynski, M. Misiak and J. Rosiek, *Dimension-Six Terms in the Standard Model Lagrangian*, *JHEP* **10** (2010) 085 [[1008.4884](#)].
- [92] E. E. Jenkins, A. V. Manohar and M. Trott, *Renormalization Group Evolution of the Standard Model Dimension Six Operators I: Formalism and lambda Dependence*, *JHEP* **10** (2013) 087 [[1308.2627](#)].
- [93] W. Dekens and P. Stoffer, *Low-energy effective field theory below the electroweak scale: matching at one loop*, *JHEP* **10** (2019) 197 [[1908.05295](#)].
- [94] A. Crivellin, S. Davidson, G. M. Pruna and A. Signer, *Renormalisation-group improved analysis of $\mu \rightarrow e$ processes in a systematic effective-field-theory approach*, *JHEP* **05** (2017) 117 [[1702.03020](#)].
- [95] E. E. Jenkins, A. V. Manohar and P. Stoffer, *Low-Energy Effective Field Theory below the Electroweak Scale: Anomalous Dimensions*, *JHEP* **01** (2018) 084 [[1711.05270](#)].
- [96] HFLAV collaboration, *Averages of b-hadron, c-hadron, and τ -lepton properties as of 2018*, *Eur. Phys. J. C* **81** (2021) 226 [[1909.12524](#)].

- [97] S. B. et al.", "Hflav-tau winter 2022 report."
<https://hflav-eos.web.cern.ch/hflav-eos/tau/winter-2022/>, June, 2022.
- [98] R. Decker and M. Finkemeier, *Radiative corrections to the decay tau → pi (K) tau-neutrino. 2*, *Phys. Lett. B* **334** (1994) 199.
- [99] R. Decker and M. Finkemeier, *Short and long distance effects in the decay tau → pi tau-neutrino (gamma)*, *Nucl. Phys. B* **438** (1995) 17 [[hep-ph/9403385](#)].
- [100] R. Decker and M. Finkemeier, *Radiative corrections to the decay tau → pi tau-neutrino*, *Nucl. Phys. B Proc. Suppl.* **40** (1995) 453 [[hep-ph/9411316](#)].
- [101] W. J. Marciano and A. Sirlin, *Radiative corrections to pi(lepton 2) decays*, *Phys. Rev. Lett.* **71** (1993) 3629.
- [102] A. Pich, *Precision Tau Physics*, *Prog. Part. Nucl. Phys.* **75** (2014) 41 [[1310.7922](#)].
- [103] BELLE-II collaboration, *The Belle II Physics Book*, *PTEP* **2019** (2019) 123C01 [[1808.10567](#)].
- [104] M. Finkemeier, *Radiative corrections to pi(l2) and K(l2) decays*, *Phys. Lett. B* **387** (1996) 391 [[hep-ph/9505434](#)].
- [105] V. Cirigliano and I. Rosell, *Two-loop effective theory analysis of pi (K) → e anti-nu/e [gamma] branching ratios*, *Phys. Rev. Lett.* **99** (2007) 231801 [[0707.3439](#)].
- [106] NA62 collaboration, *Precision Measurement of the Ratio of the Charged Kaon Leptonic Decay Rates*, *Phys. Lett. B* **719** (2013) 326 [[1212.4012](#)].
- [107] KLOE collaboration, *Precise measurement of $\Gamma(K \rightarrow e\nu(\gamma))/\Gamma(K \rightarrow \mu\nu(\gamma))$ and study of $K \rightarrow e\nu\gamma$* , *Eur. Phys. J. C* **64** (2009) 627 [[0907.3594](#)].
- [108] JPARC E36 collaboration, *Measurement of the $\Gamma(K^+ \rightarrow e^+\nu)/\Gamma(K^+ \rightarrow \mu^+\nu)$ branching ratio using stopped positive kaons at J-PARC*, *PoS HQL2018* (2018) 032.
- [109] PiENU collaboration, *Improved Measurement of the $\pi \rightarrow e\nu$ Branching Ratio*, *Phys. Rev. Lett.* **115** (2015) 071801 [[1506.05845](#)].
- [110] PEN collaboration, *PEN experiment: a precise test of lepton universality*, in *13th Conference on the Intersections of Particle and Nuclear Physics*, 11, 2018, [1812.00782](#).
- [111] V. Cirigliano, G. Ecker, H. Neufeld, A. Pich and J. Portoles, *Kaon Decays in the Standard Model*, *Rev. Mod. Phys.* **84** (2012) 399 [[1107.6001](#)].
- [112] FLAVIANNET WORKING GROUP ON KAON DECAYS collaboration, *An Evaluation of $|V_{us}|$ and precise tests of the Standard Model from world data on leptonic and semileptonic kaon decays*, *Eur. Phys. J. C* **69** (2010) 399 [[1005.2323](#)].
- [113] ALEPH, DELPHI, L3, OPAL, LEP ELECTROWEAK collaboration, *Electroweak Measurements in Electron-Positron Collisions at W-Boson-Pair Energies at LEP*, *Phys. Rept.* **532** (2013) 119 [[1302.3415](#)].
- [114] A. Filipuzzi, J. Portoles and M. Gonzalez-Alonso, *$U(2)^5$ flavor symmetry and lepton universality violation in $W \rightarrow \tau\nu_\tau$* , *Phys. Rev. D* **85** (2012) 116010 [[1203.2092](#)].
- [115] PARTICLE DATA GROUP collaboration, *Review of Particle Physics*, *PTEP* **2020** (2020) 083C01.
- [116] *The International Linear Collider Technical Design Report - Volume 2: Physics*, [1306.6352](#).
- [117] CLIC collaboration, *The CLIC Potential for New Physics*, [1812.02093](#).

- [118] FCC collaboration, *FCC Physics Opportunities: Future Circular Collider Conceptual Design Report Volume 1*, *Eur. Phys. J. C* **79** (2019) 474.
- [119] FCC collaboration, *FCC-ee: The Lepton Collider: Future Circular Collider Conceptual Design Report Volume 2*, *Eur. Phys. J. ST* **228** (2019) 261.
- [120] ALEPH collaboration, *Determination of the Number of Light Neutrino Species*, *Phys. Lett. B* **231** (1989) 519.
- [121] ALEPH, DELPHI, L3, OPAL, SLD, LEP ELECTROWEAK WORKING GROUP, SLD ELECTROWEAK GROUP, SLD HEAVY FLAVOUR GROUP collaboration, *Precision electroweak measurements on the Z resonance*, *Phys. Rept.* **427** (2006) 257 [[hep-ex/0509008](#)].
- [122] ATLAS collaboration, *Search for the lepton flavor violating decay Z → eμ in pp collisions at \sqrt{s} TeV with the ATLAS detector*, *Phys. Rev. D* **90** (2014) 072010 [[1408.5774](#)].
- [123] ATLAS collaboration, *Search for lepton-flavor-violation in Z-boson decays with τ-leptons with the ATLAS detector*, *Phys. Rev. Lett.* **127** (2022) 271801 [[2105.12491](#)].
- [124] M. Dam, “Tau physics at the fcc, 15th workshop on tau physics.” <https://indico.cern.ch/event/632562/>, 2018.
- [125] CEPC STUDY GROUP collaboration, *CEPC Conceptual Design Report: Volume 2 - Physics & Detector*, [1811.10545](#).
- [126] A. Crivellin, M. Hoferichter and P. Schmidt-Wellenburg, *Combined explanations of $(g-2)_{\mu,e}$ and implications for a large muon EDM*, *Phys. Rev. D* **98** (2018) 113002 [[1807.11484](#)].
- [127] MEG collaboration, *Search for the lepton flavour violating decay $\mu^+ \rightarrow e^+ \gamma$ with the full dataset of the MEG experiment*, *Eur. Phys. J. C* **76** (2016) 434 [[1605.05081](#)].
- [128] BABAR collaboration, *Searches for Lepton Flavor Violation in the Decays $\tau^{+-} \rightarrow e^{+-}$ gamma and $\tau^{+-} \rightarrow \mu^{+-}$ gamma*, *Phys. Rev. Lett.* **104** (2010) 021802 [[0908.2381](#)].
- [129] BELLE collaboration, *Search for lepton-flavor-violating tau-lepton decays to $\ell\gamma$ at Belle*, *JHEP* **10** (2021) 19 [[2103.12994](#)].
- [130] MEG II collaboration, *The design of the MEG II experiment*, *Eur. Phys. J. C* **78** (2018) 380 [[1801.04688](#)].
- [131] SINDRUM collaboration, *Search for the Decay $\mu^+ \rightarrow e^+ e^+ e^-$* , *Nucl. Phys. B* **299** (1988) 1.
- [132] K. Hayasaka et al., *Search for Lepton Flavor Violating Tau Decays into Three Leptons with 719 Million Produced Tau+Tau- Pairs*, *Phys. Lett. B* **687** (2010) 139 [[1001.3221](#)].
- [133] A. Blondel et al., *Research Proposal for an Experiment to Search for the Decay $\mu \rightarrow eee$* , [1301.6113](#).
- [134] MU3E collaboration, *Status of the Mu3e Experiment at PSI*, *EPJ Web Conf.* **118** (2016) 01028 [[1605.02906](#)].
- [135] A. Cerri et al., *Report from Working Group 4: Opportunities in Flavour Physics at the HL-LHC and HE-LHC*, *CERN Yellow Rep. Monogr.* **7** (2019) 867 [[1812.07638](#)].
- [136] R. Kitano, M. Koike and Y. Okada, *Detailed calculation of lepton flavor violating muon electron conversion rate for various nuclei*, *Phys. Rev. D* **66** (2002) 096002 [[hep-ph/0203110](#)].

- [137] T. Suzuki, D. F. Measday and J. P. Roalsvig, *Total Nuclear Capture Rates for Negative Muons*, *Phys. Rev. C* **35** (1987) 2212.
- [138] SINDRUM II collaboration, *A Search for muon to electron conversion in muonic gold*, *Eur. Phys. J. C* **47** (2006) 337.
- [139] A. Baldini et al., *A submission to the 2020 update of the European Strategy for Particle Physics on behalf of the COMET, MEG, Mu2e and Mu3e collaborations*, [1812.06540](#).
- [140] COMET collaboration, *Conceptual design report for experimental search for lepton flavor violating mu- - e- conversion at sensitivity of 10**(-16) with a slow-extracted bunched proton beam (COMET)*, .
- [141] MU2E collaboration, *Mu2e Technical Design Report*, [1501.05241](#).
- [142] A. Crivellin and M. Hoferichter, *β Decays as Sensitive Probes of Lepton Flavor Universality*, *Phys. Rev. Lett.* **125** (2020) 111801 [[2002.07184](#)].
- [143] M. Kirk, *Cabibbo anomaly versus electroweak precision tests: An exploration of extensions of the Standard Model*, *Phys. Rev. D* **103** (2021) 035004 [[2008.03261](#)].
- [144] A. Crivellin, M. Hoferichter and C. A. Manzari, *Fermi Constant from Muon Decay Versus Electroweak Fits and Cabibbo-Kobayashi-Maskawa Unitarity*, *Phys. Rev. Lett.* **127** (2021) 071801 [[2102.02825](#)].